

AN INTEGRATED IMAGING APPROACH TO THE STUDY OF THE OXIDANT  
EFFECTS OF AIR POLLUTIONS ON HUMAN LUNG CELLS

Wan-Yun Cheng

A dissertation submitted to the faculty of the University of North Carolina at Chapel Hill in  
partial fulfillment of the requirements for the degree of Doctor of Philosophy in the  
Department of Environmental Sciences and Engineering.

Chapel Hill

2011

Approved by:

Dr. James M. Samet

Dr. Avram Gold

Dr. Michael Chua

Dr. Lee Graves

Dr. Urmila Kodavanti

Dr. Kenneth Sexton

## Abstract

WAN-YUN CHENG: An Integrated Imaging Approach to the Study of the Oxidant Effects of Air Pollutants on Human Lung Cells  
(Under the direction of Dr. James M. Samet)

Air pollution is one of the most common environmental exposures imposed on humans in urban areas on a daily basis. Molecular toxicology studies of the inflammatory effects of ambient air pollutants typically focus on the activation of signaling events that lead to the transcriptional activation of relevant inflammatory genes. While there is a growing body of evidence that oxidative stress plays a critical role in adverse responses induced by a broad array of environmental agents, an integration of the study of oxidant effects in mechanistic studies is hampered by methodological shortcomings and limitations such as sensitivity and specificity. The causative relationship between signaling pathways and adverse outcomes stimulated by specific ambient contaminants has been described. In addition, the generation of oxidative stress has been implicated as an initiating event that leads to adverse responses triggered by exposure to environmental toxicants. However, due to their transient nature, reactivity, and low abundance, detection of reactive oxygen species (ROS) is methodologically challenging. The application of new genetically encoded reporters provides the opportunity to interface real-time measurement of oxidative stress into mechanistic studies with increased temporal and spatial resolution. The studies herein are aimed at integrating imaging analyses of oxidative stress endpoints in molecular signaling of the inflammatory effects of

environmental oxidants. We conducted a study using zinc and 1,2-naphthoquinone as model toxicants to (1) develop an integrated imaging method for measurement of redox potential, ROS levels, and mitochondrial dysfunction; (2) examine the role of oxidative stress in the initiation of signaling events that lead to inflammatory gene expression; and (3) create an advanced imaging method to perform simultaneous measurements of redox changes and ROS production.

## ACKNOWLEDGMENT

I would like to first express my appreciation to Dr. James M. Samet not only for his mentorship in my doctoral training but also his full support of several milestones in my personal life. Next, I extend my sincere gratitude to the members of my doctoral dissertation committee, Dr. Michael Chua, Dr. Avram Gold, Dr. Lee Graves, Dr. Urmila Kodavanti, and Dr. Kenneth Sexton for their time, suggestions, and scientific guidance.

My full appreciation goes out to the Clinical Research Branch community for the care I received over the years. I would like to particularly honor those who have come before me, Dr. Thomas Hofer and Dr. Tamara Tal, and extend a deep thanks to Rober Silbajoris, Eugene Gibbs, Ana Rappold, Haiyan Tong, Lisa Dailey, and Samantha Snow for their company and involvement in my matriculation as a scientist and adjustment to a new culture. I would also like to thank Dr. Philip Bromberg for his scientific contributions to my study design and research directions as well as his insightful counsel in regards to my personal development.

Finally, I thank my family for their deep love and support. I would specially like to recognize my husband, Jim, for his consistent understanding, care, and encouragement.

## TABLE OF CONTENTS

<b>LIST OF TABLES.....</b>	<b>ix</b>
<b>LIST OF FIGURES.....</b>	<b>x</b>
<b>LIST OF ABBREVIATIONS.....</b>	<b>xii</b>
<b>Chapter I. Background and significance.....</b>	<b>1</b>
1-A. Air pollution induced adverse health effects.....	1
1-B. Oxidative stress .....	4
1-C. Major cellular sources of ROS .....	8
1-D. Mechanisms underlying elevated levels of oxidative stress induced by environmental exposures .....	12
1-E. Limitations of current analytical methods .....	16
1-F. The advantages of new probes for ROS and redox status in living cells.....	18
1-G. Development of Dynamic Spectral Unmixing Microscopy methodology for the study of toxicant-induced oxidative stress. ....	26
1.H Conclusions .....	27
1.I Hypothesis and specific aims of this doctoral research .....	28
<b>Chapter II. An Integrated Imaging approach to the study of oxidative stress     generation by mitochondrial dysfunction in living cells .....</b>	<b>31</b>

2-A. Introduction .....	31
2-B. Materials and Methods .....	33
2-B-1. Cell culture and experimental settings.....	33
2-B-2. Measurement of H <sub>2</sub> O <sub>2</sub> . .....	35
2-B-3. Measurement of mitochondrial membrane potential. ....	35
2-B-4. Cardiac mitochondrial swelling assay.....	36
2-B-5. Measurement of redox potential in mitochondria. ....	37
2-B-6. Statistical analysis. ....	38
2-C. Results .....	38
2-C-1. Zinc-induced H <sub>2</sub> O <sub>2</sub> production visualized by PG1 in living cells. ....	38
2-C-2. Identification of the source of Zn <sup>2+</sup> -induced H <sub>2</sub> O <sub>2</sub> . ....	42
2-C-3. Zinc-induced mitochondrial dysfunction. ....	44
2-C-4. Visualization of Zn <sup>2+</sup> -induced oxidative stress in mitochondria.....	49
2-D. Discussion .....	51
<b>Chapter III. Linking oxidative events to inflammatory and adaptive gene expression induced by exposure to an organic PM component .....</b>	<b>56</b>
3-A. Introduction .....	56
3-B. Materials and Methods .....	59
3-B-1. Reagents .....	59
3-B-2. Synthesis of fluorescent reporter genes in lentiviral vector .....	59
3-B-3. Cell culture and viral transduction .....	60

3-B-4. Cell Exposure .....	60
3-B-5. Measurement of redox potential and hydrogen peroxide.....	61
3-B-6. RT-PCR.....	61
3-B-7. Statistical Analysis .....	62
3-C. Results .....	62
3-C-1. 1,2-NQ induces rapid oxidant changes. ....	62
3-C-2. Overexpression of catalase blunts 1,2-NQ-induced H <sub>2</sub> O <sub>2</sub> production. ....	65
3-C-3. Overexpression of catalase differentially inhibits 1,2-NQ-induced gene expression. ....	67
3-C-4. 1,2-NQ induces intracellular production of H <sub>2</sub> O <sub>2</sub> . ....	70
3-C-5. Identification of the mitochondrion as the source of 1,2-NQ-induced H <sub>2</sub> O <sub>2</sub> .....	73
3-C-6. 1,2-NQ-induced gene expression is differentially linked to mitochondrial activity and H <sub>2</sub> O <sub>2</sub> availability. ....	77
3-D. Discussion .....	79

**Chapter IV. Live cell detection of redox changes and hydrogen peroxide  
production using dynamic spectral unmixing microscopy (DynSUM) ..... 86**

4-A. Introduction .....	86
4-B. Materials and Methods .....	89
4-B-1. Reagents .....	89
4-B-2. Cell culture and viral transduction .....	89
4-B-3. Measurement of redox potential and hydrogen peroxide.....	89

4-B-4. Statistical Analysis .....	90
4-C. Results and Discussion .....	90
4-C-1. The optical properties of roGFP and HyPer.....	90
4-C-2. The application of DynSUM on roGFP and HyPer .....	94
4-C-3. DynSUM in mitochondria.....	98
4-C-4. The application of DynSUM to the study of redox changes in human lung cells exposed to an environmental electrophile.....	101
4-D. Summary .....	105
<b>Chapter V. Concluding Remarks.....</b>	<b>108</b>
5-A. The implication of oxidative stress in this study.....	110
5-B. Toxicological applications of the imaging approach to oxidant detection.....	118
5-C. PM induced oxidant toxicity and its evaluation .....	123
5-D. From imaging oxidative stress in vitro to protecting the public health from environmental exposures .....	126
<b>REFERENCES .....</b>	<b>129</b>

## LIST OF TABLES

Table 2-A. The effect of inhibitors on Zn <sup>2+</sup> -induced H <sub>2</sub> O <sub>2</sub> production.....	43
Table 4- A. The distribution of signal between HyPer, roGFP and remainder channels as a percentage of the total. ....	97

## LIST OF FIGURES

Figure 1- A. Modes of mitochondrial operation that lead to superoxide production.....	11
Figure 1- B. Structural features of roGFP2 (George T Hanson et al. 2004). .....	23
Figure 1- C. The paradigm of chemical compounds induced inflammation that is mediated by oxidative stress.....	30
Figure 2- A. Visualization of zinc-induced H <sub>2</sub> O <sub>2</sub> production by PG1 fluorescence in A431 cells.....	41
Figure 2- B. Measurement of mitochondrial membrane potential visualized by JC-1 in A431 cells treated with zinc. ....	45
Figure 2- C. Zinc-induced mitochondrial dysfunction measured using the swelling assay.....	48
Figure 2- D. Zinc-induced oxidative stress in mitochondria. ....	50
Figure 3- A. Measurement of redox change and H <sub>2</sub> O <sub>2</sub> production visualized by roGFP-cyto and HyPer-cyto in BEAS-2B cells with 1,2-NQ treatment.....	64
Figure 3- B. Catalase overexpression blunted 1,2-NQ-induced hydrogen peroxide signals but not redox changes.....	66
Figure 3- C. Dose- and time-dependent 1,2-NQ-induced inflammatory and adaptive gene expression were differentially inhibited by catalase overexpression.....	68
Figure 3- D. 1,2-NQ-induces mitochondrial hydrogen peroxide production.....	71
Figure 3- E. Confocal imaging of 1,2-NQ-induced hydrogen peroxide production in mitochondria.....	75

Figure 3- F. Differential role of mitochondrial H <sub>2</sub> O <sub>2</sub> in 1,2-NQ-induced gene expression.....	78
Figure 3- G. Proposed scheme of 1,2-NQ-induced effects. ....	85
Figure 4- A. Demonstration of HyPer and roGFP under oxidizing and reducing treatments. ....	93
Figure 4- B. The application of DynSUM on roGFP and HyPer. ....	96
Figure 4- C. The application of DynSUM in mitochondria. ....	99
Figure 4- D. Utilizing DySUM for the exposure to an environmental electrophile.....	103
Figure 5- A. Glutaredoxin as a general mediator of reversible protein thiol oxidation (Merzlyak et al. 2007; Subach et al. 2008). ....	117

## LIST OF ABBREVIATIONS

1,2-NQ	1-2 naphthoquinone
8-OHDG	8-Hydroxy, 2-deoxyguanosine
AdCAT	Adenoviral vector encoding human <i>catalase</i>
AdGFP	Adenoviral vector encoding green fluorescent protein
AP-1	Activator protein-1
AU	Arbitrary units
BSA	Bovine serum albumin
CCCP	Carbonyl cyanide 3-chlorophenylhydrazone
CFP	Cyan fluorescent protein
CLSM	Confocal laser scanning microscopy
COX-2	Cyclooxygenase-2
CREB	cAMP response element-binding protein
CSI	Confocal spectral imaging
CyA	Cyclosporine A
DCFH	2,7-dichlorodihydrofluorescein diacetate
DEP	Diesel exhaust particles
DMEM	Dulbecco's modified Eagle's medium
DPI	Diphenyleneiodonium

DynSUM	Dynamic spectral unmixing microscopy
eGFP	Enhanced GFP
EGFR	Epidermal growth factor receptor
EPA	Environmental Protection Agency
ESR	Electron spin resonance
FBS	Fetal bovine serum
FMN	Flavin mononucleotide
FRET	Fluorescence resonance energy transfer
GFP	Green fluorescent protein
GPX	Glutathione peroxidase
Grx	Glutaredoxin
Grx	Glutathione reductase
GSH	Reduced glutathione
GSSG	Oxidized glutathione
H <sub>2</sub> O <sub>2</sub>	Hydrogen peroxide
HNE	4-hydroxy-2-nonenal
HO-1	Heme oxygenase-1
I $\kappa$ B	NF- $\kappa$ B inhibitor

IL-6	Interlukin 6
IL-8	Interlukin 8
JC-1	5,5',6,6'-tetrachloro-1,1',3,3'-tetraethylbenzimidazolylcarbocyanine iodide
JNK	c-Jun N-terminal protein kinase
KCN	Potassium cyanide
Keap1	Kelch-like ECH-associated protein
KGM-Gold	Keratinocyte growth medium
MAPK	Mitogen-Activated Protein Kinase
MDA	Malondialdehyde
NA	Numerical aperture
NADH	Nicotinamide adenine dinucleotide
NaN <sub>3</sub>	Sodium azide
NF-κB	Nuclear factor-κB
PBS	Phosphate-buffered saline
PG-1	Peroxy Green 1
PM	Particulate matter
PTP	Protein tyrosine phosphatases
RET	Reverse electron transport

roGFP	Redox-sensitive GFPs
ROS	Reactive oxygen species
SOD	Superoxide dismutases
TBARS	Thiobarbituric acid reactive substance
TMRM	Tetramethyl rhodamine methyl ester
TNF- $\alpha$	Tumor Necrosis Factor-alpha
wtGFP	Wild-type GFP
YFP	Yellow fluorescent protein
Zn <sup>2+</sup>	Zinc ion
ZnSO <sub>4</sub>	Zinc sulfate
$\alpha$ KGDH	$\alpha$ -ketoglutarate dehydrogenase

## **Chapter I. Background and significance**

### **1-A. Air pollution induced adverse health effects**

Air pollution is one of the most common daily human environmental exposures in urban areas. It is currently estimated that more than 160 million Americans live in areas that exceed federal air pollution standards (EPA 2007). Air pollution is associated with multiple adverse health effects including pulmonary inflammation, decreased lung function, and exacerbation of pulmonary and cardiovascular disease, which lead to increased incidence of morbidity and mortality (Ruckerl et al. 2011). Many components of air pollution fall into 1 of 2 categories: particulate matter and gases. They may come from natural or man-made sources with the potential to have numerous interactions. Currently, the United States Environmental Protection Agency (EPA 2007) regulates 6 “Criteria” Air Pollutants: particulate matter (PM), ozone, carbon monoxide, nitrogen oxides, sulfur dioxide and lead. Of these, ambient levels of PM and ozone most frequently exceed air pollution standards (Laumbach 2010). While there are a variety of sources of air pollution and different forms of air pollutants, most air pollutants, other than CO and lead, are strong oxidants and therefore

oxidative stress is a common feature of the toxicity of many air pollutants (Pope 2010).

Many epidemiological studies have pointed out that PM, especially combustion-derived particles in urban areas, is an important risk factor for cardiopulmonary disease and mortality (Ruckerl et al. 2011). PM has multiple sources, including vehicle exhaust, wild fires, industrial emissions and road dust which pose different health risks based on the size and chemical composition of the particles. EPA has set national standards to protect against adverse health effects associated with exposures to fine (particles less than or equal to 2.5  $\mu\text{m}$  in diameter, PM<sub>2.5</sub>) and coarse particles (particles less than or equal to 10  $\mu\text{m}$  in diameter, PM<sub>10</sub>). A positive correlation has been reported between mortality rates and PM<sub>10</sub>/PM<sub>2.5</sub> exposures (Ruckerl et al. 2011). Particle size is a critical factor regarding PM induced health issues due to its correlation with particle deposition. Particle deposition is dependent on particle size in that large particles deposit primarily in the nasopharyngeal and tracheobronchial region, while nano sized particles deposit preferentially in the alveolar region (Nel et al. 1998; Samet et al. 2000).

The lung and the cardiovascular system are the main targets of PM-induced adverse health effects. Small airway inflammation is the major type of pulmonary injury induced by PM, which leads to symptoms such as exacerbation of asthma, airway obstruction, and reduced gas exchange (Zelikoff et al. 2003). An association between PM exposure and elevated rates of respiratory tract

infection is observed, as well as dysfunction such as impaired lung clearance (Brook et al. 2004). Exposure to PM is also a risk factor for cardiovascular injuries including stroke, heart attack, and sudden death (Brook et al. 2004). Systemic circulation of proinflammatory mediators and enhancements in atherogenesis are attributed to PM-induced cardiovascular effects (Li et al. 2003; Nel 2005). Furthermore, PM-induced inflammation is suggested as the general mechanism in pulmonary and cardiovascular injuries.

It has been established that the organic and metal components in PM can induce proinflammatory effects mediated through oxidative stress (Chang et al. 2000; Claiborn et al. 2002). Zinc is one of the most abundant soluble metals associated with ambient PM (Nemery 1990; Blanc et al. 1993). Inhalation of elevated levels of zinc oxide has been linked to an acute flu-like symptom called metal fume fever which induces airway inflammation and increased production of TNF- $\alpha$  and IL-6 (Kodavanti et al. 2002; Riley et al. 2003). Under experimental settings, zinc exposure results in production of inflammatory related chemokines and cytokines (Pautke et al. 2005).

As a component of air pollution, diesel exhaust particles (Sagai et al. 1993; Bai et al. 2001) are present in ambient air as a major contributor to PM in urban areas. DEP are complex mixtures that contain more than 40 toxic air contaminants. Structurally, DEP contain a carbon core with metals and many adsorbed organic compounds such as polycyclic aromatic hydrocarbon quinines. DEP exhibits toxicity consistent with the effects of quinones (Li et al. 2003).

Quinones found in PM can generate reactive oxygen species (ROS) directly, through redox cycling (the process of catalyzing recurring oxidation and reduction reactions), or as a byproduct of the covalent modification of important cellular enzymes such as cytochrome P450 (Finkelstein and Johnston 2004).

### **1-B. Oxidative stress**

Oxidative stress is a common feature in the mechanisms of cellular injury induced by a broad range of environmental agents (Steinberg et al. 1990). Such environmental oxidative stress can result directly from the effects of oxidizers, electrophiles, free radical-generating compounds such as ozone (Santa-Maria et al. 2005), quinones (Valko et al. 2005) and redox active transition metal ions (Ercal et al. 2001). Environmental oxidative stress can also involve the depletion of cellular antioxidant defense mechanisms or dysregulation of oxidative metabolism processes in the cell (Kelly et al. 1998).

Oxygen metabolism is the major source of ROS in normal physiology, whereas oxidizing enzymes and xenobiotics can also produce significant amounts of ROS (Kelly et al. 1998). Cells have well established defense systems with antioxidant enzymes such as superoxide dismutases (SOD) and catalase to scavenge ROS. However, elevated levels of ROS exceeding the ability of the cellular antioxidant defenses to detoxify oxidant assault results in oxidative stress and may cause lipid peroxidation, protein alterations, and DNA damage

(Kowaltowski et al. 2009). Adverse health effects such as aging, obesity, and inflammation are related to signaling events initiated by ROS.

Among the ROS species, hydrogen peroxide has been highlighted for its fulfillment of all the chemical and biological properties required of a “second messenger” (Kowaltowski et al. 2009).  $H_2O_2$  has a tightly regulated enzymatic production and degradation system. Importantly,  $H_2O_2$  reacts with specific target cysteine residues in dedicated environments and are capable of initiating various signaling cascades at low-levels in the cell (Forman et al. 2010). Posttranslational modification such as the creation of glutathionylated signaling proteins and intramolecular disulfides are critical for  $H_2O_2$ -modulated redox signaling (Jones 2008). Other than ROS, there is a growing awareness of radical-free oxidant insults which focuses on the disruption of thiol redox circuits. Thiol containing proteins have been recognized for redox regulation through reversible structural modifications. Cellular signaling, structural, and regulatory proteins are modulated through sulfur switches such as cysteine oxidation. Cysteine also participates in macromolecular interactions including DNA binding, membrane binding, and tethering to the cytoskeleton (Faraci and Didion 2004).

The cellular ROS defense systems contain enzymatic and nonenzymatic antioxidants. SOD are a major class of enzymatic antioxidants that catalyze the dismutation of superoxide to hydrogen peroxide. SOD can be found in many cellular compartments including cytoplasm, mitochondria, nucleus, lysosomes, and extra cellular matrix (Valko et al. 2006). Another enzymatic antioxidant,

catalase, provides further and rapid conversion for hydrogen peroxide into water and oxygen (Pastore et al. 2001; Nakamura et al. 1997). Also, glutathione is critical for hydrogen peroxide breakdown by which reduced glutathione (GSH) converts hydrogen peroxide into oxygen with catalysis by glutathione peroxidase (GPX). The concentration of reduced glutathione in normal cells is 1- 5 mM which is responsible for maintaining the cellular redox status, direct scavenging of singlet oxygen, and regenerating antioxidants such as vitamin C and E (Pinchuk et al. 1998; Awasthi et al. 2003; Trachootham et al. 2008).

While cells are maintaining a normal physiological state, the presence of ROS can modify macromolecule structure in a reversible fashion as well as regulate cellular function. However, elevated oxidative stress with excessive ROS generation would lead to irreversible damage by attacking lipids, proteins and DNA. Lipids are highly susceptible to oxidation. The radical oxidation of polyunsaturated fatty acids would generate peroxy radicals and be followed by cyclization reactions to produce reactive alkyl radicals and aldehydes such as malondialdehyde (MDA) and 4-hydroxy-2-nonenal (HNE). These lipid peroxidation products can further interact with DNA or proteins and alter signaling pathways (Trachootham et al. 2008). Furthermore, ROS such as hydroxyl radical and peroxynitrite are known for targeting proteins to create reversible or irreversible oxidative damage (Valko et al. 2006). Several amino acid residues are sensitive to oxidation including lysine, arginine, histidine, proline, threonine, cysteine and methionine (Stadtman 2004; Radi et al. 2001). Sulfur containing amino acids can undergo oxidations including reversible protein

cross-linkages and irreversible nitrosylation (Trachootham et al. 2008). These thiol-based redox switches have been regarded as major cellular regulators by participating in gene regulation under oxidant insults. As for DNA, it is subject to oxidant damage in nearly all of its components such as purine, pyrimidine, and sugar backbone (Haghdoust et al. 2005). DNA adducts such as 8-hydroxy, 2-deoxyguanosine (8-OHDG) are popular markers for DNA oxidation (Trachootham et al. 2008). Physiological processes including differentiation, maturation, and trafficking of vesicles are influenced by lipid, protein, or DNA oxidant modification (Irani 2000). On the other hand, unbalanced generation of ROS may lead to aberrant prolonged cell survival or disease with excessive cell death (Rahman and MacNee 2000). Therefore, the regulation of redox balance is critical for maintaining cellular homeostasis.

The relationship between oxidative stress and inflammation is well established (Rahman and MacNee 2000). ROS generation is stimulated by oxidants or oxidative damage of target organelles and followed by activation of nuclear factor- $\kappa$ B (NF- $\kappa$ B) and activator protein-1 (AP-1) (Rahman and MacNee 2000). The NF- $\kappa$ B inhibitor (I $\kappa$ B) binds and inactivates NF- $\kappa$ B within the cytoplasm. The presence of ROS initiates phosphorylation, ubiquitination, and degradation of I $\kappa$ B by altering the ratio of GSH/GSSG (Tak and Firestein 2001). The free NF- $\kappa$ B complex translocates into the nucleus and regulates gene expression involved in inflammation (Roebuck 1999). AP-1 activation involves phosphorylation of the c-Jun N-terminal protein kinase (JNK) targeting to c-Jun/c-Jun (homodimer) or c-Fos/c-Jun (heterodimer). The activation of NF- $\kappa$ B

and AP-1 can regulate antioxidant (MnSOD, HO-1) and pro-inflammatory (IL-8, TNF- $\alpha$ , COX-2) gene expression (Andreyev et al. 2005).

### **1-C. Major cellular sources of ROS**

The generation of ROS can come from both exogenous and endogenous sources. There is a variety of exogenous ROS sources such as environmental pollutants, irradiations, and chemicals. Many endogenous ROS sources have been studied including mitochondria, microsomes, peroxisomes, NADPH oxidase, cytochrome c oxidase, and xanthine oxidase.

Mitochondria are the site of oxidative conversion of organic carbon into cellular energy, thereby making ROS an inevitable by-product during the respiratory reaction for this organelle. There are at least seven enzymes responsible for ROS production in mammalian mitochondria including cytochrome b5 reductase, monoamine oxidases, dihydroorotate dehydrogenase, dehydrogenase of alpha-glycerophosphate, succinate dehydrogenase, aconitase, and alpha-ketoglutarate dehydrogenase complex (Starkov 2008). Many factors, including genetic defects or environmental factors (radiation or toxins), could trigger oxidative stress in mitochondria. Therefore, mitochondria are frequently named as a major source of ROS in cells (Starkov 2008). The mitochondrial ROS defense systems are important for scavenging superoxide and H<sub>2</sub>O<sub>2</sub> present in cells (Starkov 2008). Being a source/sink/target of ROS, mitochondrial redox

signaling can activate several pathways within itself as well as the cytosol and different organelles such as nucleus (Murphy 2009).

There are several factors that determine the rate of superoxide generation in mitochondria which can be expressed as the following:

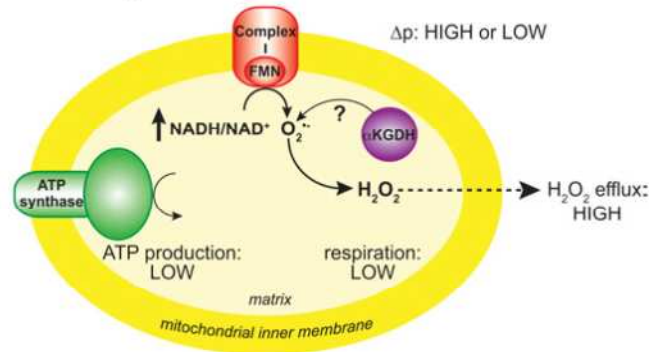
$$\left( \frac{d[\text{O}_2^{\bullet-}]}{dt} \right)_E = k_E [\text{O}_2] P_R [E]$$

[E] is the concentration of the enzyme or protein that contains electron carriers for the reduction of O<sub>2</sub> to superoxide. P<sub>R</sub> is the ratio of the redox form of the enzyme that can react with O<sub>2</sub>. [O<sub>2</sub>] represents the local oxygen concentration and k<sub>E</sub> is the second-order rate constant between the enzyme and O<sub>2</sub> in order to form superoxide (Murphy 2009).

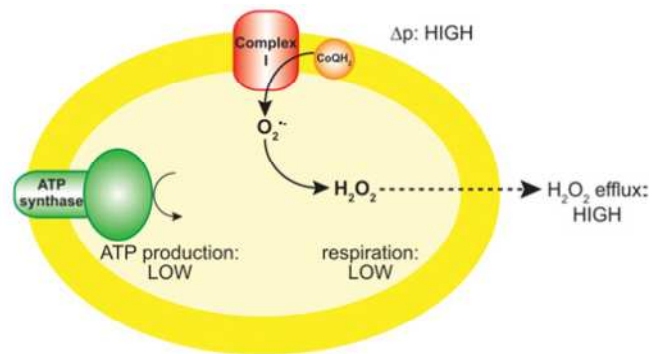
The major location for mitochondrial ROS production is complex I (Kussmaul and Hirst 2006; Hirst et al. 2008). The inhibition of the respiratory chain can lead to superoxide formation through low ATP production and elevated concentration of nicotinamide adenine dinucleotide (NADH). Studies in isolated mitochondria demonstrate that superoxide production is modulated by reduced flavin mononucleotide (FMN), and the status of FMN is controlled by the NADH/NAD<sup>+</sup>-ratio (Hinkle et al. 1967). Another mechanism for ROS production in complex I is through reverse electron transport (RET). RET involves a series of reactions that allow electrons to be transferred against the gradient, from reduced

coenzyme Q to  $\text{NAD}^+$  instead of oxygen (Lambert and Brand 2004) and therefore increases the  $\text{NADH}/\text{NAD}^+$  ratio. Studies of complex I inhibitors, for example rotenone, indicate the ROS generation sequence as the following: reduced CoQ  $\rightarrow$  rotenone binding site  $\rightarrow$  ROS generation site  $\rightarrow$   $\text{NAD}^+$  (Murphy 2009).

**MODE 1: high NADH/NAD<sup>+</sup>**



**MODE 2: high Δp and high CoQH<sub>2</sub>/CoQ**



**MODE 3: normal mitochondrial function**

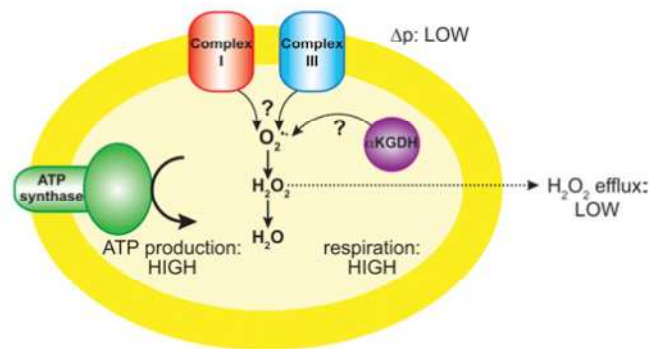


Figure 1- A. Modes of mitochondrial operation that lead to superoxide production. (Zhang et al. 1998).

Another major source of mitochondrial superoxide production is complex III. Complex III is functionalized as the site for CoQ oxidation by using Cytochrome C as an electron acceptor. The inhibition of complex III with antimycin, which interrupts the electron transfer to the  $Q_i$ -site, can result in robust superoxide production (Murphy 2009). However, the superoxide production in complex III under normal physiological conditions is far lower than complex I and therefore negligible (Murphy 2009).

In addition to the electron transfer chain, there are many other sources of superoxide production in mitochondria which can be generally categorized as sites that are related to the NADH and CoQ pools (Starkov et al. 2004). As mentioned earlier, high NADH/NAD<sup>+</sup> ratio contribute to superoxide production. This observation is not only true for complex I but also applies to other enzymes linked to the NADH pool such as  $\alpha$ -ketoglutarate dehydrogenase ( $\alpha$ KGDH). Under normal mitochondrial function with high respiration rate and ATP production, the contribution of superoxide production is more significant from sites like  $\alpha$ KGDH rather than complex I (Nel et al. 1998; Lim et al. 1998). Overall, the production of ROS from mitochondria is a major contributor of cellular oxidative stress from metabolic sources.

#### **1-D. Mechanisms underlying elevated levels of oxidative stress induced by environmental exposures**

Oxidative stress is believed to play an important role in PM-mediated toxicity in the respiratory tract. The mechanistic connection between DEP

exposure and inflammatory responses is held to hinge on the elevated level of oxidant stress and presence of ROS (Li et al. 2003; Kumagai et al. 1997).

Although DEP is a complicated mixture with thousands of components, the transition metals and organic chemical components in DEP have been shown to induce the generation of ROS including superoxide radical and hydrogen peroxide, as well as, nitric oxide (1995).

Quinones are fully conjugated cyclic dione structures derived from aromatic compounds by conversion of an even number of  $-\text{CH}=\text{}$  groups into  $-\text{C}(=\text{O})-$  groups (Bolton et al. 2000). While there are naturally occurring quinones such as vitamins K1 and K2, xenobiotic quinones have been of toxicological interest for their ability to induce DNA adduct formation which leads to mutagenesis (Bai et al. 2001; Rodriguez et al. 2004). A variety of quinone species are found in DEP which implies a significant human exposure to these compounds (Endo et al. 2007; Miura et al. 2011). The adverse effects caused by quinones range from acute cytotoxicity and immunotoxicity to carcinogenesis. Quinone toxicities can be summarized into two primary initiating mechanisms: first, a 1,4-Michael addition reaction leading to covalent modification of cellular targets (Rodriguez et al. 2004) and, second, ROS generation through redox cycling (Penning et al. 1999). Different quinones could undergo either or both pathways to initiate signaling events. The conjugation reaction for quinones has been extensively studied for its highly reactive properties and the addition of various nucleophiles (Penning et al. 1999). This reaction can form stable DNA adducts through 1,4-Michael addition, which is a mutagenic process (Nel et al.

1998). Other than the mutagenetic effects posed by DNA adducts, quinones can undergo enzymatic or non-enzymatic redox cycling for ROS generation (Jaspers et al. 2009); however, little is known about the biological consequences in this process related to inflammation.

As mentioned above, ROS can initiate signaling events and inflammatory gene expression. Evidence indicates that DEP may induce inflammatory responses (Jakober et al. 2007). DEP is the major component of fine PM derived from incomplete combustion (Donaldson et al. 2005). Extensive studies in human, animal, and cellular models have pointed out that DEP, most likely the organic content, induces inflammation by elevating oxidative stress (Donaldson et al. 2005). The activation of pro-inflammatory mediators by DEP is believed to relate to classical redox sensitive signaling pathways like MAPK, and transcription factors, such as NF- $\kappa$ B and AP-1 (Jakober et al. 2007). Benzoquinone and naphthoquinone are two of the most abundant quinone species in diesel emissions (Bai et al. 2001; Rodriguez et al. 2004). These observations lead to the hypothesis that quinones may induce inflammatory gene expression through oxidant-dependent signaling.

1-2 naphthoquinone (1,2-NQ) is a reactive electrophile associated with diesel exhaust particles (Monks et al. 1992) that has been shown to have cytotoxic, mutagenic and immunotoxic effects (Kikuno et al. 2006; Iwamoto et al. 2007). 1,2-NQ is believed to inactivate protein tyrosine phosphatases (PTP) that act as negative regulators for EGFR (Kikuno et al. 2006; Iwamoto et al. 2007).

This reaction induces potent contraction of guinea pig tracheal rings by activation of receptor tyrosine kinases (Sun et al. 2006). Also, nitric oxide synthase in endothelial cells is inactivated by 1,2-NQ exposure (Kuwahara et al. 2006; Tsatsanis et al. 2006). Although it can undergo both reactions, the toxicity posed by 1,2-NQ is most likely initiated by covalent binding, which has been associated with the activation of signaling pathways that can lead to the expression of pro-inflammatory proteins such as IL-8 and COX-2 (Kuroda et al. 2010) and the adaptive protein HO-1 (Valko et al. 2005).

Zinc, a redox inert transition metal, is found ubiquitously in plants and animals. The literature ascribes contradictory effects in regards to zinc-induced oxidative stress. Zinc is viewed as an antioxidant under deficiency conditions (Schwarzlander et al. 2009). However, elevated levels of  $Zn^{2+}$  induce cellular damage with production of ROS (Donaldson et al. 2005). Occupational and environmental exposures to elevated concentrations of  $Zn^{2+}$  have resulted in adverse health effects such as metal fume fever and inflammatory responses (Samet et al. 1998; Wu et al. 1999). It is suggested that the underlying mechanism of cellular injuries caused by zinc exposure occurs by the triggering of signaling pathways involving  $Ca^{2+}$ , MAPK, and PI3K (Link and von Jagow 1995; Lohman and Remington 2008). Previous studies point to  $Zn^{2+}$ -induced inhibition of mitochondrial respiration by binding to complex III and bc1 complex (Abraham M. Brown et al. 2000). Furthermore, mitochondrial energy metabolism is inhibited through  $\alpha$ -ketoglutarate dehydrogenase complexing with  $Zn^{2+}$  (Bossy-Wetzel et al. 2004a). In addition, it has been shown that treatment with soluble

Zn<sup>2+</sup> results in substantial respiration blockage, mitochondrial structural alterations, mitochondrial permeability transition changes, and ROS production in isolated mitochondria (Donaldson et al. 2005).

As the model toxicants in this study, Zn<sup>2+</sup> and quinones are known for their correlation with inflammation and classical signaling pathways (Nemery 1990; Blanc et al. 1993). Elevated levels of inflammatory mediators such as interleukin 8 (IL-8), interleukin 6 (IL-6), and Tumor Necrosis Factor-alpha (TNF- $\alpha$ ) are associated with Zn<sup>2+</sup> exposure (Samet et al. 1998; Wu et al. 1999; Jaspers et al. 2000; Kim et al. 2006; Samet et al. 2003; Wu et al. 2004). Our research group has demonstrated that Zn<sup>2+</sup> initiates several signaling events, including activation of epidermal growth factor receptor (EGFR), Ras, NF- $\kappa$ B, AP-1, JNK, ERK and Mitogen-Activated Protein Kinase (MAPK), which are all upstream signaling events for inflammatory responses (Cao et al. 2007a, 2009; Cao et al. 2007b; Pourazar et al. 2005; Tal et al. 2008). In addition, we have reported that diesel exhaust can activate EGFR, Src, and STAT3 with enhanced COX-2 and IL-8 expression all of which lead to inflammatory responses (Esterbauer 1996). Thus, evidence shows that Zn<sup>2+</sup> and quinones can stimulate inflammatory mediator expression via several signaling pathways.

### **1-E. Limitations of current analytical methods**

A variety of biochemical and analytical methods are commonly used for the study of oxidative stress in living cells. Traditional methods have relied on

indirect evidence such as deficiency of antioxidants or the measurements of damaged DNA, protein, and lipid by-products. For instance, a thiobarbituric acid reactive substance (TBARS) is a well-established index for lipid peroxidation. Colorimetric, fluorimetric and chromatographic assays can be utilized for the detection of MDA, the bi-product of lipid oxidation (Palmieri and Sblendorio 2007). Spin trapping with electron spin resonance (ESR) spectroscopy is a way to detect free radicals by measuring the formation of radical adducts. Normally, there are two groups of compounds, nitroso and nitron, used for trapping. The application of spin trapping ESR demonstrates high sensitivity for ROS detection; however, the stability of spin trapping, interference of the probe with biological systems, and artifacts are concerns regarding these approaches (Crow 1997). In general, the detection of ROS by means of the approaches mentioned above involve the disruption of cells, which may interfere with the results. It could generate oxidation artifacts, limit dynamic interpretation and impair subcellular compartment detection during cell lyses process. Furthermore, physiological production of oxidants by non-phagocytic cells involves the generation of relatively low levels of ROS, making the detection of ROS generation by relevant cellular targets of inhaled pollutants such as epithelial cells especially difficult.

Fluorescence microscopy can perform measurements that are focused on individual living cells over a prolonged period of time. 2,7-dichlorodihydrofluorescein diacetate (H<sub>2</sub>DCF-DA) and its variants are widely used for H<sub>2</sub>O<sub>2</sub> detection when imaging live cells. However, DCFH has low specificity and is oxidized by different oxidant species including peroxyxynitrite,

nitric oxide, and  $H_2O_2$  in various experimental conditions (Ohashi et al. 2002). Furthermore, DCFH can not only be activated by ROS but also by heme and hemoproteins, which reduces the credibility of its oxidative stress detection (Marchesi et al. 1999). Photoreduction is another limitation for DCFH as oxidation occurs when the dye is incubated with reducing agents and stimulated with visible light irradiation (Miller et al. 2007). These fluorescent dyes are noted for their drawbacks including low specificity, non-reversibility, and limited organelle targeting potential.

#### **1-F. The advantages of new probes for ROS and redox status in living cells**

Peroxy Green 1 (PG-1) was the first fluorescence-based indicator developed specifically for  $H_2O_2$  detection, with the sensitivity for  $H_2O_2$  production from non-phagocytic cells responding to physiological signals (Miller et al. 2007). PG-1 consists of fluorescein conjugated to a chemoselective boronate switch that responds to  $H_2O_2$  with high specificity (Rhee 2007). As a chemical based ROS sensor, PG-1 represents a significant improvement over DCFH in that it offers superior specificity, sensitivity, and stability (Dickinson et al. 2011; Lippert et al. 2011a; Chung et al. 2011; Lippert et al. 2011b). Although PG-1 is not specifically targeted to any intracellular compartments, when used in combination with classical inhibitors, as presented in chapter II, it can be used to infer an intracellular source of  $H_2O_2$  production. Furthermore, Dr. Chang, who first engineered PG-1, is working on improving chemical tools for studying ROS biology. The Chang research group developed boronate group based-fluorescence

indicators with characterizations such as different ROS detection, subcellular compartment targeting capability, and two photon competences (Dickinson and Chang 2011) (Reers et al. 1991). These newly expanded chemical tools allow advanced ROS detection under reaction-based approaches.

Reagents also exist for the evaluation of mitochondrial function by imaging methods. The mitochondrial membrane potential indicator, 5,5',6,6'-tetrachloro-1,1',3,3'-tetraethylbenzimidazolylcarbocyanine iodide (JC-1), has been used since the 1990s (Li et al. 1999). It is a ratiometric dye with two distinct emissions (maximum at 527 nm and 590 nm) that varies depending on its concentration. Under normal conditions, mitochondria actively pump the dye against its concentration gradient, resulting in a high JC-1 concentration (J-aggregates with red color), while disruption of mitochondrial membrane potential results in the release of JC-1 into the cytosol (J monomer with green color). In other words, the changes of JC-1 color represent the viability of the mitochondria. Loss of mitochondrial membrane potential indicates cellular dysfunction and initiates signaling events that lead to ROS production (Belousov et al. 2006).

In addition to chemical based fluorescence probes, another strategy for ROS measurement is through the use of protein-based fluorophores. Generally, fluorescent proteins are fused/engineered with redox-active domains such as transcription factors or antioxidants to achieve specific ROS detection or sense changes in redox balance in a cellular system. Green fluorescent protein (GFP) based redox/ROS probes have been developed since 2000 and have received a lot

of attention due to several advantages including reversibility, stability, sensitivity and specificity regarding their detection of physiologically relevant oxidant event. Additionally, there are two excitation maxima observed in GFP based on the protonation state of the chromophore. Ratiometric fluorophores exhibit two excitation maxima that can be monitored sequentially in real-time. Typically, the emission at one of the excitation peaks is constant in intensity relative to the other and can be used to control for variations in signal intensity caused by differences in extraneous factors. It can minimize errors associated with differences in protein expression level, cell thickness, and uneven illumination as well as photobleaching.

The genetically encoded sensor, HyPer, was developed for hydrogen peroxide detection by Belousov et al. This sensor is a fusion of YFP and the regulatory domain of OxyR (OxyR-RD) and was generated by the insertion of circularly permuted YFP into OxyR coding sequence (Choi et al. 2001). OxyR is an *E. coli* transcription factor that is specifically sensitive to H<sub>2</sub>O<sub>2</sub>. Hydrogen peroxide reacts with the critical cysteine in OxyR-RD protein to create a cysteine sulfenic acid followed by the formation of an intramolecular disulfide bridge (Belousov et al. 2006). cpYFP is inserted nearby the critical OxyR hydrogen peroxide sensing domain (C199 and C208) between position 205 and 206 (Meyer and Dick 2010). HyPer can be used directly for the ratiometric measurement of intracellular hydrogen peroxide with no exogenous chemical compounds. According to the manufacturer, the HyPer protein has nanomolar affinity to H<sub>2</sub>O<sub>2</sub>, and our laboratory has observed micro molar affinity for HyPer in BEAS-2B

cells. HyPer has been shown to express a 3 to 4 fold dynamic range *in vitro* (Belousov et al. 2006). The high sensitivity and specificity of HyPer makes it very useful for its application in signaling studies. Detection of physiological levels of H<sub>2</sub>O<sub>2</sub> was performed by using HyPer in HeLa cells and was found to be expressed in different sub-cellular compartments including the cytosol, mitochondria and nucleus (Ostergaard et al. 2001).

Sensitive reporters for redox potential have been designed based on variants of green fluorescent protein (roGFP and rxYFP). These genetically encoded reporters were presented by two independent research groups as redox sensors with two fluorescence excitation maxima which allow ratiometric analysis (George T Hanson et al. 2004) (Shimomura et al. 1962; Ormo et al. 1996). Wild-type GFP (wtGFP) isolated from jelly fish has an 11-stranded beta barrel shielding an internal alpha helix (Bjornberg et al. 2006). The chromophore of wtGFP consists of three amino acids (S65/Y66/G67). Beta strands 7 and 10 extend into the core of wtGFP adjacent to the chromophore. Therefore, the engineering strategy for redox fluorescence indicator development is targeted to the amino acids with the potential to distort/alter the chromophore and, therefore, fluorescence emission intensity through a reversible reaction such as a disulfide bond formation (Dooley et al. 2004). The redox-sensitive GFP (roGFP) developed by Dr. Remington's group has two surface-exposed, thiol-containing, cysteines placed at positions 147 and 204 on beta strands 7 and 10 in both wtGFP and enhanced GFP (eGFP), close to the chromophore (Cannon and James Remington 2009). Disulfide formation between the cysteine groups promotes protonation of

the chromophore and alters emission intensity. Therefore, oxidizing conditions induce the formation of a disulfide bridge between these 2 cysteines, which ultimately alters the emission intensity depending upon the excitation wavelength (Meyer and Dick 2010). roGFP2 uses eGFP as a backbone, which is preferable due to enhanced intensity, better compatibility with general laser excitation (404 and 488 nm), and better resistance to photoswitching (George T Hanson et al. 2004).

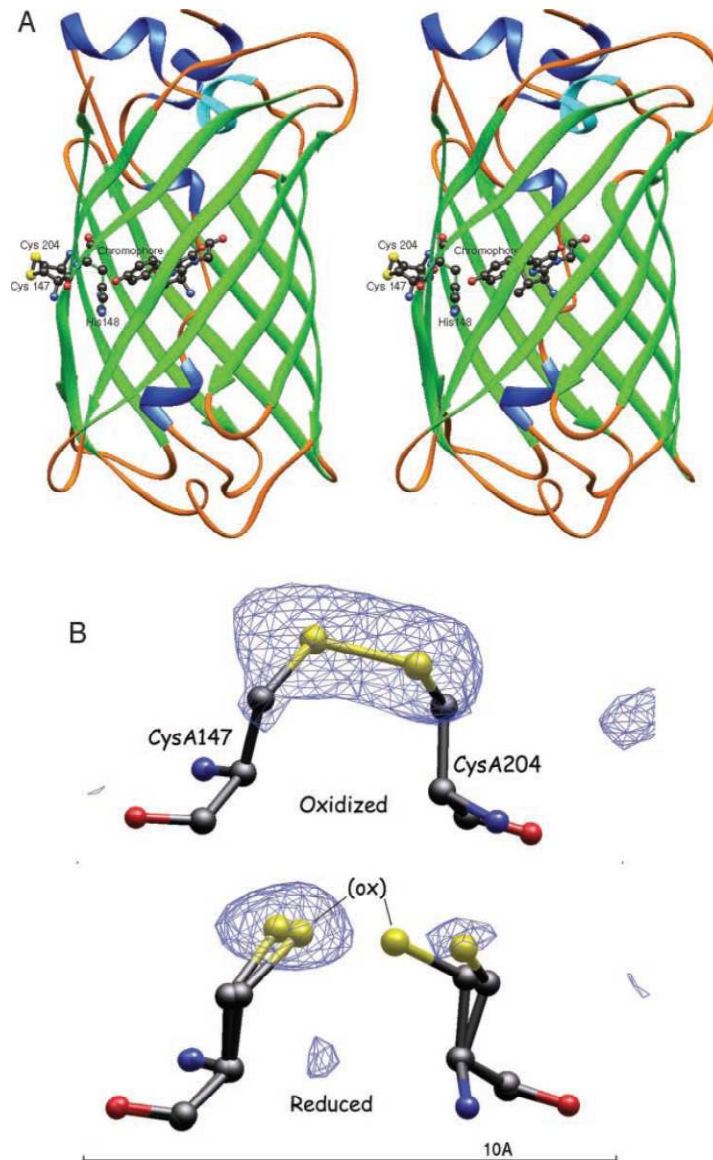


Figure 1- B. Structural features of roGFP2 (George T Hanson et al. 2004).  
 A. The key structure of roGFP including the chromophore and engineered cysteine.  
 B. the critical cysteine, Cys147 and Cys204, under oxidized (top panel) and reduced (bottom panel) environments.

These roGFP variants are engineered for the detection of intracellular thiol-disulfide equilibria (Lohman and Remington 2008; Dooley et al. 2004; Cannon and Remington 2006), and therefore provide a non-invasive method for the measurement of cellular redox potential with improved response rate, selectivity of midpoint potential, and specific cellular compartment expression (Valko et al. 2005; Schwarzlander et al. 2009). These sensors have been used for monitoring redox status in plant cells and ischemic neuronal cells under various conditions (Ostergaard et al. 2001; George T Hanson et al. 2004).

The midpoint potential of roGFP2 is approximately -272 mV which makes it suitable for detection in reducing compartments such as the cytosol, mitochondria and chloroplast stroma (Austin et al. 2005). However, since roGFP is fully oxidized in environments such as endoplasmic reticulum or lysosome, it is desirable to also have roGFP variants with higher midpoint potential (Lohman and Remington 2008). A second generation of roGFPs, roGFP1-R12 and roGFP1-iX were established by Lohman and Remington that had a higher midpoint potential, -230mV (Meyer and Dick 2010). Validation of the dynamic range of the second generation roGFP in oxidizing compartments is required (Dooley et al. 2004).

The measurement of redox potential reflects the state of oxidant stress present in the cytosol. Although there are multiple redox pairs in the cell, GSH/GSSG is the dominant redox pair in the cytosol. Studies conducted with the

use of specific inhibitors reveal that roGFP largely senses the balance of the glutathione redox pool (Cobbett et al. 1998; Meyer et al. 2007; Vernoux et al. 2000; Vesce et al. 2005), specifically the concentration of GSSG, which is typically very small in resting physiological conditions. Several experimental lines of evidence confirm that roGFP communicates with the glutathione redox couple through the intervention of glutaredoxin (Grx) (Meyer and Dick 2010). The rate limiting step for roGFP to equilibrate with the glutathione pool  $2\text{GSH}/\text{GSSG}$  is the availability of endogenous Grx (Meyer and Dick 2010). In other words, the kinetics of roGFP2 is restricted by the abundance and activity of Grx which varies in species, cell types, and cellular locations. Therefore, the development of next generation roGFP focuses on coupling redox-sensitive reporters to Grx. Grx1-roGFP fusion protein is the third generation of redox-sensitive fluorescent protein with better sensitivity and faster response time (Dickinson et al. 2001).

Taken together, the combination of ratiometric fluorescent probes and confocal microscopy offers considerable improvements over existing methods for the detection of oxidative stress, specifically, in regard to temporal and spatial resolution as well as sensitivity. As mentioned above, detection of ROS and oxidative stress is challenging due to the transient nature of the events and the sensitivity required for the detection. Although several parameters should be taken into consideration while acquiring data, imaging analysis can achieve decisecond detection, effectively providing near real-time measurements. Equally important is the ability to observe the locations of the oxidative events of interest

with subcellular resolution (e.g., redox changes in mitochondria). This is valuable in tracking the origin and propagation of signaling events and understanding the etiology of oxidative stress. Lastly, the use of photomultiplier and advanced camera-based detectors provides improved sensitivity and quantitative resolution for the detection of low concentrations of ROS and the development of small changes in redox status. In the current study, genetically encoded probes can detect ROS concentrations in the micro molar range in nonphagocytic cells. The combined application of an imaging approach based on these new sensors of ROS and redox status is a major innovation in the current series of studies, as it is used to integrate oxidative stress into the existing molecular toxicology paradigm for the study of the effects of inhaled pollutants

#### **1-G. Development of Dynamic Spectral Unmixing Microscopy methodology for the study of toxicant-induced oxidative stress.**

Spectral unmixing refers to the protocol by which the measured spectrum of a mixed pixel is decomposed into a collection of constituent spectra (Dickinson et al. 2001; Berg 2004; Ecker et al. 2004; Larson 2006; Zimmermann et al. 2003; Zucker and Lerner 2005; Zucker et al. 2007). Spectral unmixing techniques have been used in the physical sciences for the analysis of satellite-based imaging for several decades. This technique was introduced from planetary systems to cellular systems in the recent decade (Monks et al. 1992). In the biological application, spectral unmixing is used for discriminating between the fluorescence signals emitted by multiple fluorophores with overlapping spectra. Most filter methods

for either widefield or confocal microscopy only allow separation of distinct channels, such as blue, green and red. The development of the confocal spectral imaging (CSI) microscope permits simultaneous study of multiple probes with overlapping emission spectra (Finkelstein and Johnston 2004) (Steinberg et al. 1990). The CSI instruments achieve spectral unmixing by acquiring emission spectra from different probes and comparing the signal with reference spectra. The distance between the peaks in the individual spectra, the resolution of the instrument and the relative intensity of the emitted fluorescence from each probe are critical determinants of the accuracy of spectral unmixing.

In this dissertation work, a novel dynamic spectral unmixing approach was developed, validated and applied for the monitoring of H<sub>2</sub>O<sub>2</sub> levels and redox changes induced in real time in living cells undergoing exposure to environmental oxidants.

## **1.H Conclusions**

Molecular toxicology studies of the inflammatory effects of ambient air pollutant exposure typically focus on the activation of signaling events that lead to the transcriptional activation of relevant inflammatory genes. While there is a growing body of evidence that oxidative stress plays a critical role in adverse responses induced by a broad array of environmental agents, an integration of the study of oxidant effects in mechanistic studies is hampered by methodological shortcomings and limitations such as sensitivity and specificity. The causative

relationship between signaling pathways and adverse outcomes stimulated by specific ambient contaminants has been described previously. Studies conducted in this laboratory and elsewhere have implicated the generation of oxidative stress as an initiating event that leads to adverse responses triggered by exposure to environmental toxicants. However, due to their transient nature, reactivity and low concentration, the detection of ROS and oxidant responses has been methodologically challenging. This dissertation herein is aimed at integrating imaging analyses of oxidative stress endpoints with chemical and genetic indicators in molecular signaling studies. Also, in the current study, we utilized transition metal and organic components found in DEP as our model toxicants to elucidate the role of oxidative stress as a mechanistic link between exposure to environmental electrophiles and the expression of inflammatory proteins.

## **1.I Hypothesis and specific aims of this doctoral research**

One of the major mechanisms by which ubiquitous components of ambient air pollution, such as quinones and  $Zn^{2+}$ , induce toxicity is by the generation of exogenous or endogenous ROS. While ROS generation is involved in inflammatory processes, the link between exposure and inflammation has not been examined. The lack of reliable quantitative methods is a major impediment in the integration of the role of oxidant stress induced inflammation in molecular toxicology studies. The application of new genetically encoded reporters provides the opportunity to interface real time measurement of oxidative stress into mechanistic studies with increased temporal and spatial resolution. The studies

herein are aimed at integrating imaging analyses of oxidative stress endpoints in molecular signaling studies of the inflammatory effects of environmental oxidants. The overall hypothesis of this research project is that imaging approaches can facilitate examination of the role of oxidative stress in mechanistic studies of the inflammatory effects from air pollution exposures.

The hypothesis is addressed in three specific aims in this dissertation. We conducted a study using zinc and quinone as model toxicants to (1) develop an integrated imaging method for measurement of redox potential, ROS levels, and mitochondrial dysfunction; (2) examine the role of oxidative stress in the initiation of signaling events that lead to inflammatory gene expression; and (3) create an advanced imaging method to perform simultaneous measurements of redox changes and ROS production.

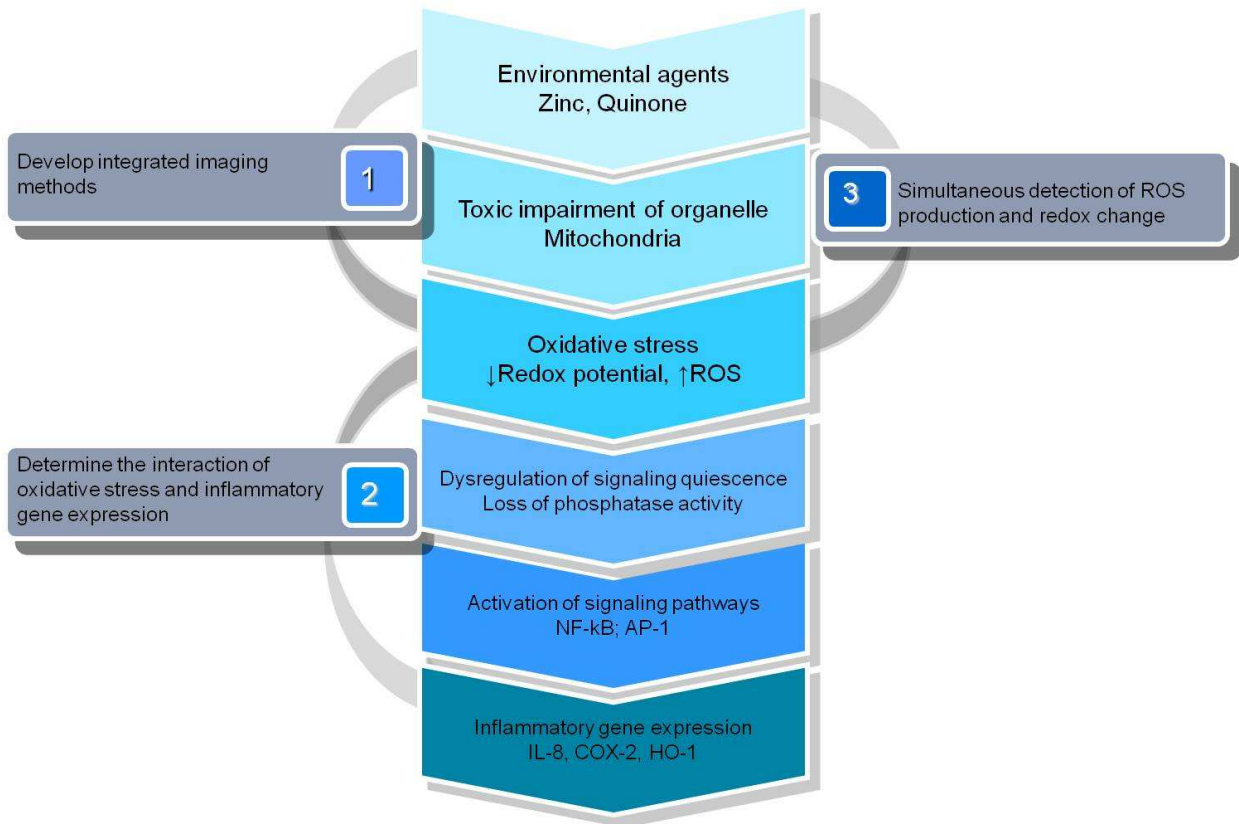


Figure 1- C. The paradigm of chemical compounds induced inflammation that is mediated by oxidative stress.

Environmental agents induced toxic impairments to organelles which lead to elevation of oxidative stress. The oxidant events would then change redox homeostasis and activate signaling pathways followed by inflammatory and adaptive gene expression.

## **Chapter II. An Integrated Imaging approach to the study of oxidative stress generation by mitochondrial dysfunction in living cells<sup>1</sup>**

### **2-A. Introduction**

Oxidative stress is a common feature of the mechanism of injury induced by a broad range of environmental agents (Valko et al. 2005). Such environmental oxidative stress can result directly from the effects of oxidizers, electrophiles, or free radical-generating compounds such as ozone (Ercal et al. 2001), quinones (Kinter 1995), and redox-active transition metal ions (Kelly and Mudway 2003). Environmental oxidative stress can also involve the depletion of cellular antioxidant defense mechanisms or dysregulation of oxidative metabolism processes in the cell (Aust and Eveleigh 1999).

Analytical methods used to study oxidative stress often focus on the detection of oxidized biomolecules such as oxidized lipids (Monks et al. 1992), proteins (Crow 1997), and DNA (Marchesi et al. 1999; Rota et al. 1999). Direct detection of reactive oxygen species (Andreyev et al. 2005) involved in cellular

---

<sup>1</sup> The main findings of Specific Aim 1 were published in “Wan-Yun Cheng, Haiyan Tong, Evan W. Miller, Christopher J. Chang, James Remington, Robert M. Zucker, Philip A. Bromberg, James M. Samet, and Thomas P.J. Hofer (2010). An Integrated Imaging approach to the study of oxidative stress generation by mitochondrial dysfunction in living cells. *Environ Health Perspect* 118:902–908.”

oxidative stress in living cells has relied heavily on the use of the fluorescent indicator 2,7-dichlorodihydrofluorescein diacetate (H<sub>2</sub>DCF-DA) (Lam et al. 2001). Unfortunately, the interpretation of data obtained with this indicator has been limited by its lack of specificity and by experimental artifacts that include photoinstability, autoxidation, and photoconversion (Senft et al. 2002).

Mitochondria are a known source of partially reduced oxygen species generated as a by-product of oxidative metabolism in the cell (Valko et al. 2005). Dysregulation of mitochondrial function with metabolic inhibitors has been shown to induce the release of ROS and associated oxidative stress (Ouhabi et al. 1998; Smiley et al. 1991). Toxicologically, a wide variety of environmental contaminants ranging from aromatic hydrocarbons (Rhee 2007; Cannon and Remington 2008) to heavy metal ions (Kim et al. 2006; Tal et al. 2006) have been shown to impair mitochondrial respiration, with ensuing production of ROS. A number of assays measure indices of mitochondrial function, such as ATP concentration, citrate synthase activity, and membrane potential (Tang et al. 2001), but the methodologies used to measure mitochondrial redox potential are limited.

In the present study, we used an integrated imaging approach to the investigation of environmental oxidative stress resulting from mitochondrial dysfunction. By applying established and recently introduced indicators, this integrated approach allows real-time measurement of mitochondrial membrane potential, hydrogen peroxide (H<sub>2</sub>O<sub>2</sub>) levels, and redox status in living cells

(Zucker and Lerner 2005; Zucker et al. 2007; Lerner and Zucker 2004; Zucker 2006a, b). A431 skin carcinoma cells were used as representative of rapidly growing cells with high metabolic rate and energy use that could be inferred to have a correspondingly high mitochondrial activity. Zinc sulfate ( $\text{ZnSO}_4$ ) was used as a soluble form of the zinc ion ( $\text{Zn}^{2+}$ ) that is also environmentally relevant, because sulfate salts are known to predominate among soluble metal salts released by combustion processes. In addition, we used zinc pyrithione, which is used as a mildewcide in outdoor paints, making skin cells a relevant cell type to study with this agent.

We report that exposure to  $\text{Zn}^{2+}$ , a ubiquitous ambient contaminant that has been shown to induce inflammatory (Miller et al. 2007) and cytotoxic responses (Riganti et al. 2004), results in an intracellular accumulation of  $\text{H}_2\text{O}_2$  that is associated with a decrease of mitochondrial reducing redox potential and depolarization of the mitochondrial membrane. These findings demonstrate the utility of an integrated application of imaging techniques for the study of mechanisms of environmental oxidative stress in living cells with improved spatial and temporal resolution as well as specificity.

## **2-B. Materials and Methods**

### **2-B-1. Cell culture and experimental settings.**

A431 human skin carcinoma cells (no. CRL-1555; American Type Culture Collection, Manassas, VA, USA) were used for live cell imaging experiments.

The cells were cultured in Dulbecco's modified Eagle's medium (DMEM; catalog no. 11995, GIBCO, Grand Island, NY, USA) and supplemented with 10% fetal bovine serum (FBS) and 5  $\mu\text{g}/\text{mL}$  gentamicin at 37°C, 5% CO<sub>2</sub>. Cells were seeded on round glass cover slips (22 mm in diameter, thickness #1) in six-well culture plates at 150,000–250,000 cells per well. Cultures were deprived of growth factors overnight prior to study. The A431 cells were preloaded with Peroxy Green 1 (PG1) or 5,5',6,6'-tetrachloro-1,1',3,3'-tetraethylbenzimidazolylcarbocyanine iodide [JC-1 (T3168; Invitrogen, Carlsbad, CA, USA)], and the cover slip cultures were fitted into a custom-made stainless-steel chamber filled with 500  $\mu\text{L}$  phosphate-buffered saline (PBS), which was supplemented with 1 g/L glucose and kept at 37°C with a stage heater. Conventional and spectral confocal microscopy analyses were conducted using a Nikon Eclipse C1Si confocal microscope (Nikon Instruments Inc., Melville, NY, USA) that was equipped with TE 2000 microscope. Light was delivered to the sample with a 60  $\times$  Plan Apo 1.4 numerical aperture (NA) objective; the system also uses diode lasers of 404 nm, 488 nm, 561 nm, and 633 nm. Prior to each experiment, the confocal microscope was tested for field illumination alignment, optical efficiency, colocalization, and axial resolution (Bogeski et al. 2006); and the lens was inspected and cleaned before use. Cells were exposed sequentially to ZnSO<sub>4</sub> (catalog no. Z-0251; Sigma, St. Louis, MO, USA) at concentrations between 10  $\mu\text{M}$  and 100  $\mu\text{M}$  with or without 4  $\mu\text{M}$  of the Zn<sup>2+</sup>-specific ionophore pyrithione, given at 5 min. The inhibitors apocynin (100  $\mu\text{M}$ ) (Tal et al. 2006), wortmannin (10  $\mu\text{M}$ ), diphenyleneiodonium (DPI; 25  $\mu\text{M}$ ) (Shutes et al. 2007),

carbonyl cyanide 3-chlorophenylhydrazone (CCCP; 10  $\mu$ M) (Miller et al. 2007), and Ly294002 (10  $\mu$ M; all inhibitors were obtained from Sigma), plus compound 56 (C56, 10  $\mu$ M; Calbiochem, San Diego, CA, USA) (EPA 2007) and EHT 1864 (5  $\mu$ M; provided by C.J. Der, University of North Carolina–Chapel Hill) (George T Hanson et al. 2004) were applied 30 min prior to adding  $Zn^{2+}$ .  $H_2O_2$  (1 mM), CCCP (10  $\mu$ M), or dithiothreitol (DTT; Sigma; 10 mM) was added at the end of experiments as positive controls.

### 2-B-2. Measurement of $H_2O_2$ .

$H_2O_2$  production was monitored using the fluorescein-like Peroxy Green 1 (PG1) dye (Tal et al. 2006). PG1 is a boronate probe with high specificity for  $H_2O_2$ . A431 cells grown on glass cover slips were labeled in 5  $\mu$ M PG1 for 15 min at 37°C in PBS glucose solution prior to measurement. PG1 fluorescence was excited using an argon laser (at  $\lambda = 488$  nm), and the emission spectrum was monitored in a range of  $\lambda = 490$  nm to 570 nm over 32 channels with 2.5 nm band pass. Signal intensity was quantified at the PG1 emission peak at 523 nm.

### 2-B-3. Measurement of mitochondrial membrane potential.

The mitochondrial membrane potential was monitored using the fluorescent indicator JC-1. In the presence of physiological mitochondrial membrane potentials, JC-1 forms aggregates that fluoresce with an emission peak at 588 nm. Loss of membrane potential favors the monomeric form of JC-1, which has an emission peak at 530 nm. Cells were labeled with 5  $\mu$ M JC-1 in DMEM supplemented with 10% FBS and 1  $\mu$ g/mL gentamicin at 37°C. After 15

min incubation, cells were washed with PBS twice and placed in the chamber with 500  $\mu$ L PBS glucose. JC-1 fluorescence intensity was monitored with dual excitation at 488 nm and 561 nm and an emission scan range of 490–650 nm (32 channels, 5 nm per channel). Mitochondrial membrane potential was inferred from the ratio of fluorescence intensity of emission maximum at 593 nm and 538 nm, which represented the J-aggregate and monomeric forms, respectively.

#### 2-B-4. Cardiac mitochondrial swelling assay.

Adult pathogen-free female CD-1 mice, which were purchased from Charles River (Raleigh, NC, USA), were used as the source of the cardiac mitochondria. Animals were housed at the U.S. Environmental Protection Agency (Miller et al. 2007) animal care facility (accredited by the Association for Assessment and Accreditation of Laboratory Animal Care) and given ad libitum access to both water and food. Animal care was given in accordance with institutional guidelines, and animals were treated humanely, with regard to alleviating suffering. The studies were conducted with approval by the EPA Institutional Animal Care and Use Committee. Mice were euthanized with an intraperitoneal injection of sodium pentobarbital (80 mg/kg body weight), and hearts were excised and weighed. Freshly isolated mitochondria were prepared from the ventricles by differential centrifugation. Briefly, heart tissues were homogenized with three strokes of a polytron homogenizer in ice-cold homogenization buffer containing 225 mM mannitol, 75 mM sucrose, 5 mM morpholinepropanesulfonic acid, and 2 mM taurine, with 0.2% bovine serum

albumin (BSA; pH 7.4). The homogenate was transferred to a glass homogenizer and homogenized for five strokes on ice. After centrifugation at 2,500 rpm for 5 min at 4°C, the supernatant was removed and centrifuged at 8,000 rpm for 5 min. The pellet was sequentially washed with homogenization buffer three times and resuspended in homogenization buffer plus 5 mM KH<sub>2</sub>PO<sub>4</sub>. The protein concentration was determined with BSA as a standard by a Bradford assay.

The mitochondria (50 µg) were incubated in buffer containing 120 mM KCl, 10 mM Tris HCl, and 5 mM KH<sub>2</sub>PO<sub>4</sub> at room temperature. After adding 10 mM glutamate and 2 mM malate, the light scattering of mitochondria was measured at 540 nm for 40 min with a 96-well plate spectrophotometer (POLARstar Optima; BMG, Alexandria, VA, USA). We initiated calcium- or zinc-induced mitochondrial swelling by adding 250 µM calcium or 100 µM zinc and measured for another 20 min. The absorbance was normalized to the initial absorbance.

#### 2-B-5. Measurement of redox potential in mitochondria.

The genetically encoded mitochondria-targeted form of the genetically encoded fluorescent reporter redox-sensitive green fluorescent protein (MTroGFP1) was used for the measurement of redox potential in mitochondria (Riganti et al. 2004; Bogeski et al. 2006; Shutes et al. 2007; Vanhaesebroeck et al. 2001). Fugene 6 (catalog no. 11815091001; Roche, Mannheim, Germany) was used for transfection according to the manufacturer's protocol. The MTroGFP1 plasmid was mixed with Fugene 6 for 30 min at room temperature and applied to

the A431 cells for 48 hr. Tetramethyl rhodamine methyl ester (TMRM; catalog no. T-668, Invitrogen), a mitochondria-specific dye, was used to validate the transfection by incubating 500 nM TMRM with transfected cells for 15 min and by visualizing with excitation at 561 nm and with emission filter of 605/75 nm (Chroma Technology Corp, Rockingham, VT, USA). Green fluorescence was derived from excitation at both 404 nm and 488 nm with an emission detected using a band-pass filter of 525/50 nm (Chroma). The results were calculated by ratioing the emissions excited by 488 nm and 404 nm laser sequentially.

#### 2-B-6. Statistical analysis.

Imaging data were collected with Nikon EZ-C1 software and quantified by EZ-C1 and Nikon Elements. Figures were plotted with mean  $\pm$  SE, with three repeat experiments. An average of 5–10 cells with different fluorescence intensities were collected as regions of interests in each experiment and quantified with Nikon EZ-C1 and Nikon Elements software (Nikon Instruments). Pairwise comparisons were carried out using Student's t-test; a p-value of  $< 0.05$  was considered statistically significant.

### **2-C. Results**

#### 2-C-1. Zinc-induced H<sub>2</sub>O<sub>2</sub> production visualized by PG1 in living cells.

As a model toxicant for these studies, we used Zn<sup>2+</sup>, a non-redox-active metal that is ubiquitously found associated with particulate matter in ambient air and occupational settings. Addition of noncytotoxic concentrations (Guthrie and

Welch 2008) of  $Zn^{2+}$  and pyrithione (10–100  $\mu M$   $ZnSO_4$  plus 4  $\mu M$  pyrithione) to A431 cells resulted in a time-dependent elevation in intracellular concentrations of  $H_2O_2$  as detected by an increase in PG1 fluorescence intensity (Figure 2-A).  $H_2O_2$  added as positive control resulted in a marked increase (550%) in PG1 fluorescence (Figure 2-A). Spectral analysis of PG1 fluorescence excited with 488 nm revealed an emission peak at 523 nm (Figure 2-A), consistent with published reports (George T Hanson et al. 2004). Sequential images were captured at 30-sec intervals and plotted as the relative fluorescence intensity normalized to initial intensity. Cells exposed to 100  $\mu M$   $Zn^{2+}$  for 10 min showed a 64% increase in PG1 fluorescence intensity relative to starting levels. PG1-loaded resting cells not exposed to  $Zn^{2+}$  observed during the same testing period showed < 4% increase in fluorescence intensity (Figure 2-A). Similar to resting cells, A431 cells incubated in 4  $\mu M$  pyrithione alone did not show an increase in PG1 fluorescence intensity (data not shown).

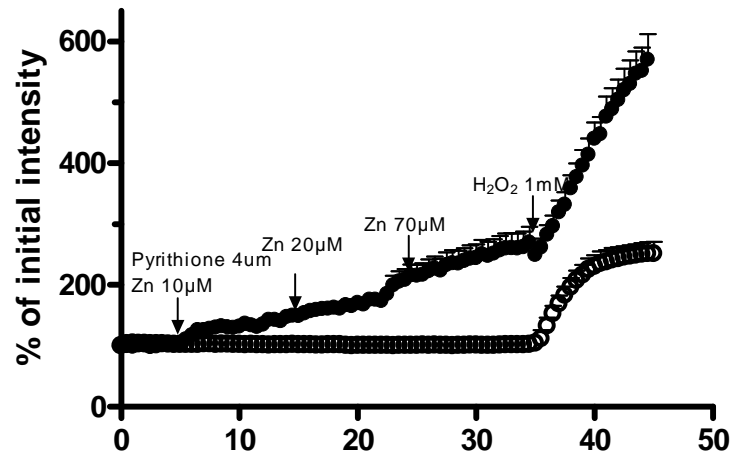
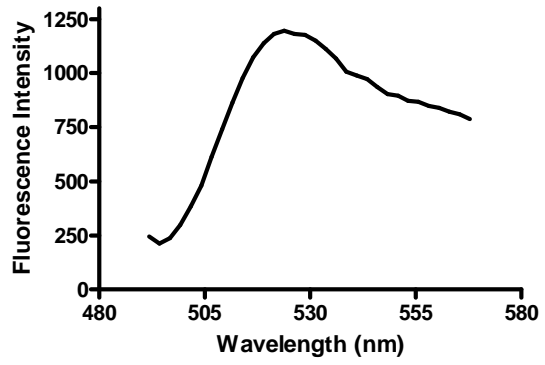
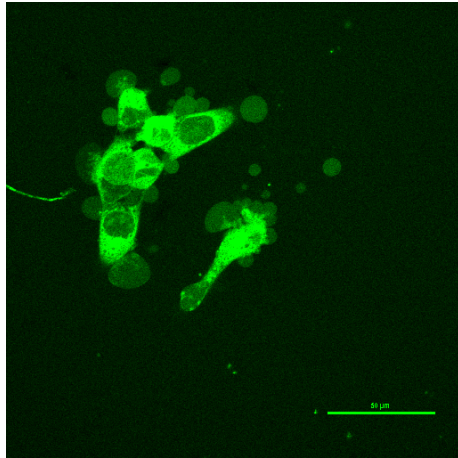
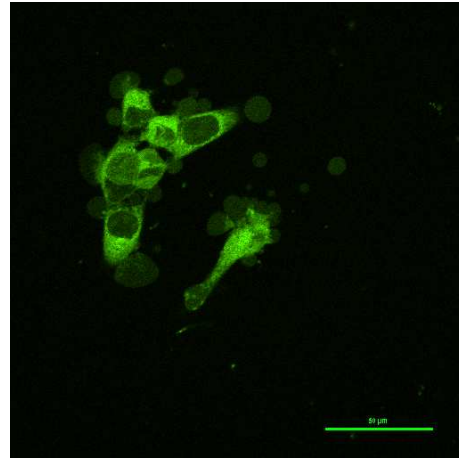
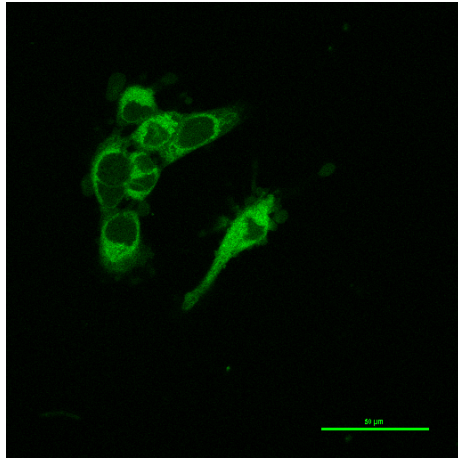


Figure 2- A. Visualization of zinc-induced H<sub>2</sub>O<sub>2</sub> production by PG1 fluorescence in A431 cells.

A431 cells were incubated with vehicle alone for 5 min (a), 100 μM zinc sulfate for 30 min (b), or 1 mM H<sub>2</sub>O<sub>2</sub> given at 45 min (c). (d) Emission spectra confirmation of PG1 fluorescence with peak at 523 nm; intensity is shown in arbitrary units (AU). (e) Time course of H<sub>2</sub>O<sub>2</sub> production detected by PG1 fluorescence in resting cells and in cells stimulated with 10 μM Zn plus 4 μM pyrithione at 5 min, 20 μM Zn at 15 min, or 70 μM Zn at 25 min; H<sub>2</sub>O<sub>2</sub> (1 mM) was added at 35 min as a positive control for both experimental conditions. Triplicate observations were made for control and stimulated cells with an average of 10 cells in each run. Data are mean ± SE.

### 2-C-2. Identification of the source of Zn<sup>2+</sup>-induced H<sub>2</sub>O<sub>2</sub>.

As shown in Figure 2-A, Zn<sup>2+</sup>-stimulated H<sub>2</sub>O<sub>2</sub> production was visualized as an increase in fluorescence disseminated throughout the cytosol. To identify the intracellular source of H<sub>2</sub>O<sub>2</sub>, cells were pretreated with the nicotinamide adenine dinucleotide phosphate oxidase inhibitors apocynin or DPI, the epidermal growth factor receptor kinase activity inhibitor C56, the phosphoinositide 3-kinase activity inhibitors wortmannin or Ly294002, the Rac GTPase kinase inhibitor EHT 1864, or the mitochondrial uncoupler CCCP, prior to exposure to Zn<sup>2+</sup> (George T Hanson et al. 2004). With the exception of CCCP, the application of these inhibitors did not have statistically significant effects on Zn<sup>2+</sup>-induced H<sub>2</sub>O<sub>2</sub> production in A431 cells (Table 2-A). Pretreatment with CCCP induced a statistically significant 32% inhibition in PG1 fluorescence intensity relative to Zn<sup>2+</sup> alone. Treatment with other reagents resulted in less than 10–20% inhibition of the H<sub>2</sub>O<sub>2</sub>-dependent PG1 fluorescence production induced by Zn<sup>2+</sup> (Table 2-A). These findings implicate mitochondria as the source of Zn<sup>2+</sup>-induced H<sub>2</sub>O<sub>2</sub> production.

Table 2-A. The effect of inhibitors on Zn<sup>2+</sup>-induced H<sub>2</sub>O<sub>2</sub> production.

<b>Inhibitor <sup>a</sup></b>	<b>Conc.</b>	<b>% Inhibition</b>
<b>Apocynin</b>	100 μM	21
<b>DPI</b>	25 μM	7
<b>C56</b>	10 μM	3
<b>Wortmannin</b>	10 μM	10
<b>Ly294002</b>	10 μM	0
<b>EHT 1864</b>	5 μM	5
<b>CCCP</b>	10 μM	32*

a. Cells incubated with inhibitors in various concentrations 30 min prior to 100 μM Zn<sup>2+</sup> exposure. Inhibition effects were calculated by comparison of Zn<sup>2+</sup> induced PG1 fluorescence after 30 min exposure with or without prior inhibitor treatment.

\* denotes statistically significant difference from vehicle control, p < 0.05

### 2-C-3. Zinc-induced mitochondrial dysfunction.

The maintenance of the electron transport chain proton gradient by functional mitochondria establishes a transmembrane electrical potential that can be monitored using the fluorescence indicator JC-1. Intrinsically a green indicator with an emission maximum at 529 nm in monomeric form, JC-1 accumulates in functional mitochondria in concentrations sufficient to form J-aggregates, which leads to a shift of the emission maximum to 588 nm (Figure 2-B). Zinc-induced mitochondrial depolarization led to a change in the equilibrium of JC-1 observed as a shift of the JC-1 emission maximum to a shorter wavelength (Figure 2-B), corresponding to an emission peak shift from 588 nm to 538 nm (Figure 2-B). The ratio of the fluorescence emission at 538 and 588 nm represents the degree of  $Zn^{2+}$ -induced mitochondrial depolarization (Valko et al. 2005). Loss of mitochondrial membrane potential was observed 10 min after cells were exposed to 100  $\mu M$   $Zn^{2+}$  and 4  $\mu M$  pyrithione, and continued to rise for 30 min (Figure 2-B). CCCP was added at the end of each experiment as a positive control. As shown in Figure 2-B, the addition of CCCP did not induce a further increase in fluorescent intensity in cells exposed to  $Zn^{2+}$ , suggesting a complete depolarization of mitochondrial potential induced by  $Zn^{2+}$  in A431 cells.

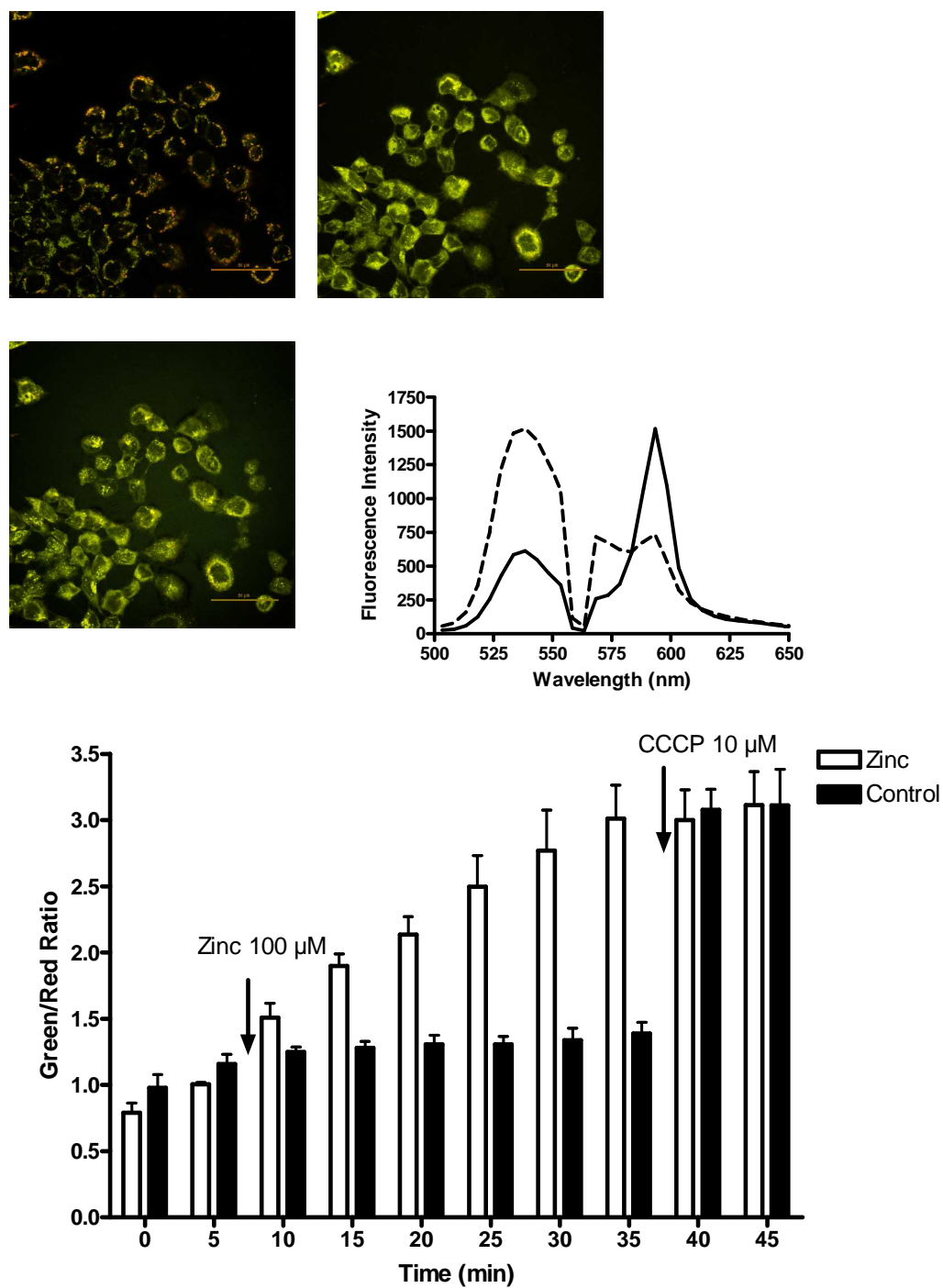


Figure 2- B. Measurement of mitochondrial membrane potential visualized by JC-1 in A431 cells treated with zinc.

A431 cells treated with vehicle alone (A) or with 100  $\mu\text{M}$  zinc before (B) and after addition of 10  $\mu\text{M}$  CCCP (C) as a positive control. (D) The spectrum of JC-1 is shown under 2 different conditions; control cells (solid line) and depolarized cells (dashed line). Intensity is shown in arbitrary units (AU). (E) Measurement of JC-1 fluorescence intensity (taken as the ratio of green to red) in control and  $\text{Zn}^{2+}$ -exposed A431 cells; 100  $\mu\text{M}$  zinc plus 4  $\mu\text{M}$  pyrithione were added at 5 min, and 10  $\mu\text{M}$  CCCP was added to both groups at 35 min. Images were obtained with simultaneous excitation of 488 nm and 561 nm laser and emission scan range between 490 nm and 650 nm using a 5 nm band pass. Triplicate observations were made for control and stimulated cells with an average of 10 cells in each run. Data are mean  $\pm$  SE.

As an independent measurement of mitochondrial function, we next examined the effect of  $Zn^{2+}$  exposure on the mitochondrial membrane transition pore using the mitochondrial swelling assay in isolated cardiac mouse mitochondria. This particular assay requires a large number of isolated mitochondria that would be impractical to obtain from cultured cells. Therefore, mouse heart mitochondria were used for this purpose as a model suitable for toxicological testing. Treatment with  $Zn^{2+}$  and pyrithione resulted in significant swelling of isolated mitochondria. The addition of calcium (positive control) induced spontaneous swelling, indicated by a 17% decrease in absorbance at 4 min, whereas the addition of zinc induced a similar effect, with a 15% decrease in absorbance (Figure 2-C). These results independently confirmed that  $Zn^{2+}$  directly affects mitochondrial function.

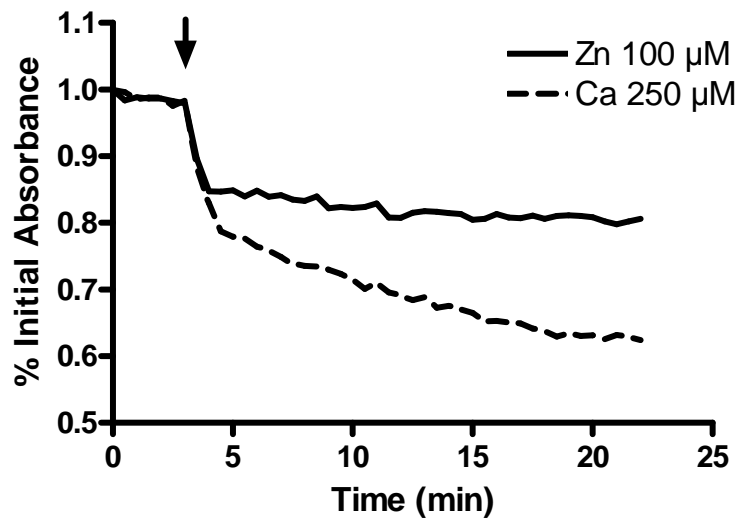


Figure 2- C. Zinc-induced mitochondrial dysfunction measured using the swelling assay.

A suspension of isolated cardiac mitochondria was monitored for absorbance at 550 nm after the addition of 100  $\mu\text{M}$   $\text{Zn}^{2+}$  or 250  $\mu\text{M}$  calcium ion. Absorbance values were normalized to the initial reading. Data represent three independent experiments.

#### 2-C-4. Visualization of Zn<sup>2+</sup>-induced oxidative stress in mitochondria.

The data presented above indicate that the mitochondrion is a target of Zn<sup>2+</sup>-mediated toxicity and a potential source of ROS and oxidative stress. To examine the effect of Zn<sup>2+</sup> exposure on mitochondrial redox potential, we used MTroGFP1 (Crow 1997). This genetically encoded reporter responds to changes in redox status with changes in the relative intensity of fluorescence at 510 nm upon excitation with its two excitation maxima, 404 and 488 nm. Cells transfected with MTroGFP1 displayed the expected green fluorescence in a pattern that was exclusively associated with mitochondria (Figure 2-D). Confirming the localization of the sensor, the MTroGFP1 fluorescence colocalized with a validated mitochondrial indicator, TMRM (Figure 2-D). Exposure of these cells to 100 μM Zn<sup>2+</sup> and 4 μM pyrithione induced a rapid increase in the ratio of fluorescence at 404/488, indicating a less reduced redox state (Figure 2-D). This Zn<sup>2+</sup>-induced change corresponded to a loss of mitochondrial reducing potential, from a value previously reported to be -288 mV (Ohashi et al. 2002), toward a more positive redox potential, starting within 2 min and reaching a plateau by 10 min (Figure 2-D). Subsequent addition of 10 mM DTT as a positive control restored a negative mitochondrial redox potential.

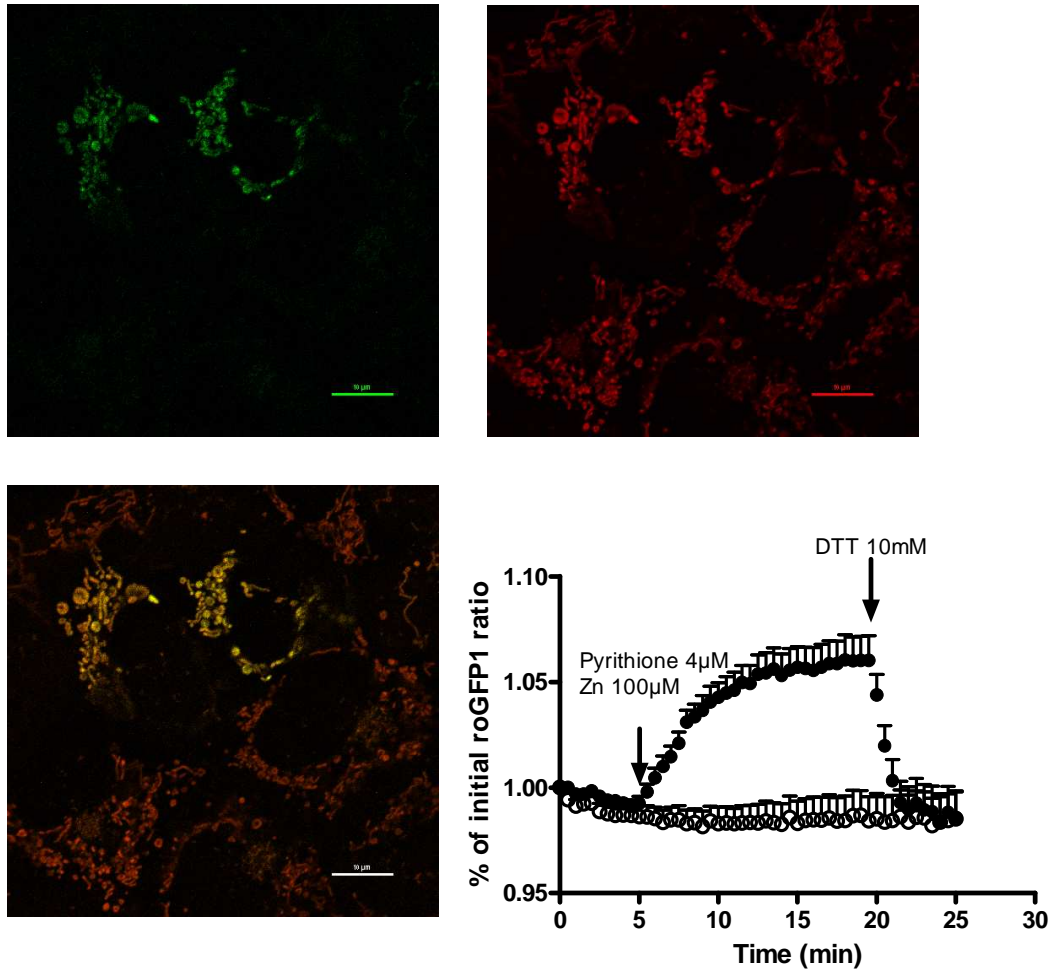


Figure 2- D. Zinc-induced oxidative stress in mitochondria.

(A) A431 cells transfected with MTroGFP1 demonstrate green fluorescence associated with mitochondria. (B) Cells incubated with the mitochondrial indicator TMRM, shown as red fluorescence. (C) Colocalization of the two images. (D) Mitochondrial redox potential was monitored as the ratio of fluorescence intensity under 404/488 excitation normalized to the value at 0 min; vehicle or 100  $\mu\text{M}$   $\text{Zn}^{2+}$  plus 4  $\mu\text{M}$  pyrithione was added at 5 min. DTT (10 mM) was added at 20 min as a positive control. Data were grouped from 20 cells studied over three separate experiments, expressed as mean  $\pm$  SE.

## 2-D. Discussion

Oxidative stress is increasingly recognized as an important feature of the mechanism of toxic action that is common to many structurally disparate environmental contaminants (Marchesi et al. 1999). However, a significant limitation in the investigation of oxidative stress in toxicology has been the availability of an integrated methodological approach for real-time detection of reactive oxidant species and oxidative damage in living cells. Compared with conventional biochemical assays, live-cell imaging offers superior temporal and spatial resolution of intracellular processes. In the present study, we have employed an integrated imaging approach to study oxidative stress associated with mitochondrial dysfunction in cells exposed to the environmental air pollutant  $Zn^{2+}$ . The detection of specific ROS is an important feature of this approach. The indicator H2DCF-DA and its variants have been used widely for ROS detection by imaging of living cells. However, several limitations are associated with H2DCF-DA, including a lack of ROS specificity and its susceptibility to oxidation by different species such as peroxynitrite, nitric oxide, superoxide, and  $H_2O_2$  under various experimental conditions (Miller et al. 2007). In addition, H2DCF-DA can also be oxidized by heme and hemoproteins (Miller et al. 2007) and is subject to photoreduction (Rhee 2007), further reducing the reliability of ROS detection with this indicator.

Using PG1, we visualized  $Zn^{2+}$ -stimulated  $H_2O_2$  production in living cells. Although PG1 is not specifically targeted to an intracellular compartment, when

used in combination with classical inhibitors, as we did in this study, it can be used to infer an intracellular source of H<sub>2</sub>O<sub>2</sub> within the cell. PG1 consists of a fluorescein-like dye conjugated to a chemoselective boronate switch that responds to H<sub>2</sub>O<sub>2</sub> with high specificity (Miller et al. 2007). PG1 is the first fluorescence-based molecular indicator for the specific detection of H<sub>2</sub>O<sub>2</sub> with sufficient sensitivity to detect low concentrations of peroxide such as those produced by nonphagocytes responding to physiological signals (George T Hanson et al. 2004). Thus, as an ROS sensor, PG1 represents a significant improvement over H2DCF-DA in that it offers superior specificity, sensitivity, and stability (Lohman and Remington 2008; Dooley et al. 2004; Cannon and Remington 2006). Miller et al. (Schwarzlander et al. 2009; Vesce et al. 2005) showed that PG1 has high specificity for H<sub>2</sub>O<sub>2</sub> relative to a wide range of other oxygen, nitrogen, chlorine, and organic oxidant species. Lending credence to these findings, in the present study we showed that Zn<sup>2+</sup>, a transition metal incapable of producing ROS by redox cycling, induces H<sub>2</sub>O<sub>2</sub> production detected by PG1 fluorescence, which we independently show to be the result of mitochondrial dysfunction induced by Zn<sup>2+</sup> exposure.

A critical element of the approach applied in this study is monitoring redox potential using redox-sensitive variants of green fluorescent protein (roGFPs). These genetically encoded reporters were first described by Hanson et al. (Link and von Jagow 1995; Lohman and Remington 2008) as redox potential sensors with two fluorescence excitation maxima, thus permitting ratiometric analysis that minimizes errors associated with variations in indicator

concentration (roGFP expression), illumination intensity, and cell thickness. The roGFP sensors were genetically engineered to respond to changes in intracellular thiol-disulfide equilibria (Hanson et al. 2004) and therefore provide a noninvasive method for measuring cellular redox potential. The roGFP sensors feature fast response rates and selectivity for midpoint potential and for subcellular compartment targeting (A. M. Brown et al. 2000). They have been used for monitoring redox status in plant cells and ischemic neuronal cells under various conditions (Bossy-Wetzel et al. 2004b). Here, we used a mitochondria-targeted version, MTroGFP1, to monitor the effect of  $Zn^{2+}$ -induced oxidative stress. The reporter responded as expected to treatment with exogenous oxidants ( $H_2O_2$ ) and reducing agents (DTT) within 2 min. Our findings show that  $Zn^{2+}$  induces a rapid decrease of mitochondrial reducing potential, consistent with the independent measurements of reduced mitochondrial membrane potential and opening of the mitochondrial permeability pore.

Previous studies point to  $Zn^{2+}$ -induced inhibition of mitochondrial respiration by binding to the bc1 complex (Kim et al. 2006; Tal et al. 2006). Furthermore, mitochondrial energy metabolism is known to be inhibited through  $\alpha$ -ketoglutarate dehydrogenase complexation by  $Zn^{2+}$  (Franklin and Costello 2009). In addition, it has been shown that treatment with soluble  $Zn^{2+}$  has resulted in substantial respiration block, mitochondrial structural alterations along with mitochondrial permeability transition changes, and ROS production in isolated mitochondria (Tang et al. 2001). Exposure to  $Zn^{2+}$  is also associated with dysregulation of signaling leading to increased expression of inflammatory

mediators (Link and von Jagow 1995), as well as apoptotic (Pautke et al. 2005) and necrotic cell death (Monks et al. 1992). Based on current understanding, the impairment of mitochondrial function observed in this study can be seen as an underlying mechanism through which the oxidant responses are caused by  $Zn^{2+}$  exposure, or interpreted to represent a secondary effect of the oxidant stress induced by  $Zn^{2+}$ . Additional studies will be required to elucidate the complex mechanisms that underlie the oxidative stress associated with  $Zn^{2+}$  toxicity.

As our findings with  $Zn^{2+}$  in this study demonstrate, by integrating the MTroGFP redox sensor and the JC-1 sensor of mitochondrial membrane potential with conventional methods to determine mitochondrial function (the swelling assay and metabolic inhibitors), it is possible to elucidate the mechanism of oxidative stress induced by exposure to environmental agents. The conclusion that oxidative stress induced by  $Zn^{2+}$  originates in the mitochondria is supported by the following findings in the present study: a) the partial inhibition of  $Zn^{2+}$ -stimulated  $H_2O_2$  production in the cytosol by the mitochondrial respiration uncoupler CCCP, b) the observation that  $Zn^{2+}$  exposure induces mitochondrial depolarization, c) the finding that  $Zn^{2+}$  induces mitochondrial swelling (in isolated cardiac mitochondria), and d) the decrease of reducing redox potential induced by  $Zn^{2+}$  exposure.

The methodologies used in this study are broadly applicable to other oxidative stressors such as redox active transition metals and organic oxidants. Using BEAS 2B cells as a model of the human airway epithelium, we have

observed that the diesel exhaust organic constituents 1,2-naphthoquinone and  $\square$ p-benzoquinone induce  $\text{H}_2\text{O}_2$  production and a change in redox potential in both cytosolic and mitochondrial compartments (Cheng WY et al., unpublished observations).

The timeline of events measured with the integrated approach using real-time imaging of living cells in this study seems to support a sequence in which exposure to  $\text{Zn}^{2+}$  results in mitochondrial dysfunction, possibly an arrest of electron transport (Kelly et al. 1998), causing an accumulation and release of partially reduced oxygen species, which gives rise to the increase in cytoplasmic  $\text{H}_2\text{O}_2$  detected as increased PG1 fluorescence subsequent to mitochondrial depolarization and redox changes.

The change in redox potential detected by the MTroGFP1 sensor appears to precede  $\text{Zn}^{2+}$ -induced depolarization of mitochondria reported by the color shift in JC-1 fluorescence. However, it is likely that the relative timing of the changes in fluorescence reported by the sensors and indicators used in this study is also influenced by differences between their individual response rates. Thus, it is not currently possible to precisely establish the sequence of events based on changes in the fluorescence intensity of different sensors. Future studies will focus on refining this integrated approach to factor in response rates in a dynamic system and thus more accurately reflect the temporal sequence of cellular events involving mitochondrial dysfunction and ROS generation leading to oxidative stress induced by ambient toxicants.

## **Chapter III. Linking oxidative events to inflammatory and adaptive gene expression induced by exposure to an organic PM component<sup>2</sup>**

### **3-A. Introduction**

Oxidant stress is a commonly described mechanistic feature of the toxicity of environmental contaminants (Pautke et al. 2005). Multiple pathophysiological effects of environmental exposures, including cancer, fibrosis and inflammation, have been associated with oxidant damage to macromolecules such as lipids, proteins and DNA (Monks et al. 1992). Oxidant stress induced by a toxicant is invariably a multifaceted process involving exogenous and endogenous reactions between xenobiotic and cellular macromolecules. Toxic exposures often elicit cellular responses that are intrinsically oxidant in that they involve production of ROS and/or the loss of intracellular reducing potential. Oxidative cellular responses to exposure to oxidizing agents can also occur and thus the elucidation of the events involved and the order in which they occur presents significant analytical challenges (Li et al. 2003; Kumagai et al. 1997).

---

<sup>2</sup> The main findings of Specific Aim 2 were published in “Wan-Yun Cheng; Jenna Currier; Philip A. Bromberg; Robert Silbajoris; Steven O. Simmons; and James M. Samet (2011). Linking oxidative events to inflammatory and adaptive gene expression induced by exposure to an organic PM component. *Environmental Health Perspective.*”

Oxidant stress is believed to play an important role in air pollutant-mediated toxicity in the respiratory tract. Transition metals and organic chemical components of diesel exhaust particles (Rahman and MacNee 2000; Becker et al. 2005) have been shown to induce the generation of various ROS (Cheng et al. 2010), including superoxide radical, H<sub>2</sub>O<sub>2</sub>, and nitric oxide (Bai et al. 2001; Rodriguez et al. 2004). The relationship between oxidative stress and altered expression of inflammatory and adaptive genes has been well established for a variety of air pollutants (Monks et al. 1992).

While established methods for the measurement of oxidant damage to cells and tissues exist, they are relatively insensitive and often provide only inferential mechanistic information. On the other hand, detection of primary oxidative events resulting from environmental exposures is inherently challenging due to the transient nature of the events involved as well as the relatively low levels of oxidant reactants that are generated. Imaging approaches offer the distinct advantages of providing high temporal and spatial resolution, as well as the high sensitivity necessary to detect early indicators of oxidative stress in cells exposed to environmental agents. Recently, we described an integrated imaging approach for the real-time measurement of redox potential changes and H<sub>2</sub>O<sub>2</sub> generation resulting from mitochondrial dysfunction in living cells exposed to the non-redox active transition metal Zn<sup>2+</sup> (Endo et al. 2007; Miura et al. 2011). In the present study, we expand this approach to include an investigation of the relationship between specific oxidant events in the cytosol and mitochondria and

altered gene expression induced by the redox-active air contaminant, 1,2-naphthoquinone (1,2-NQ).

1,2-NQ is a reactive electrophile associated with diesel exhaust particles (Rodriguez et al. 2004) that has been shown to have cytotoxic, mutagenic and immunotoxic effects (Kikuno et al. 2006; Iwamoto et al. 2007; Sun et al. 2006). Quinone toxicity has been found to involve two primary initiating mechanisms: first, a 1,4-Michael addition reaction leading to covalent modification of cellular targets (Kuwahara et al. 2006; Tsatsanis et al. 2006) and, second, ROS generation through redox cycling (Kuroda et al. 2010). Previous studies have shown that 1,2-NQ attacks protein-tyrosine phosphatases (G. T. Hanson et al. 2004), which has been associated with the activation of signaling pathways that can lead to the expression of pro-inflammatory proteins such as IL-8 and COX-2 (EPA 2007) and the adaptive protein HO-1 (Simmons et al. 2011). While multiple studies have suggested a role for ROS generation and inflammatory processes, the link between oxidant stress and inflammatory and adaptive gene expression has not been examined following exposure to environmental electrophiles.

Here we report that exposure to 1,2-NQ results in a rapid loss of intracellular reducing potential and increased production of H<sub>2</sub>O<sub>2</sub> of mitochondrial origin, and that these endpoints associate differentially with the induction of inflammatory and adaptive gene expression.

## **3-B. Materials and Methods**

### 3-B-1. Reagents

Tissue culture media and supplements were obtained from Lonza (Walkersville, MD). Adenoviral vectors were procured from the Gene Therapy Center Virus Vector Core Facility (University of NC at Chapel Hill, NC). Common laboratory reagents were obtained from Sigma Chemical Co. (St. Louis, MO). Basic laboratory supplies were purchased from Fisher Scientific (Raleigh, NC).

### 3-B-2. Synthesis of fluorescent reporter genes in lentiviral vector

The genetically encoded fluorescent reporter roGFP2 is a redox sensitive ratiometric probe established for detection of oxidative stress in the cytosol and mitochondria (Reddel et al. 1988). The plasmid for this protein was a generous gift from Dr. S. James Remington (University of Oregon, Eugene, OR). HyPer is a genetically encoded probe specific for H<sub>2</sub>O<sub>2</sub> detection and was purchased from Evrogen (Axxora, San Diego, CA). The two genes, roGFP2 and HyPer, were isolated from pEGFP-N1 and pQE30 vector by BamHI and HindIII digest and cloned into the lentiviral transfer vector pTLRED (Tal et al. 2010). HEK293T cells were co-transfected with purified transfer vector plasmids and lentiviral packing mix (Open Biosystems, Huntsville, AL). The resulting supernatants from the individual transfections were concentrated once by low-speed centrifugation through an Amicon Ultra 100kD centrifuge filter unit (Millipore; Billerica, MA), and the retentates were aliquoted and stored at -80°C. Viral titers were determined

in HEK293T cells stably expressing the rTTA3 transactivator (E10 cells) by transduction with serially diluted vector stocks as previously described (Livak and Schmittgen 2001).

### 3-B-3. Cell culture and viral transduction

Transformed human airway epithelial cells (BEAS-2B) (Pastore et al. 2001) were maintained in serum-free keratinocyte growth medium (KGM-Gold, Lonza). For imaging purposes, BEAS-2B cells grown to 50% confluency were transduced with lentiviral vectors carrying roGFP2 or HyPer genes targeting them to either the cytosol or mitochondria under the multiplicity of infection of 5 as previously described (Cheng et al. 2010). For catalase overexpression, BEAS-2B cells were transduced with an adenoviral vector encoding human *catalase* (AdCAT), *green fluorescent protein* (AdGFP), or empty vector for 4 h using an MOI of 100. The adenoviral constructs were removed after transduction and the cells were passaged in KGM-Gold.

### 3-B-4. Cell Exposure

Growth factor-deprived BEAS-2B cells were exposed to 10-150  $\mu\text{M}$  1,2-NQ for the 0-4 h. Cells expressing roGFP2 or HyPer were treated under observation with a Nikon Eclipse C1Si confocal imaging system (Nikon Instruments Inc., Melville, NY). In separate experiments, cells were analyzed using a PolarStar Optima microplate reader (BMG Labtech, Durham, NC) prior to and during treatment with 1,2-NQ. For gene expression analyses, BEAS-2B cells were exposed to 1-10  $\mu\text{M}$  1,2-NQ for 4 h and changes in the levels of specific

transcripts were analyzed using RT-PCR. In some experiments, cells were pretreated 30 min prior to exposure with the inhibitors diphenyleneiodonium (DPI; 25  $\mu$ M), CCCP (10  $\mu$ M), rotenone (10  $\mu$ M), sodium azide ( $\text{NaN}_3$ ; 2 mM), potassium cyanide (KCN; 10  $\mu$ M) and cyclosporine A (CyA; 10  $\mu$ M).

### 3-B-5. Measurement of redox potential and hydrogen peroxide

Confocal microscopy analyses were conducted using a C1Si system that was equipped with an Eclipse Ti microscope. Green fluorescence was derived from excitations at 404 and 488 nm while emission was detected using a band-pass filter of 525/50 nm (Chroma, Bellows Falls, VT). The results were calculated by ratioing the emissions excited by 488 nm and 404 nm lasers sequentially with a scanning frequency of 60s. The optical settings for the plate reader were similar to those used in the microscope, with excitation at 485/12 and 400/10 and emission at 520/30 (Chroma).

### 3-B-6. RT-PCR

Subconfluent BEAS-2B cells were exposed to varying concentrations of 1,2-NQ for 0-4 h. Relative gene expression in BEAS-2B cells was quantified using the real-time PCR, ABI Prism 7500 Sequence Detection System (Applied Biosystems, Foster City, CA). Total RNA was isolated using an RNeasy kit (Qiagen, Valencia, CA) and reverse transcribed to generate cDNA using a High Capacity cDNA Reverse Transcription kit (Applied Biosystems) . Oligonucleotide primer pairs and dual-labeled fluorescent probes for *IL-8*, *COX-2*, *HO-1*,  $\beta$ -*Actin*, and *Catalase* were obtained from Applied Biosystems. The

relative abundance of mRNA levels was determined using the  $2^{-\Delta\Delta CT}$  method (Jakober et al. 2007; Inoue et al. 2007a; Cho et al. 2004).  *$\beta$ -Actin* mRNA was used to normalize levels of the mRNAs of interest.

### 3-B-7. Statistical Analysis

Imaging data were collected with Nikon EZ-C1 software (Nikon). An average of 5–10 cells was collected as regions of interests in each experiment and quantified using Nikon Elements software (Nikon). Data are expressed as mean values and standard error of the mean of three repeated experiments. The linear regression of plate reader results was calculated with GraphPad Prism (La Jolla, CA) and the slope of the regression line was plotted against 1,2-NQ concentrations. Pairwise comparisons were carried out using Student's t-test  $P < 0.05$  was taken as statistically significant.

## **3-C. Results**

### 3-C-1. 1,2-NQ induces rapid oxidant changes.

The genetically encoded fluorescent probes roGFP-cyto and HyPer-cyto were used to monitor changes in redox potential and  $H_2O_2$  production, respectively, in BEAS-2B cells exposed to 1,2-NQ. The cells were observed for 5 min to establish a baseline signal prior to treatment with either vehicle (control) or  $100\mu M$  1,2-NQ for 15 min. As shown in Figure 3-A, treatment with  $100\mu M$  1,2-NQ induced a rapid increase in the ratiometric fluorescence intensity of cytosolic roGFP2, corresponding to a marked loss of intracellular reducing potential that

peaked and stabilized at 20 min (Figure 3-A). The intracellular redox potential in cells exposed to vehicle alone remained stable during the same time period (Figure 3-A). Similarly, cells expressing HyPer-cyto responded with an increase in fluorescence ratio intensity, indicating elevated levels of H<sub>2</sub>O<sub>2</sub> following exposure to 1,2-NQ, relative to control cells (Figure 3-A).

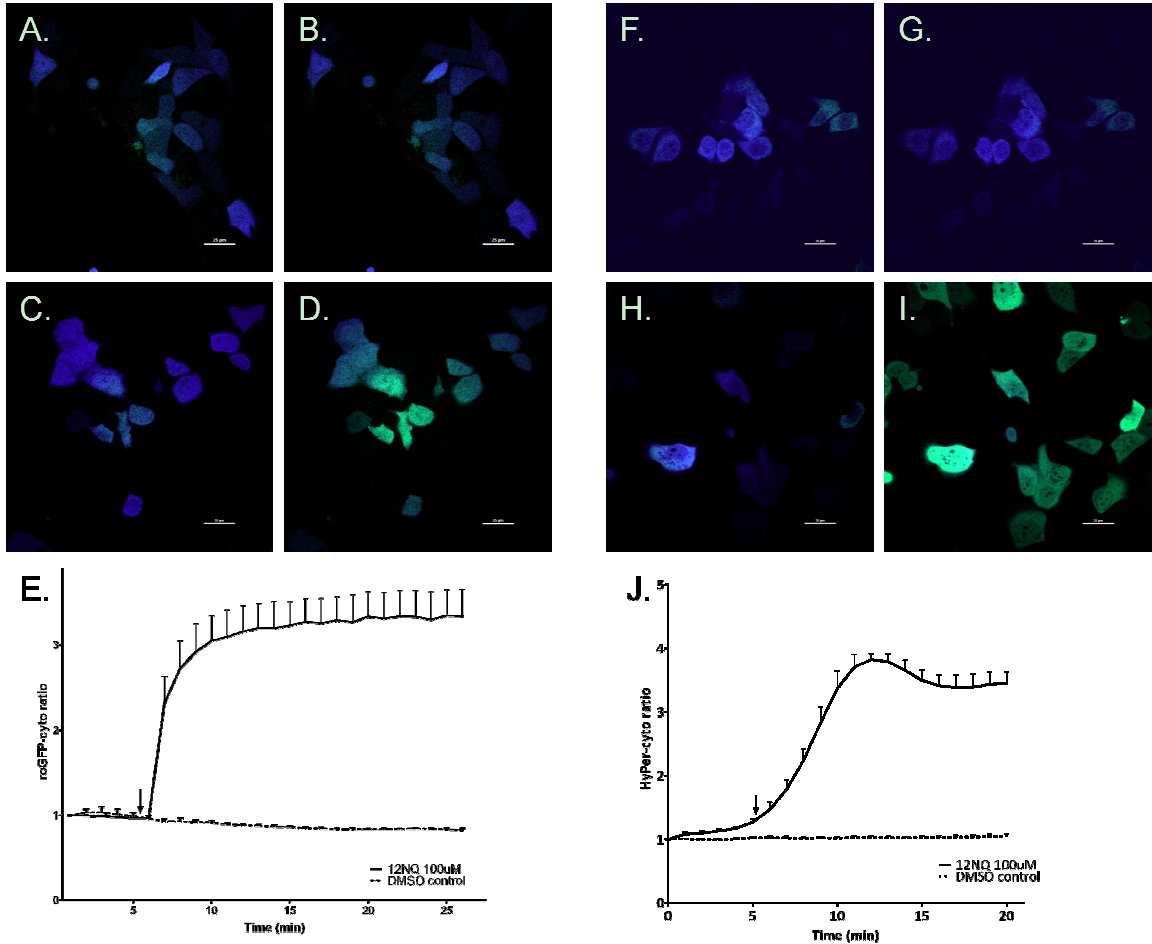


Figure 3- A. Measurement of redox change and H<sub>2</sub>O<sub>2</sub> production visualized by roGFP-cyto and HyPer-cyto in BEAS-2B cells with 1,2-NQ treatment. BEAS-2B cells expressing roGFP-cyto were imaged under resting conditions (A, C) or treatment with either DMSO as vehicle control (B) or 100 μM 1,2-NQ (D). Pseudo-color images correspond to a ratiometric calculation obtained by dividing fluorescence intensities acquired at 404 nm laser excitation over that obtained under 488 nm illumination. Time course of redox changes monitored by roGFP-cyto ratios in cells stimulated with 0 or 100 μM 1,2-NQ (E). Cells expressing HyPer-cyto were visualized before (F, H) and after treatments with 0 (G) or 100 μM 1,2-NQ (I). Pseudo-color images were generated from the ratio of 510 emission intensity under 488 nm over 404 nm excitations. Measurements of HyPer-cyto ratios were expressed in (J) with control and 1,2-NQ-exposed BEAS-2B cells. The arrows mark the time of addition of DMSO or 100 μM 1,2-NQ. Shown are mean  $\pm$  SE (n=3). The scale bar indicates 20 μm.

### 3-C-2. Overexpression of catalase blunts 1,2-NQ-induced H<sub>2</sub>O<sub>2</sub> production.

In order to explore the interaction between changes in redox potential and H<sub>2</sub>O<sub>2</sub> generation, we studied the effect of 1,2-NQ in BEAS-2B cells overexpressing catalase. Preliminary experiments established that catalase mRNA levels were 4-fold higher in BEAS-2B cells transduced with AdCAT relative to controls (data not shown). Treatment of catalase-overexpressing BEAS-2B cells with 100 μM 1,2-NQ induced a loss of reducing potential that was not significantly different from that observed in BEAS-2B cells transduced with an empty vector (Figure 3-B). In contrast, 1,2-NQ-induced H<sub>2</sub>O<sub>2</sub> production was effectively ablated in BEAS-2B cells overexpressing catalase (Figure 3-B).

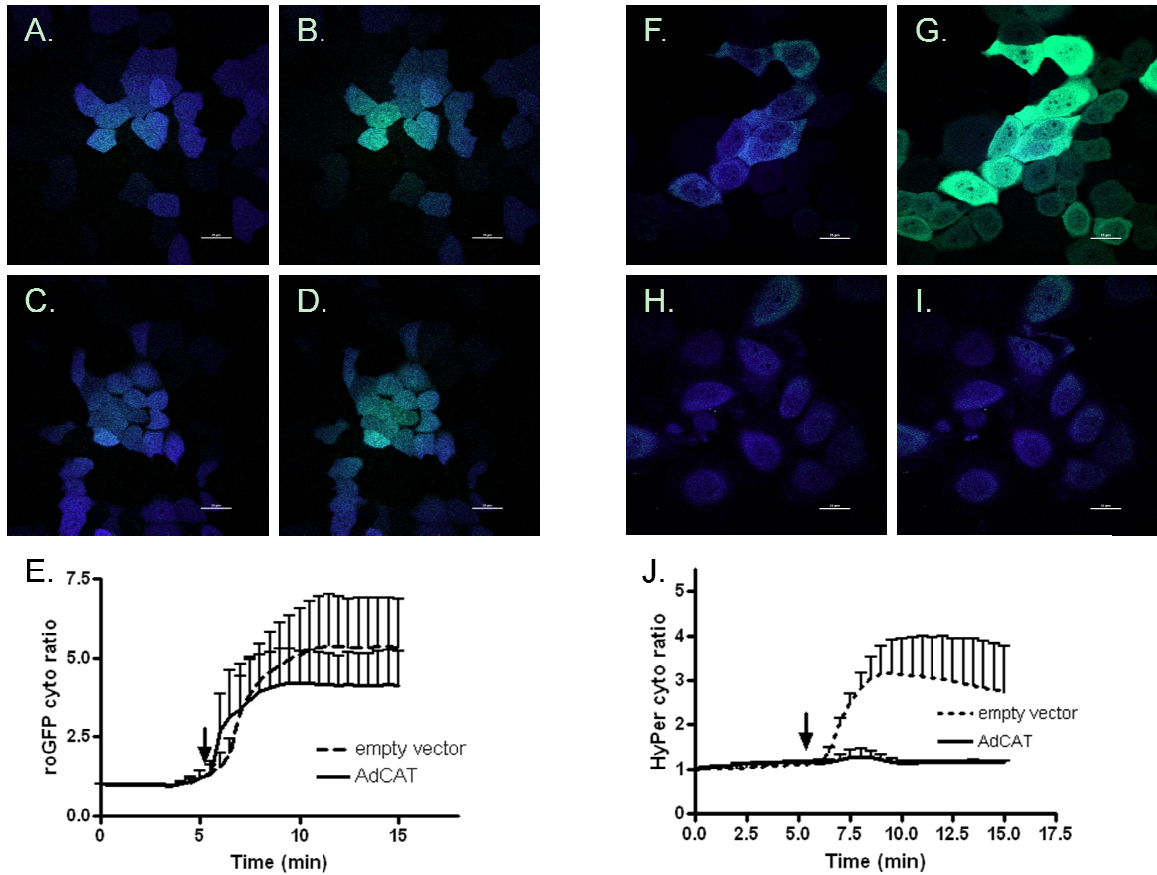


Figure 3- B. Catalase overexpression blunted 1,2-NQ-induced hydrogen peroxide signals but not redox changes.

Stably transduced BEAS-2B cells expressing roGFP-cyto (A-D) or HyPer-cyto (F-I) received either an empty vector (A, B, F, G) or adenoviral vector encoding catalase (AdCAT) (C, D, H, I) were exposed to 0 or 100 μM 1,2-NQ. Time courses of roGFP-cyto ratios (E) or HyPer-cyto (J) were plotted for cells receiving empty vector (dashed line) or AdCAT (solid line). Arrows mark the addition of DMSO or 100 μM 1,2-NQ. Shown are mean  $\pm$  SE (n=3). The scale bar indicates 20 μm.

3-C-3. Overexpression of catalase differentially inhibits 1,2-NQ-induced gene expression.

We next examined the effect of 1,2-NQ exposure on the expression of the pro-inflammatory genes *IL-8* and *COX-2* and the adaptive, oxidant responsive gene *HO-1*. Exposure of BEAS-2B cells to 1-10  $\mu$ M 1,2-NQ or vehicle for 0-4 h resulted in dose- and time-dependent inductions in *IL-8*, *COX-2* and *HO-1* mRNA (Figure 3-C), with maximal respective increases of 5-, 4-, and 30-fold relative to vehicle controls observed at 4 h of exposure. In order to test the mechanistic link between gene expression and oxidant responses, we determined the effect of 1,2-NQ exposure on the induction of *IL-8*, *COX-2* and *HO-1* transcripts in BEAS-2B cells overexpressing catalase. Relative to control cells transduced with AdGFP, overexpression of catalase blunted the increases in *IL-8* and *COX-2* mRNA induced by treatment with 10 $\mu$ M 1,2-NQ for 4 h (Figure 3-C). However, the induction of *HO-1* gene expression by 1,2-NQ was significantly augmented in BEAS-2B cells that overexpressed catalase (Figure 3-C), indicating a differential role for H<sub>2</sub>O<sub>2</sub> in 1,2-NQ-induced inflammatory and adaptive gene expression.

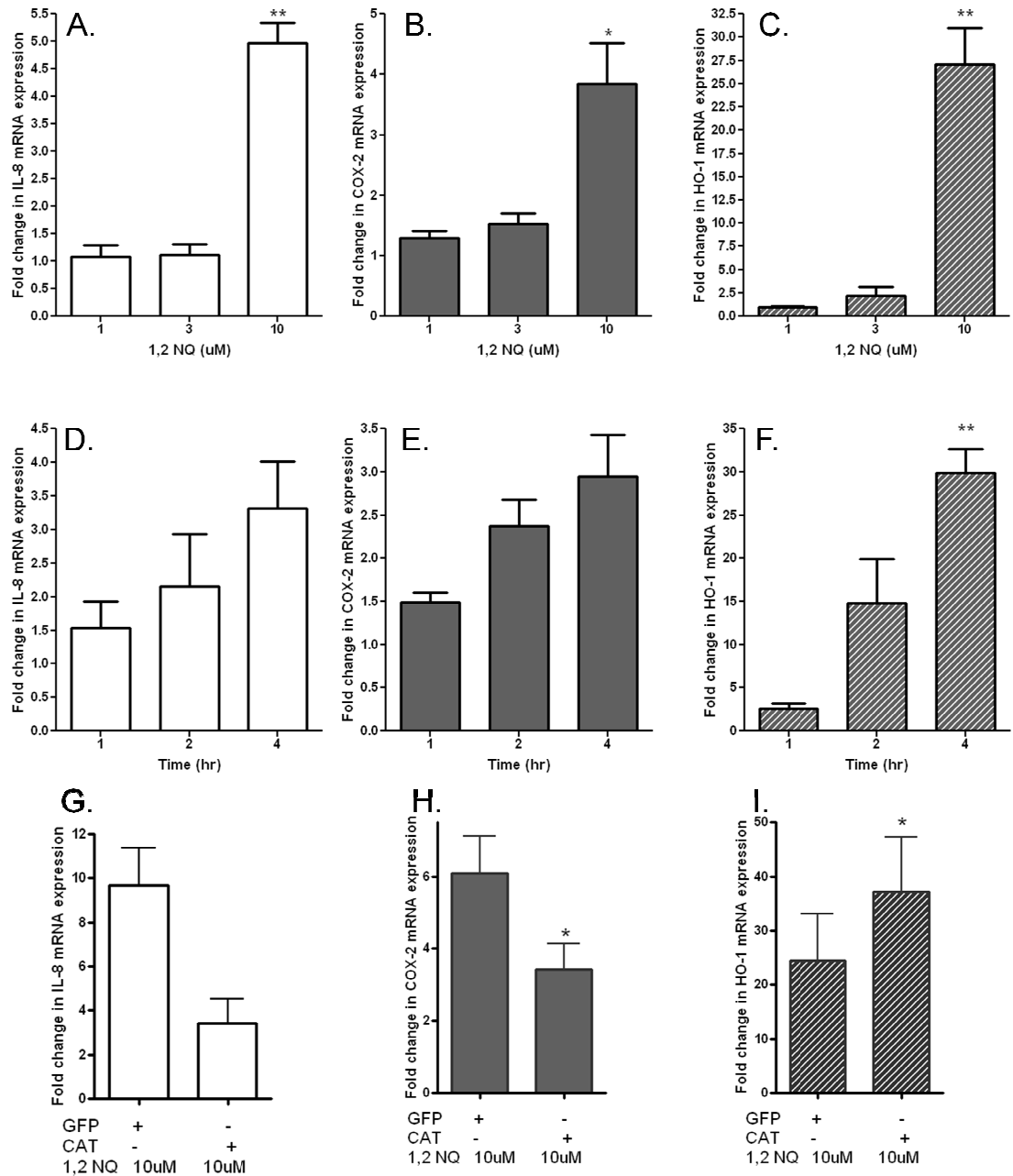


Figure 3- C. Dose- and time-dependent 1,2-NQ-induced inflammatory and adaptive gene expression were differentially inhibited by catalase overexpression. Levels of *IL-8* (A,D,G), *COX-2* (B,E,H), and *HO-1* (C,F,I) mRNA were measured using TaqMan-based RT-PCR, normalized to levels of  $\beta$ -Actin mRNA, and expressed as fold increases over vehicle control. For the data shown in panels A-C and G-I cells were exposed for 4 h. The 1,2-NQ concentration used to expose cells in the experiments shown in D-F was 10  $\mu$ M. Transcript levels after

treatment with 1,2-NQ in BEAS-2B cells transduced with AdCAT or AdGFP (G,H,I). . \*p<0.05, \*\*p<0.01, n=3.

#### 3-C-4. 1,2-NQ induces intracellular production of H<sub>2</sub>O<sub>2</sub>.

To identify the source of H<sub>2</sub>O<sub>2</sub> production shown in Figure 3-A, we investigated possible mechanisms through which 1,2-NQ exposure of BEAS-2B cells could result in the generation of H<sub>2</sub>O<sub>2</sub>. Considering the possibility that 1,2-NQ generates H<sub>2</sub>O<sub>2</sub> extracellularly, we employed a plate reader assay to monitor fluorescence changes in BEAS-2B cells expressing roGFP-cyto or HyPer-cyto with various 1,2-NQ concentrations (10-150 μM) in the presence or absence of exogenous catalase. As shown in Figure 3-D, the inclusion of extracellular catalase did not significantly affect the magnitude or time of onset of 1,2-NQ-induced H<sub>2</sub>O<sub>2</sub> generation in BEAS-2B cells as detected by HyPer-cyto. However, in agreement with the microscopy findings shown in Figure 3-B, adenoviral mediated overexpression of catalase in BEAS-2B cells ablated H<sub>2</sub>O<sub>2</sub> production induced by 1,2-NQ treatment (Figure 3-D). Neither extracellular catalase nor overexpression of catalase had any effect on the loss of cytoplasmic reducing potential observed in roGFP-cyto expressing BEAS-2B cells treated with 1,2-NQ (Figure 3-D).

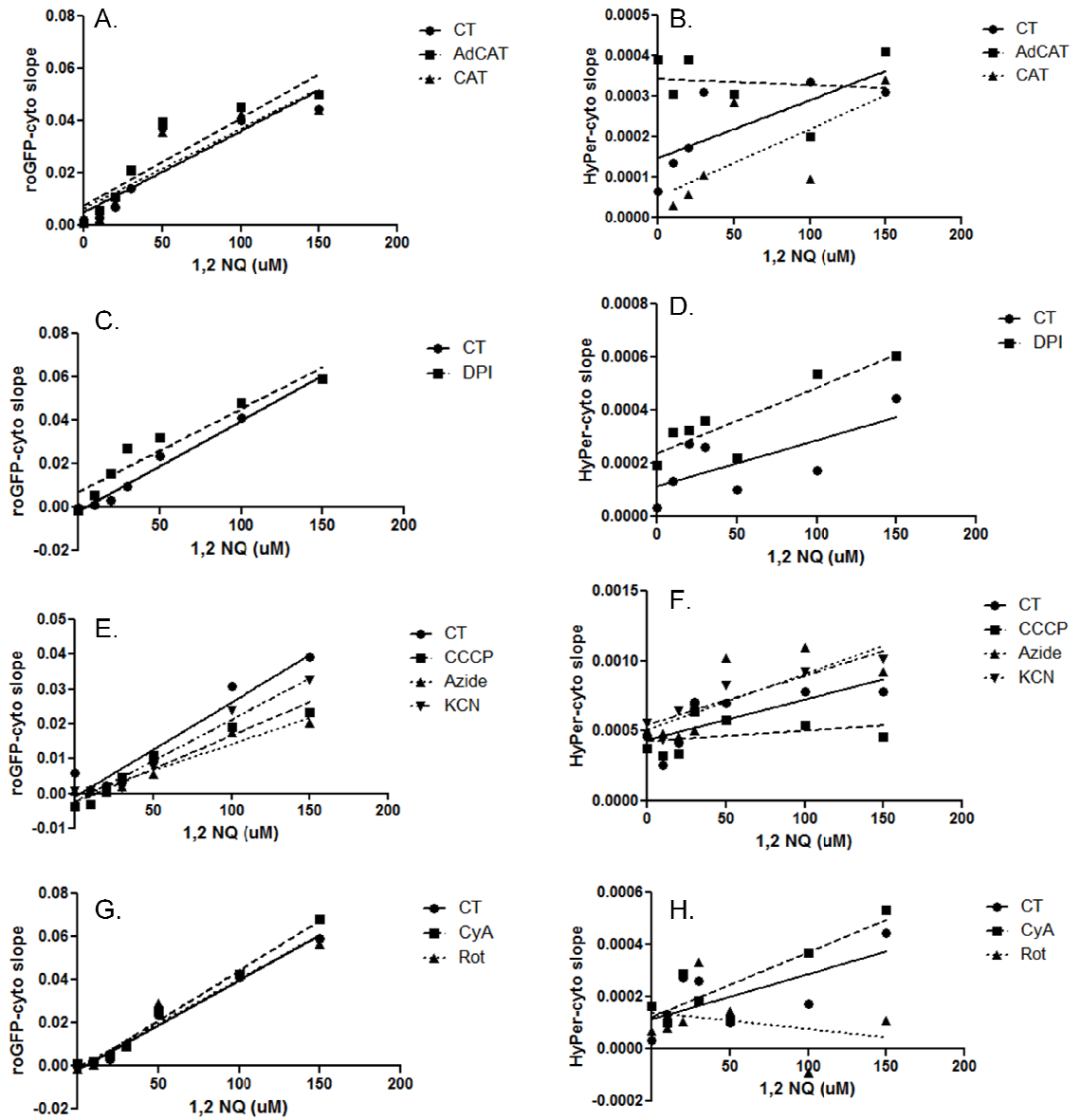


Figure 3- D. 1,2-NQ-induces mitochondrial hydrogen peroxide production. Redox potential and hydrogen peroxide levels were monitored in roGFP-cyto- (panels A,C,E,G) or HyPer-cyto- (panels B,D,F,H) expressing BEAS-2B cells exposed to 0-150  $\mu$ M 1,2-NQ. Shown are responses to 1,2 NQ in AdCAT BEAS-2B cells relative to wild type BEAS-2B cells (CT), and in wild type BEAS-2B cells exposed in the presence or absence of exogenous catalase (Inoue et al. 2007a; Inoue et al. 2007b) (panels A, B). BEAS-2B cells were pretreated with vehicle or the NADPH oxidase inhibitor DPI (25  $\mu$ M, panels, panels C, D), or 10  $\mu$ M of the mitochondrial inhibitors CCCP, KCN, CyA or rotenone (panels E, F, G, H), or 2 mM azide (panels E,F). Shown are means (n=3) slopes of linear

regression analyses of fluorescence intensity with error bars omitted for clarity.  
The scale bar indicates 20 $\mu$ m.

### 3-C-5. Identification of the mitochondrion as the source of 1,2-NQ-induced H<sub>2</sub>O<sub>2</sub>.

The data shown in Figure 3-D indicated that 1,2-NQ exposure elevates the intracellular concentration of H<sub>2</sub>O<sub>2</sub>, suggesting the involvement of a cellular process. We therefore examined potential cellular sources of H<sub>2</sub>O<sub>2</sub> generation in 1,2-NQ-treated cells. We first tested the involvement of H<sub>2</sub>O<sub>2</sub> generation at the cell membrane by pretreating the cells with the specific NADPH oxidoreductase inhibitor DPI 30 min prior to the addition of 10-150 μM 1,2-NQ. As shown in Figure 3-D, there were no significant differences in the production of H<sub>2</sub>O<sub>2</sub> in cells exposed to 1,2-NQ in the presence of DPI relative to cells pretreated with vehicle alone. We therefore turned our attention to possible mitochondrial sources of H<sub>2</sub>O<sub>2</sub> with the use of the mitochondrial inhibitors CCCP, NaN<sub>3</sub>, KCN, cyclosporine A and rotenone. Of these inhibitors CCCP, a mitochondrial membrane potential uncoupler, and rotenone, a mitochondrial complex I inhibitor, showed an effect on 1,2-NQ-induced H<sub>2</sub>O<sub>2</sub> in BEAS-2B cells (Figure 3-D). None of the inhibitors showed significant effects on 1,2-NQ-induced redox changes (Figure 3-D). These findings implicated the mitochondrial respiratory chain as the source of 1,2-NQ-induced H<sub>2</sub>O<sub>2</sub> production.

We then examined BEAS-2B cells expressing Hyper-mito, a version of the H<sub>2</sub>O<sub>2</sub> sensor that is targeted to the mitochondrial inner membrane. Exposure to 100 μM 1,2-NQ resulted in an elevation of ratiometric HyPer-mito fluorescence signal intensity, indicating elevated concentrations of H<sub>2</sub>O<sub>2</sub> in the mitochondria (Figure 3-E). 1,2-NQ-induced production of mitochondrial H<sub>2</sub>O<sub>2</sub> was effectively

suppressed by pretreatment of the cells with 10  $\mu$ M CCCP (Figure 3-E). These data showed 1,2-NQ-induced generation of  $H_2O_2$  in the mitochondrion and further established mitochondrial respiration as the source of  $H_2O_2$  production.

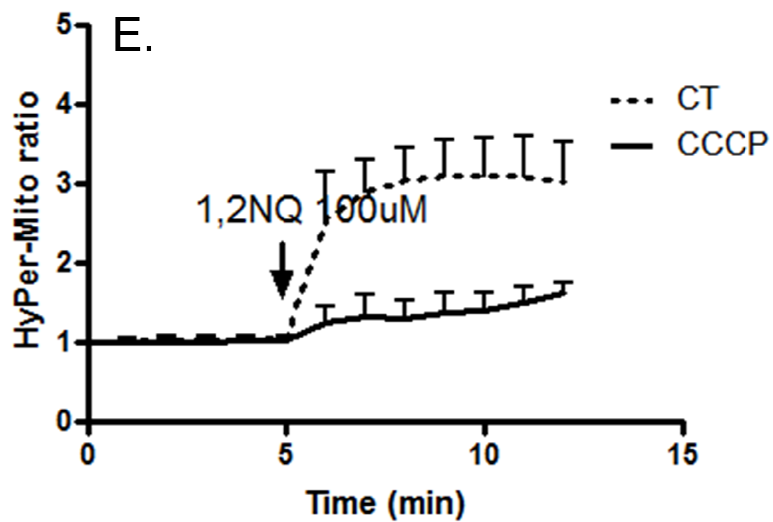
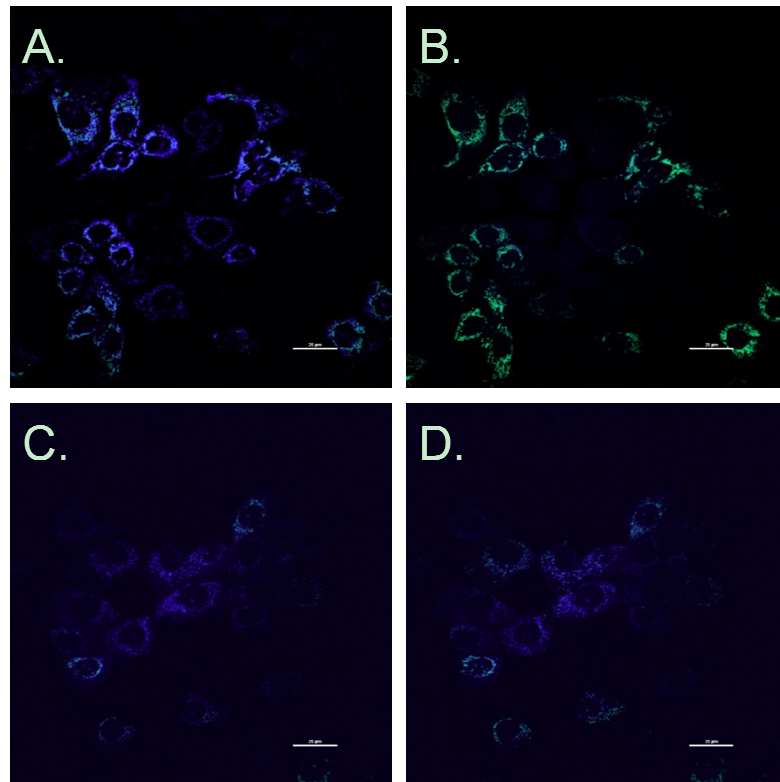


Figure 3- E. Confocal imaging of 1,2-NQ-induced hydrogen peroxide production in mitochondria.

Mitochondrial hydrogen peroxide was monitored as the ratio of HyPer-mito fluorescence emission intensity under 488/404 excitation in BEAS-2B cells expressing HyPer-mito pre-incubated with vehicle (A,B) or 10  $\mu$ M CCCP (C,D) prior (A,C) and following (B,D) exposure to 100  $\mu$ M 1,2-NQ. Plot of  $H_2O_2$

production in BEAS-2B cells expressing HyPer-mito and pretreated with vehicle (CT) or 10  $\mu$ M CCCP prior to the addition of 100 $\mu$ M 1,2-NQ (E). Data are mean  $\pm$  SE (n=3). The scale bar indicates 20 $\mu$ m.

3-C-6. 1,2-NQ-induced gene expression is differentially linked to mitochondrial activity and H<sub>2</sub>O<sub>2</sub> availability.

The role of mitochondrial metabolism in 1,2-NQ-induced inflammatory and adaptive gene expression was examined by pretreating cells with rotenone for 30 min prior to 10  $\mu$ M 1,2-NQ exposure. Rotenone inhibited the induction of *IL-8* and *COX-2* expression by 1,2-NQ (Figure 3-F). In marked contrast, the induction of *HO-1* mRNA by 1,2-NQ was potentiated by rotenone pretreatment (Figure 3-F). This finding, combined with the earlier observation that catalase overexpression also enhanced the induction of *HO-1* mRNA by 1,2-NQ, led us to hypothesize that H<sub>2</sub>O<sub>2</sub> limits 1,2-NQ-induced increases in *HO-1* mRNA. We therefore tested this hypothesis directly with the addition of 30  $\mu$ M H<sub>2</sub>O<sub>2</sub> immediately prior to 1,2-NQ treatment of BEAS-2B cells. As shown in Figure 3-F, the addition of exogenous H<sub>2</sub>O<sub>2</sub> significantly blunted the induction of *HO-1* expression by 1,2-NQ (Figure 3-F). H<sub>2</sub>O<sub>2</sub> pretreatment had no effect on 1,2-NQ-induced *IL-8* and *COX-2* expression (Figure 3-F).

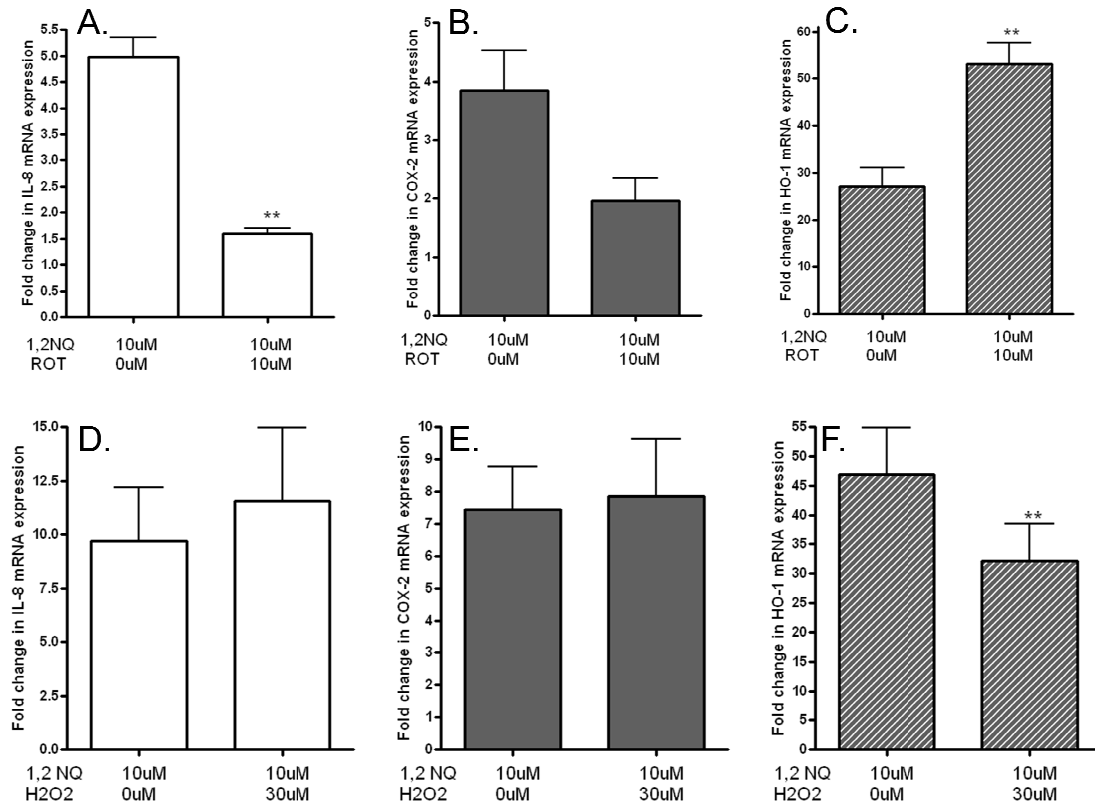


Figure 3- F. Differential role of mitochondrial H<sub>2</sub>O<sub>2</sub> in 1,2-NQ-induced gene expression.

BEAS-2B cells were pretreated with vehicle, the mitochondrial complex I inhibitor rotenone (10μM, 30 min) or H<sub>2</sub>O<sub>2</sub> (30 μM, 10 seconds) prior to the addition of 10μM 1,2-NQ for 4 h. mRNA levels of *IL-8*(A,D), *COX-2*(B,E), and *HO-1*(C,F) were measured using TaqMan-based RT-PCR, normalized to levels of *β-Actin* mRNA, and expressed as fold increases over vehicle control. Shown are means +/- SE. \*\*p<0.01, n=3.

### **3-D. Discussion**

Oxidant effects are a commonly reported mechanistic feature of the toxicity of environmental agents. In the present study, we have expanded our previously described integrated imaging approach to the investigation of mitochondrial dysfunction (Kikuno et al. 2006) to include inflammatory and adaptive gene expression changes induced by an environmental electrophile capable of inducing multiple types of oxidant stress. This study presents a mechanistic link between early oxidant events resulting from exposure to 1,2-NQ and downstream toxicological effects, specifically alterations in the expression of genes involved in inflammatory and adaptive responses in a human bronchial epithelial cell line. In preliminary studies we have observed similar oxidant responses and changes in gene expression in primary cultures of human airway epithelium (Cheng, unpublished).

As one of the organic components of the ubiquitous air contaminant DEP (Endo et al. 2007), 1,2-NQ has been shown to induce airway inflammation and to initiate deleterious effects through covalent modification or ROS generation (Sumi et al. 2010). Both activating and inhibitory effects of 1,2-NQ have been reported. For instance, recent studies have reported that 1,2-NQ induces vanilloid receptor and epidermal growth factor receptor signaling leading to guinea pig tracheal contraction (Lame et al. 2003). Inhibitory signaling effects associated with 1,2-NQ include impairment of cAMP response element-binding protein (CREB) (Groeger et al. 2009) and LPS-induced NF $\kappa$ B DNA binding activities

(Miura et al. 2011) and NF. In addition, the cytoplasm, endoplasmic reticulum, nucleus, and mitochondrion are all major targets for 1,2-NQ-induced toxicity through protein modification in lung epithelial cells (Fourquet et al. 2010). Thus, the high reactivity of 1,2-NQ can result in a diversity of molecular effects that are likely dependent on concentration and show cell type specificity.

In this study, we employed the genetically encoded fluorescence reporters roGFP2 and HyPer for the detection of redox changes and H<sub>2</sub>O<sub>2</sub> production, respectively. The exposure of 1,2-NQ induced rapid responses in both roGFP2 and HyPer in the cytosol of BEAS-2B cells indicating an acute oxidative burden stimulated by this compound. The generation of ROS and changes in redox balance can be seen as related events. However, the observation that catalase overexpression blunted the 1,2-NQ-induced increase in H<sub>2</sub>O<sub>2</sub> production without affecting the changes in redox potential suggests that H<sub>2</sub>O<sub>2</sub> production is not the cause of the redox changes. Furthermore, overexpression of catalase also protected against 1,2-NQ-induced *IL-8* and *COX-2* expression, indicating that 1,2-NQ-stimulated H<sub>2</sub>O<sub>2</sub> production is involved in the induction of inflammatory responses. This is in agreement with the reports of the involvement of H<sub>2</sub>O<sub>2</sub> in the activation of signaling pathways that regulate pro-inflammatory genes, such as NF- $\kappa$ B, p38 and JNK (Samet and Tal 2010). However, the addition of 30  $\mu$ M H<sub>2</sub>O<sub>2</sub> did not induce a statistically significant increase in *IL-8* or *COX-2* expression in response to 1,2-NQ exposure. This observation may reflect a requirement for H<sub>2</sub>O<sub>2</sub> acting as a second messenger at specific subcellular compartments in order to initiate inflammatory gene expression.

An unexpected finding is that 1,2-NQ-induced *HO-1* expression in BEAS-2B cells was not mediated by H<sub>2</sub>O<sub>2</sub>. On the contrary, the magnitude of *HO-1* induction by 1,2-NQ was enhanced by removal of H<sub>2</sub>O<sub>2</sub>. Specifically, catalase expression and impairment of mitochondrial electron transport, which effectively decrease H<sub>2</sub>O<sub>2</sub> concentrations and production, respectively, both potentiated 1,2-NQ-induced increases in *HO-1* mRNA. Furthermore, direct evidence for the suppressive effect of H<sub>2</sub>O<sub>2</sub> on 1,2-NQ-induced *HO-1* expression was also obtained using exogenous H<sub>2</sub>O<sub>2</sub>. A similar finding was reported by Miura *et al.*, who showed that pretreatment with catalase did not protect against 1,2-NQ-induced activation of Nrf2, which is a regulator of *HO-1* gene expression (Mason and Liebler 2000). This is a seemingly paradoxical finding, as H<sub>2</sub>O<sub>2</sub> is a known inducer of the Nrf2 pathway that regulates *HO-1* expression (Miura *et al.* 2011). One explanation for these observations may be that 1,2-NQ-induced *HO-1* expression requires electrophilic attack on a susceptible regulatory target, possibly a protein thiol, that is rendered unreactive to 1,2-NQ when oxidized by H<sub>2</sub>O<sub>2</sub>.

A parallel for H<sub>2</sub>O<sub>2</sub>-mediated inactivation of protein thiols is found in redox regulation of protein tyrosine phosphatases, in which the cysteine thiolate in the catalytic center of the enzyme is reversibly oxidized by H<sub>2</sub>O<sub>2</sub> (Lame *et al.* 2003). Using benzoquinone as the model toxicant, cysteine has been reported as a preferred target for quinone-induced toxicity (Iwamoto *et al.* 2007). Recently, Miura *et al.* reported that Nrf2 activation by 1,2NQ was mediated by covalent modification and subsequent degradation of Keap1 (Le *et al.* 2007). These studies point to cellular cysteine thiol groups as primary targets of electrophilic

naphthoquinone attack by covalent modification (Miller et al. 2010). From this perspective, it is intriguing that 1,2-NQ has been shown to attack and inactivate the protein tyrosine phosphatase PTP1B, albeit at an allosteric site (Xia et al. 2004). These observations lead us to speculate that biomolecular covalent modifications by 1,2-NQ are involved in *HO-1* gene expression induced by electrophilic attack. Detailed studies will be needed to elucidate the signaling mechanisms that underlie 1,2-NQ-induced gene expression.

A variety of metabolic processes are potential targets for xenobiotic-induced ROS production. While quinone species that undergo redox cycling can generate ROS in cell-free aqueous environments (Cho et al. 2004; Valavanidis et al. 2006), the lack of an effect of extracellular catalase in suppressing the 1,2-NQ-induced HyPer signal excluded an extracellular redox process as a source of the H<sub>2</sub>O<sub>2</sub>. The presence of exogenous catalase would also be expected to scavenge H<sub>2</sub>O<sub>2</sub> generated by membrane oxidoreductases, since NADPH oxidases generate H<sub>2</sub>O<sub>2</sub> in the extracellular space (Cho et al. 2004; Valavanidis et al. 2006). The failure of the oxidoreductase activity inhibitor DPI to suppress HyPer signals is consistent with this notion and thus helped shift the focus to the mitochondria as a source of 1,2-NQ-induced H<sub>2</sub>O<sub>2</sub> in this study.

The observation of H<sub>2</sub>O<sub>2</sub>-dependent fluorescence in the mitochondria confirmed that the mitochondrion is the site of H<sub>2</sub>O<sub>2</sub> production in BEAS-2B cells exposed to 1,2-NQ. Of the variety of mitochondrial inhibitors used in this study, targeting membrane potential (CCCP), complex I (Rotenone), complex IV (KCN

and  $\text{NaN}_3$ ), and the permeability transition pore (cyclosporine A), only CCCP and rotenone blunted 1,2-NQ-induced HyPer signals, indicating that the molecular target for 1,2-NQ-stimulated  $\text{H}_2\text{O}_2$  is associated with components of the upstream mitochondrial respiratory chain. A similar mitochondrial dysfunction was observed by exposing a mouse macrophage cell line to a quinone-enriched polar fraction of DEP (Benedetti et al. 1992). Furthermore, pretreatment with rotenone diminished 1,2-NQ-induced *IL-8* and *COX-2* gene expression, further establishing the functional link between the formation of mitochondrial  $\text{H}_2\text{O}_2$  and inflammatory gene expression.

The ambient concentration of 1,2-NQ has been reported to range from 13-53  $\mu\text{g/g}$  of DEP (Dickinson et al. 2001; Berg 2004). Given the ubiquitous nature of DEP as a constituent of ambient PM, plausible real-world scenarios are estimated to result in exposure of airway epithelial cells to deposited doses of 1,2-NQ during a 3 hr inhalational exposure that are about 10-fold lower than those used in this study (see supporting calculations and assumptions in Supplemental Material). Moreover, 1,2-NQ is representative of a class of organic constituents of ambient PM that includes other quinones as well as polycyclic aromatic hydrocarbons that may be metabolized to redox active quinones (Wolf and Schubler 2005).

Most studies on environmental electrophiles such as 1,2-NQ have focused on the highly reactive electrophilic properties of these compounds. Here we were able to measure early oxidative events in real time and correlate them mechanistically to gene expression changes associated with adverse responses to

electrophilic exposure. In this study, we demonstrate that 1,2-NQ induces mitochondrial H<sub>2</sub>O<sub>2</sub> production that leads to inflammatory gene expression but not the accompanying loss of reducing potential observed in the cytosol. 1,2-NQ also induces *HO-1* expression; however, our data show that it does so through a mechanism that is actually opposed by the availability of H<sub>2</sub>O<sub>2</sub>. Thus, these findings reveal dissociation between H<sub>2</sub>O<sub>2</sub> production and the loss of reducing potential induced by a frank electrophile (Figure 3-G). Ascertaining whether the loss of reducing potential is a consequence or a cause in the induction of HO-1 by 1,2-NQ requires further investigation. Taken as a whole, the experimental strategy conducted in this study represents an integrated approach for the systematic study of oxidative events that underlie adverse cellular responses to xenobiotic exposure. From a public health perspective, the inflammatory and adaptive responses induced by 1,2-NQ are consistent with the inflammatory and immunotoxic effects that are associated with human exposure to DEP and ambient PM.

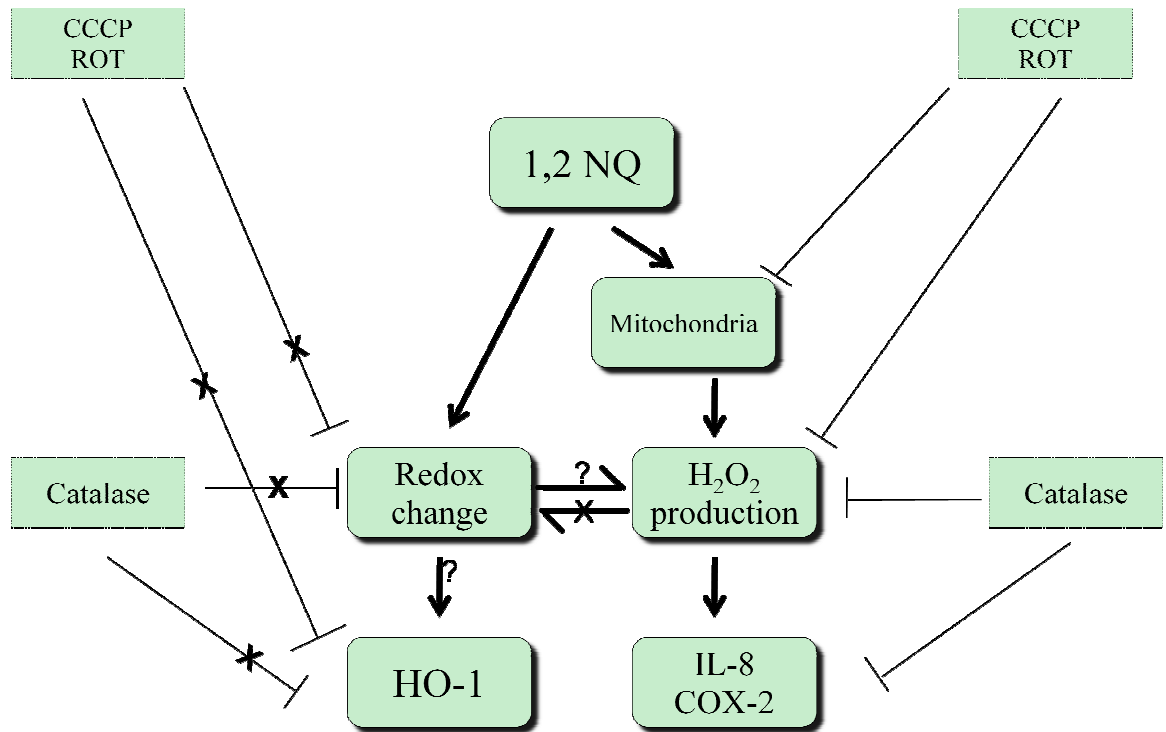


Figure 3- G. Proposed scheme of 1,2-NQ-induced effects.

## **Chapter IV. Live cell detection of redox changes and hydrogen peroxide production using dynamic spectral unmixing microscopy (DynSUM)**

### **4-A. Introduction**

In recent years, there has been a proliferation of novel imaging approaches that employ chemical or genetically-encoded sensors suitable to answer questions related to dynamic changes of molecular events with high temporal and spatial resolution. Reporter molecules based on green fluorescence protein or fluorescein have been developed over the years to detect a myriad of cellular events in living cells. However, there is a rising interest in using live-cell imaging to monitor not just individual intracellular endpoints, but to investigate the interplay between multiple molecular events as they unfold in real time within the cell. Advances in multispectral imaging instrumentation and analysis algorithms have provided an opportunity for the development of novel approaches to the resolution of fluorescence captured from two or more fluorophores derived from the same parent molecule and, therefore, emitting in the same region of the visible spectrum, with emission maxima that are only a few nanometers apart.

The first application of spectral unmixing in microscopy was reported in the 1990s (Pautke et al. 2005). The interfacing of confocal microscopy and spectral imaging created opportunities for simultaneous detection of indicators with closely overlapping emission spectra. This technique has been applied to a

variety of experimental models including human cells, plant cells, and bacteria (Ecker et al. 2004). Successful spectral unmixing with up to eight different indicators ranging between 410 to 645 nm has been reported in fixed bone specimens (G. T. Hanson et al. 2004). Spectral unmixing has been pursued in applications based on fluorescence resonance energy transfer (FRET), a technique that monitors energy transfer between two molecules and is commonly utilized to describe protein-protein interactions. The donor and acceptor pair, such as cyan fluorescent protein (CFP) and yellow fluorescent protein (YFP), in a FRET system requires a strong spectral overlap. Spectral unmixing is widely utilized as an adjunct to FRET analysis (Belousov et al. 2006).

Oxidative stress is a common feature in the mechanisms of cellular injury induced by a broad range of toxic agents (Reddel et al. 1988). The dynamics of redox events in cells has been assessed using imaging tools for fundamental intracellular processes such as signal transduction. However, ROS detection in non-phagocytic cells is fraught with challenges that include the transient nature, distinct subcellular compartmental localizations and relatively small magnitude that characterize oxidative events. In principle, these challenges can be addressed using the high sensitivity and spatial-temporal resolution approaches used by fluorescence-based confocal laser scanning microscopy (CLSM). The advent of the newly developed genetically-encoded sensors for the measurement of redox changes and ROS has recently been presented as an opportunity to gain some ground in addressing these technical difficulties.

The genetically encoded fluorescent reporter roGFP2 is a redox sensitive ratiometric probe established for the detection of oxidative stress by sensing glutathione pools with two surface exposed cysteine pairs (Larson 2006). HyPer is a genetically encoded probe specific for H<sub>2</sub>O<sub>2</sub> detection with the structure of OxyR and YFP fusion proteins (Jaspers et al. 2009). roGFP and HyPer monitor the related oxidant events of changes in redox potential and hydrogen peroxide production, respectively. Therefore, using real-time live-cell imaging to monitor the time sequence of these two related events with simultaneous detection is desirable when answering mechanistic questions such as event etiology. However, methodological limitations hamper the separation of roGFP and HyPer signals when using conventional filter-based light microscopes. roGFP has an emission peak around 512 nm whereas HyPer's emission peak is 518 nm. Although close, the emission maxima for the 2 probes are greater than 5 nm apart. In order to perform the measurement for roGFP and HyPer at the same time, we developed the dynamic spectral unmixing microscopy (DynSUM) system with a spectral confocal microscope for simultaneous detection. Here, we demonstrate the feasibility of this method with genetically encoded sensors to characterize cellular responses to oxidative challenges in a human respiratory epithelial cell line.

## **4-B. Materials and Methods**

### 4-B-1. Reagents

Tissue culture media and supplements were obtained from Lonza (Walkersville, MD, USA). Costar tissue culture plates were purchased from Corning (Corning, NY, USA). Common laboratory reagents were obtained from Sigma Chemical Co. (St. Louis, MO, USA). Basic laboratory supplies were purchased from Fisher Scientific (Raleigh, NC, USA).

### 4-B-2. Cell culture and viral transduction

Transformed human airway epithelial cells (BEAS-2B), (Cheng et al. 2011) were obtained from the Environmental Public Health Division, NHEERL, U.S. EPA, and maintained in serum-free keratinocyte growth medium (KGM-gold, Lonza). For imaging purposes, BEAS-2B cells grown to 50% confluency were transfected with Fugene 6 reagent (Roche, Mannheim, Germany) according to the manufacturer's protocol. roGFP plasmid was a generous gift from Dr. S. James Remington (University of Oregon, Eugene, OR). HyPer is a genetically encoded probe specific for H<sub>2</sub>O<sub>2</sub> detection and was purchased from Evrogen (Axxora, San Diego, CA). The two plasmids were mixed with Fugene 6 for 30 min at room temperature and applied to the BEAS cells for 48 hr.

### 4-B-3. Measurement of redox potential and hydrogen peroxide

Confocal microscopy analyses were conducted using a Nikon Eclipse C1Si confocal imaging system (Nikon Instruments Inc., Melville, NY) that was

equipped with an Eclipse Ti microscope. Light was delivered to the sample with a 63 × Plan Apo, 1.4 numerical aperture (NA) objective lens. The microscope can acquire an emission spectrum by separating the emission signal into 32 channels. Green fluorescence was derived from excitations at 404 and 488 nm while emission was scanned between 490 to 570 nm with a 2.5 nm band pass filter. The results were calculated by ratioing the emission intensity elicited by excitation of 488 nm and 404 nm lasers sequentially with a scanning frequency of 60 s. The spectral data was then fed into Nikon Elements software for spectral unmixing calculation. Although the algorithm is proprietary information, the principle of spectral unmixing involves linear regression with least squares fitting.

#### 4-B-4. Statistical Analysis

Imaging data were collected with Nikon EZ-C1 software (Nikon Instruments Inc.). Cells with different fluorescence intensities were collected as regions of interests in each experiment and quantified with Nikon Elements software (Nikon Instruments Inc.).

### **4-C. Results and Discussion**

#### 4-C-1. The optical properties of roGFP and HyPer

HyPer and roGFP are both ratiometric sensors with similar excitation maxima which are compatible with conventional CLSM lasers, 404 and 488 nm. These reporters are GFP variants and therefore have similar emission spectra, with close emission maxima at 518 and 512 nm respectively (Figure 4-A).

However, the responses for the two probes are distinct under oxidizing and reducing conditions. For cells that expressed HyPer in cytosol, the fluorescence intensity increases with 488 nm laser excitation and decreases under 404 nm laser excitation when the cells are exposed to H<sub>2</sub>O<sub>2</sub> (Figure 4-A). When exposed to the reducing agent DTT, the response of HyPer is reversed, with fluorescence intensity decreasing under 488 nm laser excitation and increased with 404 nm laser excitation. Furthermore, the response of cells expressing roGFP under different conditions is opposite from that shown by cells expressing Hyper. Under oxidizing conditions, roGFP fluorescence intensity decreases under 488 nm laser excitation and increases with 404 nm laser excitation. On the contrary, the fluorescence intensity increased from 488 nm laser excitation and decreased from 404 nm laser excitation for roGFP under reducing conditions (Figure 4-A). The time sequence data for cells expressing HyPer or roGFP under different excitation wavelengths are shown in Figure 4-A to demonstrate the behavior of these two probes, while the spectra of the two indicators are plotted in Figure 4-A as well. When cells were co-transfected with HyPer and roGFP, the combined spectrum was similar to the two indicators with emission maximum at 513 nm.

The unmixing algorithm applied in the Nikon Elements software is derived from the least squares method with linear regression (Meyer and Dick 2010). Noise and negative values are taken into account in the software. The error associated with the unmixing calculation is subjected to several parameters including spectral pattern, difference of emission intensity, and signal-to-noise ratio. The spectral profiles of cells that were co-expressing roGFP and HyPer are

shown in Figure 4-A. Distinguishing roGFP from HyPer signals from the combined spectrum is difficult. In principle, the mirror behaviors of the roGFP and HyPer facilitate their distinction when co-expressed in cells using dynamic spectral unmixing microscopy (DynSUM). However, the accuracy of unmixing algorithm decreases in proportion to the proximity of the individual fluorophores emission peaks as well as the absolute magnitude of the difference in their fluorescence intensity at the peak wavelengths. The proximity in their emission peaks and the opposing behavior of roGFP and HyPer approximates a worse-case scenario in spectral unmixing. The opposing behaviors of these fluorophores offer a great advantage as it affords experimental confirmation of fluorophore identity. However, they also introduce difficulty given that the emission maxima for roGFP and HyPer are quite close. This is because the accuracy of the unmixing process decreases with peak proximity and with the magnitude of the difference in signal strength that each fluorophores contributes to the overall (combined) spectrum. . Overall, having two probes moving toward opposite directions, therefore, increases the challenge of successful unmixing.

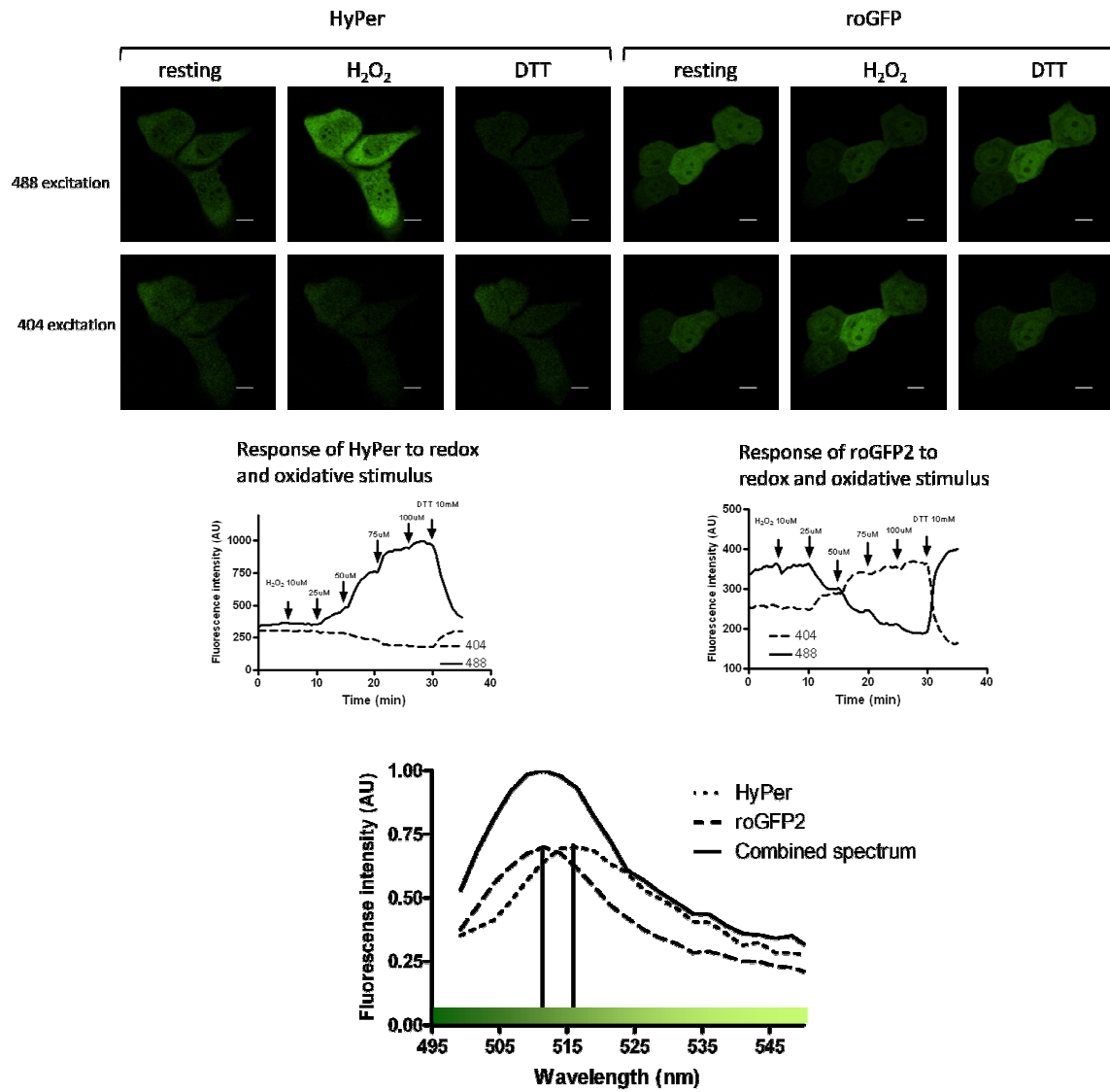


Figure 4- A. Demonstration of HyPer and roGFP under oxidizing and reducing treatments. BEAS-2B cells were transfected with either HyPer or roGFP constructs targeted to the cytosol and exposed to oxidizing or reducing agents under the excitation of 488 (first row) or 404 (second row) nm lasers. The time sequence data for each probe was demonstrated on the third row. The emission spectra were plotted on the bottom.

#### 4-C-2. The application of DynSUM on roGFP and HyPer

BEAS-2B cells were transfected with HyPer and roGFP simultaneously. Shown in Figure 4-B, left panel, first three rows, correspond to cells that were excited at 488 nm and treated sequentially with H<sub>2</sub>O<sub>2</sub> and DTT. The right panel in the same figure shows cells that were excited with the 404 nm laser. The first row of each panel shows the raw, unprocessed images of fluorescence signals obtained at each excitation wavelength, with the emission spectra collected between 490 and 570 nm using a 2.5 nm band pass filter. Raw fluorescence intensities were comparable following treatment of the cells with H<sub>2</sub>O<sub>2</sub> and DTT. The second and third rows display the results of the unmixing analysis of the raw fluorescence data, using reference spectra for HyPer and roGFP. The unmixing process used a least square fit analysis to assign pixels from the combined fluorescence signal into channels corresponding HyPer or roGFP. As expected, HyPer fluorescence intensity increased with the addition of H<sub>2</sub>O<sub>2</sub> and decreased with DTT exposure under the excitation of 488 nm laser. Conversely, roGFP fluorescence intensity decreased under H<sub>2</sub>O<sub>2</sub> challenge and increased with the addition of DTT. Excitation at 404 nm induced a reverse response for both HyPer and roGFP. The energy absorbance under the 404 nm illumination is weaker for both probes, especially so for roGFP. We therefore used pixel intensities obtained from 404 nm excitation to normalize for the signals induced by 488 nm excitation. Thus, providing ratiometric data. The images in the fourth row display the ratiometric view for unmixed HyPer and roGFP, demonstrating the viability of ratiometry in spectral unmixing.

Having demonstrated that the behavior of the co-expressed roGFP and HyPer under oxidizing and reducing treatment of the cells is qualitatively as expected, we next assessed quantitative accuracy of the resolving algorithm under basal, oxidant and reducing conditions. Based on our understanding of the unmixing algorithm in the Elements software, spectral data were calculated based on a linear regression model with least square fitting and assigned to either HyPer or roGFP channels. The unmixing process also generated signal that could not be assigned to either the roGFP or the HyPer channels, and are therefore categorized as falling into a “remainder” channel by the Elements software. These data are displayed in the fifth row of Figure 4-B. Table 4-A presents the distribution of signal between HyPer, roGFP and remainder channels as a percentage of the total. In general, approximately 20% of the signal intensity was assigned to the remainder channel under 488 nm laser excitation and 40% was assigned for the signal excited at 404 nm. The noise level is expected to be higher for the 404 excitation given the low energy absorbance for HyPer and roGFP. Thus, the successful application of DymSUM system for unmixing co-expressed HyPer and roGFP fluorescence under basal, oxidant and reducing cellular stimuli is presented in Figure 4-B.

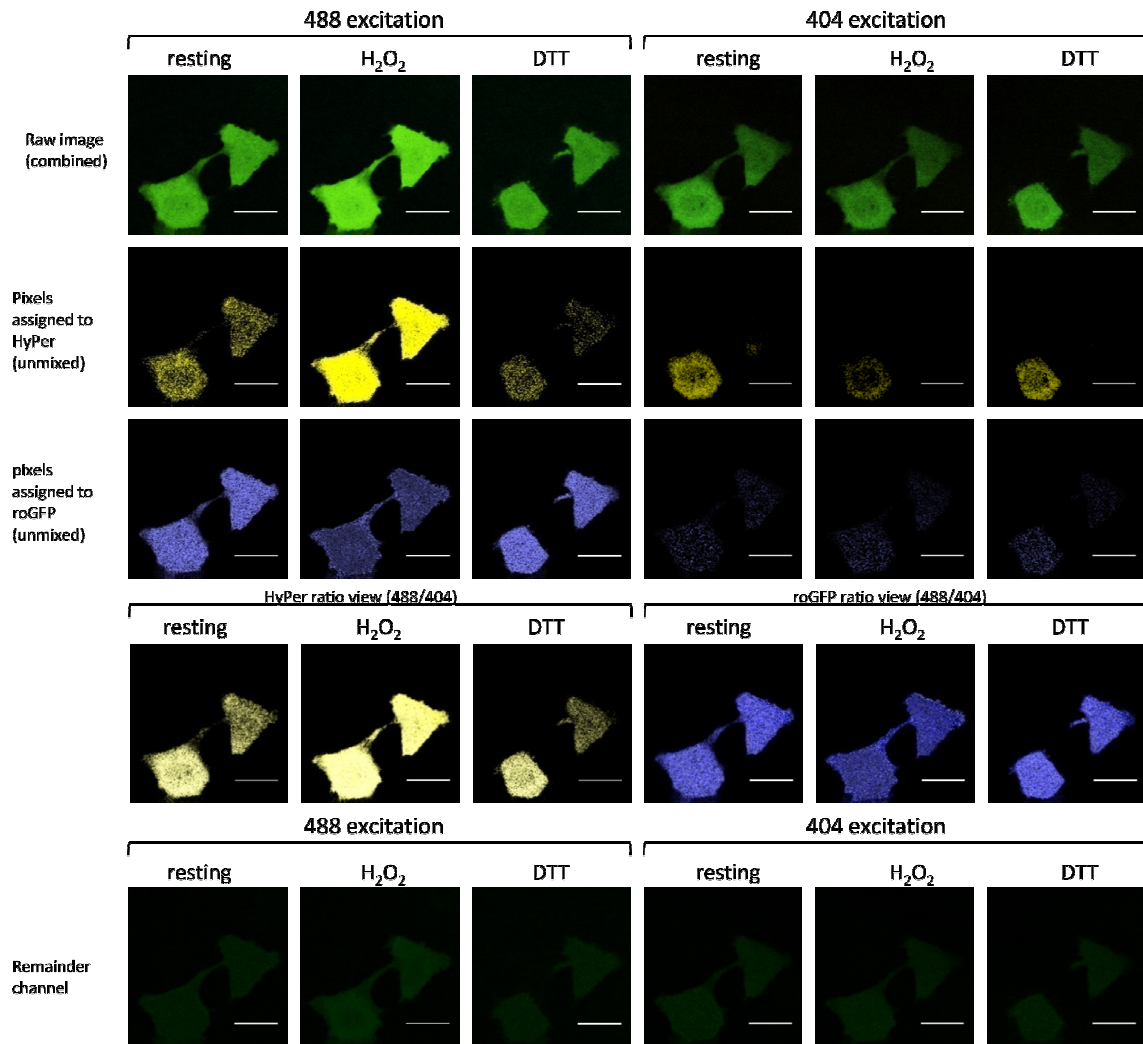


Figure 4- B. The application of DynSUM on roGFP and HyPer. The left panel shows cells that were excited with the 488 laser and exposed to oxidizing or reducing agents while the panel on the right shows cells that were excited with the 404 laser. The images on the first row of each panel are the raw, unprocessed data resulting from the corresponding excitation wavelengths. The second and third rows are unmixed images for HyPer and roGFP. Furthermore, the signals from the remainder channel are plotted in the fourth row. The last row is the ratio views of HyPer and roGFP.

Table 4- A. The distribution of signal between HyPer, roGFP and remainder channels as a percentage of the total.

	488			404		
	resting	H <sub>2</sub> O <sub>2</sub>	DTT	resting	H <sub>2</sub> O <sub>2</sub>	DTT
HyPer	24%	60%	12%	52%	36%	45%
roGFP	60%	22%	67%	14%	18%	15%
remainder	16%	17%	21%	34%	46%	40%

#### 4-C-3. DynSUM in mitochondria

We next investigated the feasibility of using DynSUM to unmix fluorescence signals in subcellular compartments. BEAS-2B cells were transfected with HyPer and roGFP targeted to the mitochondria. As shown in Figure 4-C, HyPer and roGFP were successfully co-expressed in mitochondria. The images in the first row correspond to cells expressing both sensors and excited by 488 nm (left) and 404 nm (Cannon and James Remington 2009). The unmixed images for HyPer under 488 nm excitation showed the expected responses to the addition of H<sub>2</sub>O<sub>2</sub>, namely an increase in fluorescence intensity, while the addition of DTT decreased HyPer signal intensity (Figure 4-C). The behavior of mitochondrially-targeted roGFP, as determined by unmixing of the combined emission spectrum under basal, oxidant and reducing conditions were similarly as expected, with the exposure of H<sub>2</sub>O<sub>2</sub> induced a decrease of signal under 488 excitation, while the addition of DTT induced an increase in roGFP fluorescence intensity. As seen in the cytosol, the pattern was reversed under 404 nm laser excitation (Figure 4-C). The 488/405 nm ratio view for HyPer and roGFP was demonstrated in the third row of Figure 4-C. As a demonstration of the dynamic capabilities of this analysis, time sequence data is presented in the bottom of Figure 4-C, showing the kinetics of the fluorescence changes in the mitochondrially targeted co-expressed HyPer and roGFP induced by treatment of the cells with H<sub>2</sub>O<sub>2</sub>, and DTT.

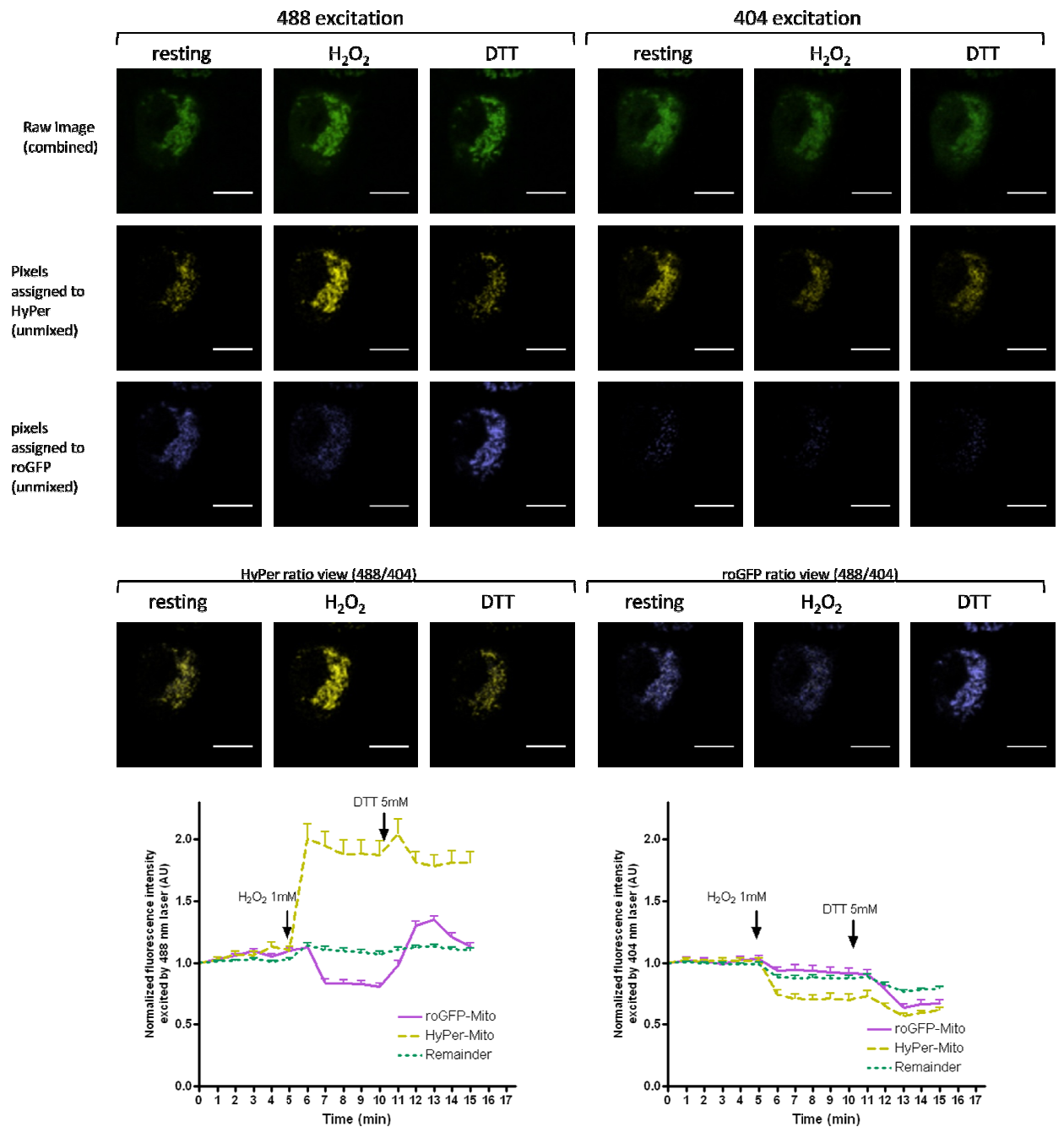


Figure 4- C. The application of DynSUM in mitochondria. BEAS-2B cells were transfected with HyPer and roGFP targeted to mitochondria. Cells were excited with 488 and 404 nm lasers and the emission spectra were monitored between 490 to 570 nm. The unmixed results are shown on the second

(HyPer) and third (roGFP) raw images. Ratio views of HyPer and roGFP were shown on the fourth row while time sequence data were plotted on the bottom series of images.

4-C-4. The application of DynSUM to the study of redox changes in human lung cells exposed to an environmental electrophile.

As presented above, DynSUM was established in cytosolic and mitochondrial compartments by using the physiologically relevant oxidant H<sub>2</sub>O<sub>2</sub> and the strong reducing agent DTT to effect maximal signal displacements in cells co-expressing roGFP and HyPer. To test the utility of DynSUM as a tool to investigate the effects of environmentally relevant cellular exposures that result in oxidant stress, 1,2-naphthoquinone (1,2-NQ), an organic component in diesel exhaust particle was used as a model toxicant. We reported previously that cells exposed to 1,2-NQ undergo a rapid loss of reducing potential and an increase in H<sub>2</sub>O<sub>2</sub> concentrations for expressing either HyPer or roGFP (Belousov et al. 2006). The ability to study the responses of roGFP and HyPer as they unfold simultaneously permits investigation of the dynamic interaction between ROS generation and redox changes induced by exposure to an environmental contaminant.

Exposure of BEAS cells co-expressing roGFP and HyPer to 1,2-NQ induced a moderate decrease in the combined 488 nm-excitation induced fluorescence intensity spectrum collected between 490 nm to 570 nm . Spectral unmixing revealed an 80 % increase in HyPer signal intensity and a 20 % reduction in roGFP signal strength. Figure 4-D also shows the ratio corresponding to these analyses. 1,2-NQ is a strong oxidant agent that induces rapid changes of redox potential and H<sub>2</sub>O<sub>2</sub> generation. By analyzing the kinetics of HyPer and

roGFP responses, similar time and slopes were observed for both sensors to reach to plateau while small recovery was observed for HyPer signal. DynSUM demonstrates a better observation potential for monitoring relevant events simultaneously in comparison with single sensor measurement.

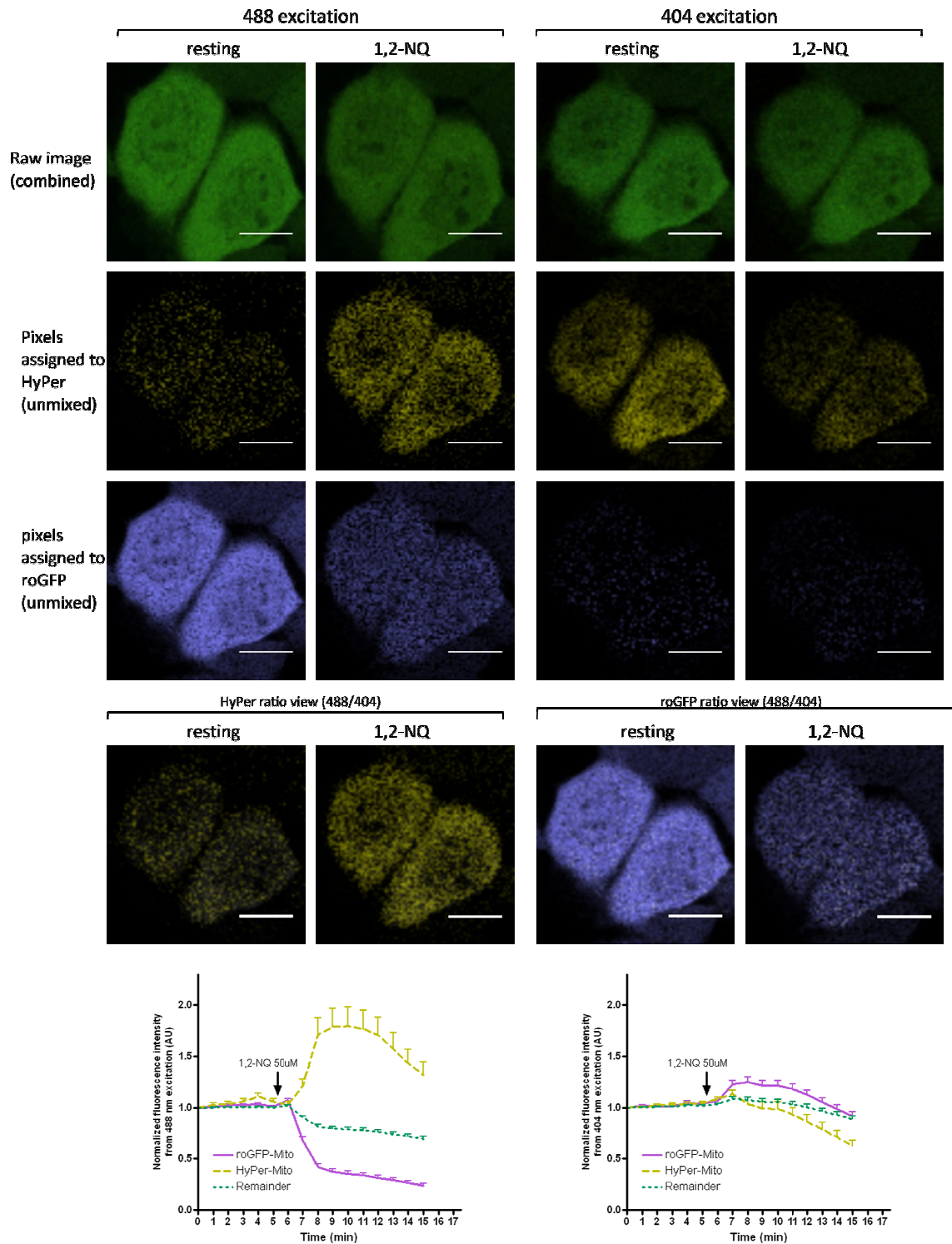


Figure 4- D. Utilizing DynSUM for the exposure to an environmental electrophile. BEAS-2B cells were transfected with HyPer and roGFP and then exposed to 1,2-NQ. The unmixed images were shown in the second (HyPer) and third (roGFP)

rows. Ratio views of HyPer and roGFP were listed on the fourth row followed by time sequence data (bottom row).

#### 4-D. Summary

Oxidative stress is a major mechanistic research focus in cell biology and toxicology. The limitations regarding oxidant studies are related to sensitivity, specificity and artifacts. Taking advantage of recent advances in reporter development, imaging techniques can achieve high temporal and spatial resolution for oxidative measurements. Several genetically encoded fluorescence sensors reported in the past decade have been engineered for the detection of oxidative events and specific ROS species (Meyer and Dick 2010). roGFP, which responds to its redox environment, specifically by interacting with the cellular glutathione pool, has several advantages including fast response time, reversibility, ratiometric detection, and relative insensitivity to pH changes (Valko et al. 2005). HyPer is the fusion protein of yellow fluorescence protein and *E. coli* transcription factor OxyR that is specific for sensing hydrogen peroxide (Rosen et al. 1995). The changes of glutathione balance and production of H<sub>2</sub>O<sub>2</sub> are two independent events that are often thought to be interrelated in biological and toxicological contexts. The application of sensitive and specific methodologies for the intracellular measurement of ROS species and redox potential in toxicological studies will improve our understanding of the role of oxidant stress in the mechanism of action of environmental contaminants.

Live cell imaging is a non-destructive method of studying biological events as they occur in real time. Fluorescence proteins prove to be appropriate as imaging indicators due to several advantages including insensitivity to

photobleaching, cellular compartment targeting potential and relative stability. Green fluorescence protein was the fluorescence protein to be widely applied as a tool for spectroscopically-based microscopy in live cells (Irani 2000). While multiplexing of GFPs has been successfully applied for the development of FRET-based methods, many useful GFP-based reporters exist that are restricted to individual use due to the fact that they share a narrow emission band spectrum. By enabling simultaneous detection of closely emitting fluorophores, spectral unmixing is a technique that broadens the number of existing reporters that can be studied in a multiplex manner and thereby greatly expands the range of interacting intracellular events that can be studied. The developments of methods such as spectral confocal microscopy, unmixing algorithm, and corresponding indicators in the past decades are the fundamental elements for the DynSUM approach to overcome the limitations mentioned above. Spectral imaging allows DynSUM to interpret multisensory detection by scanning emission spectra from fluorophores present in the cell simultaneously. A limitation of this method is the potential loss of sensitivity that results from splitting emission photons into multiple-channels in order to generate spectral profiles with sufficient time resolution. The signal-to-noise ratio may increase based on the scanning parameters used. Another limitation is the increased possibility of photobleaching of probes that may occur with laser excitation due to prolonged scanning time required in spectral acquisition.

In this project, we demonstrated the validation and application of a dynamic spectral unmixing microscopy, DynSUM. For cells that co-express

HyPer and roGFP, we were able to unmix signals from cytosol and mitochondria under oxidizing and reducing conditions in a dynamic fashion. The scanning interval can be as fast as 60 seconds. In addition to H<sub>2</sub>O<sub>2</sub> and DTT, the environmentally relevant organic electrophile 1,2-NQ was also utilized in this study for the validation of the DynSUM system. The application of DynSUM has several practical benefits such as higher efficiency and decreased material and tissue requirements, especially for clinical samples with limited availability. However, individual experiments are still recommended for verification purposes when first attempting to setup a DynSUM system for specific applications.

## **Chapter V. Concluding Remarks**

Oxidative stress is a common feature in xenobiotic injury mechanisms induced by different environmental contaminants. While there is a growing body of evidence that oxidative stress plays a critical role in adverse health effects induced by a broad array of air pollutants, an integration of the study of oxidant effects in mechanistic studies has been hampered by methodological shortcomings and limitations. These studies have employed imaging approaches to facilitate mechanistic examinations of the role of oxidative stress in the inflammatory effects induced by air pollution exposure.

Firstly, the initial investigation (Chapter II) demonstrated the feasibility of using an imaging approach for studying the toxicity induced by environmental air pollutants. In this study, an integrated imaging approach was developed and implemented to examine oxidative stress associated with mitochondrial dysfunction in cells exposed to  $Zn^{2+}$ . The detection of specific ROS is an important feature in this chapter of the present dissertation. Using PG-1, a highly sensitive and specific  $H_2O_2$  sensor,  $Zn^{2+}$ -stimulated  $H_2O_2$  production was visualized in real-time in living cells. With the use of established inhibitors, mitochondria were identified as the major intracellular source of  $Zn^{2+}$ -induced  $H_2O_2$ . Conventional detection methods were used as adjuncts to assess the extent of mitochondrial dysfunction induced by  $Zn^{2+}$  exposure, including the swelling

assay and metabolic inhibitors. Similarly, integration of the redox sensor roGFP targeted to the mitochondria, and the use of the fluorescent dye JC-1 to monitor the mitochondrial membrane potential, enabled us to elucidate the mechanism of oxidative stress induced by exposure to  $Zn^{2+}$  and other environmental agents.

Secondly, the findings presented in Chapter III revealed a mechanistic link between early oxidant events of exposure to 1,2-NQ and downstream toxicological effects involving alterations in the expression of genes whose products are responsible for inflammatory and adaptive responses in human bronchial epithelial cells. The genetically encoded fluorescence reporters roGFP2 and HyPer were employed for the detection of redox changes and  $H_2O_2$  production, respectively. Here we demonstrated that 1,2-NQ induced mitochondrial  $H_2O_2$  production leads to inflammatory gene expression but is not involved in the accompanying loss of reducing potential observed in the cytosol. 1,2-NQ was also found to induce *HO-1* expression; however, our data illustrate that it did so through a mechanism that was actually blunted by the availability of  $H_2O_2$ . In this chapter, we were able to measure early oxidative events in real-time and correlate them mechanistically to gene expression changes associated with adverse responses to exposure to a prototypic environmental electrophile.

Thirdly, a novel imaging methodology, called dynamic spectral unmixing microscopy (DynSUM), was developed for the simultaneous measurement of  $H_2O_2$  production and redox status. The two indicators, HyPer and roGFP2, measure closely related yet independent events. In Chapter IV, we show the

validation and application of the DynSUM method. For cells that were co-expressing HyPer and roGFP, we were able to spectrally unmix signals from the cytosol and mitochondria under oxidizing and reducing conditions in a dynamic fashion.

The general paradigm for xenobiotic-induced adverse health effects that has guided these studies is shown in Figure 1-C. When cells are exposed to environmental agents, there are toxic impairments of organelles which lead to an elevation of oxidative stress characterized by the loss of reducing potential and a production of ROS. These oxidative events then alter intracellular redox homeostasis which activates signaling pathways initiating changes in inflammatory and adaptive gene expression. Environmental agents such as zinc and 1,2 NQ are known to induce adverse health effects in humans. This research demonstrates the utility of an integrated approach for understanding the mechanisms involved in inducing inflammatory responses initiated by oxidative stress.

### **5-A. The implication of oxidative stress in this study**

Oxidative stress is increasingly recognized as an important feature of the mechanism of toxic action that is common to many structurally disparate environmental contaminants (Irani 2000). There are multiple phases in the cellular response to oxidative stress. Cells are equipped with a variety of tools for maintaining a reducing redox potential, such as metalloenzymes and non-

enzymatic antioxidants. Glutathione is the most abundant antioxidant that is actively maintained in a reduced state in millimolar concentrations apparently for the purpose of protecting the cells against oxidative insults. When the production of ROS or oxidized thiol proteins exceeds the capacity of these defense systems, oxidative stress begins to induce damage in cellular organelles. The elevated level of oxidative insults attacking macromolecules, lipids, proteins, and DNA, leads to dysfunction, disease development or cell death. Despite the potential for these harmful effects, free radicals such as superoxide, nitric oxide, and peroxynitrite are synthesized in phagocytic cells by NADPH oxidase or myeloperoxidase for immunological purposes, specifically to mediate host defense (Forman et al. 2010). Also, small amounts of ROS are produced for signaling purposes in order to activate specific transduction cascades. In fact, essential cellular functions, such as growth, death and survival are suspected to rely on oxidant signaling in varying cell types (Forman et al. 2010). Furthermore there is evidence that signaling molecules target major cellular sources for oxidant production, including mitochondria, cytochrome p450, NADPH oxidase, and xanthine oxidase. Signaling pathways such as MAP kinase, NF- $\kappa$ B, and caspases are then activated through the production of ROS (Forman et al. 2010) which lead to the transcription of corresponding genes.

Among the ROS species, hydrogen peroxide has been highlighted for its fulfillment of all the chemical and biological properties required of a “second messenger” (Jones 2008).  $H_2O_2$  has a tightly regulated enzymatic production and degradation system. The abundance of catalase and superoxide dismutase (SOD)

in different organelles allows a rapid break down of  $H_2O_2$  in a specific location which is useful for signaling regulation. Importantly,  $H_2O_2$  reacts with specific target cysteine residues in dedicated environments. The lack of specificity for the highly reactive hydroxyl radical and the short half life of superoxide add to the evidence that  $H_2O_2$  is the ROS species that serves as the major second messenger in cellular signaling systems (Jones 2006). Posttranslational modification such as the creation of glutathionylated signaling proteins and intramolecular disulfides are critical for  $H_2O_2$ -modulated redox signaling (Meyer and Dick 2010; Flohe 2010). Therefore research in Chapter II, III, and IV was centered on the identification of  $H_2O_2$  production using imaging methods in order to achieve high temporal and spatial detection.

Other than ROS, there is a growing awareness of radical-free oxidant insults which focuses on the disruption of thiol redox circuits. Despite the general understanding of antioxidants, thiol containing proteins have been recognized for redox regulation through reversible structural modifications. These thiol-based redox switches regulate receptor activation (platelet activation), signal transduction (PTP-1B), and transcription factor activation (Nrf-2 and NF-kB). Cellular signaling, structural, and regulatory proteins are modulated through sulfur switches such as cysteine oxidation. Cysteine also participates in macromolecular interactions including DNA binding, membrane binding, and tethering to the cytoskeleton (Wamelink et al. 2008). The cysteine has been noted for engaging in different alternations depending upon its redox state to regulate physiological function in plasma. The oxidized cysteine leads to cell adhesion or

even apoptosis depending on the degree of oxidation. On the other hand, cell proliferation through enhanced EGFR signaling was stimulated under a reduced cysteine environment (Cobbett et al. 1998; Meyer et al. 2007; Vernoux et al. 2000; Vesce et al. 2005). Although this information is provided from extracellular cysteine measurements, these observations clarify the notion that redox changes induce adverse effects in a more qualitative fashion in comparison with the description from ROS studies.

Protein thiol redox circuits in redox pathways are directed through redox-sensitive elements, typically involving glutathione and thioredoxin. Glutathione is the most abundant cellular thiol source available to modulate oxidant insults. Oxidative agents can oxidize glutathione through the use of glutathione peroxidase (Gpx) and transiently increase the intracellular glutathione redox potential. In response, oxidation-sensitive proteins form disulfide bonds through glutathionylation with the glutathione cofactor glutaredoxin (Grx). In a reducing environment, GSH attacks the disulfide bonds in redox sensitive proteins while Grx catalyzes de-glutathionylation of the proteins (Tal et al. 2008; Tal et al. 2006)(Figure 5-A). Oxidized glutathione (GSSG) is then reduced to 2 molecules of GSH through glutathione reductase (GR) and NADPH. The generation of NADPH via the pentose phosphate pathway, therefore, plays a pivotal role in redox regulation as well (Kim et al. 2006). roGFP with its two surface-exposed cysteine residues senses glutathione redox changes via the mediation of Grx (Rahman and MacNee 2000). Alterations in thiol-disulfide equilibria represent the beginning step of redox regulation and, therefore, are studied in Chapters II, III,

and IV as an essential feature of the roGFP-based methods presented in this dissertation.

An important aim of this dissertation is to correlate the early production of oxidant insult ( $H_2O_2$  production and loss of reducing potential) with downstream events such as inflammatory and adaptive gene expression. Distinct responses between ROS production and redox potential elevation by 1,2-NQ exposure (Chapter III) reveal an interesting dissociation. Inflammatory gene expression (*IL-8* and *COX-2*) mediated by mitochondrial  $H_2O_2$  may activate classical redox-sensitive transcription factors such as NF- $\kappa$ B, AP-1 and CEBP $\beta$ . On the other hand, roGFP changes report an apparent ROS free signaling regulation induced by 1,2-NQ. This is suggested by the observation that scavenging  $H_2O_2$  not only does not prevent 1,2-NQ stimulated roGFP signals but actually potentiates adaptive gene expression (*HO-1*). It is possible to speculate that a requirement for  $H_2O_2$  acting as a second messenger in order to initiate inflammatory gene expression, while, 1,2-NQ-induced *HO-1* expression requires electrophilic attack on a susceptible regulatory target, possibly a protein thiol, that is rendered unreactive to 1,2-NQ when oxidized by  $H_2O_2$ .

My predecessors in Dr. Samet's lab investigated the activation of signaling cascades and the expression of pro-inflammatory cytokines in xenobiotic-exposed airway cells. Environmental exposures (zinc and DEP) induce EGFR-dependent signaling through inhibition of EGFR-directed protein tyrosine phosphatase, PTP (Rahman and MacNee 2000). Subsequent AP-1 and NF- $\kappa$ B

activation leads to cytokine (IL-8) production (Marino and Gladyshev 2011). Oxidative stress was proposed to play a major role in mediating these signaling events. In addition, air pollution exposures stimulate oxidant release from neutrophils, macrophages and epithelial cells (Marino and Gladyshev 2011) which alter the glutathione balance by increasing GSSG concentration. The increase in glutathione redox potential has been shown to trigger lung inflammation via transcription of cytokine genes (Marino and Gladyshev 2011). In this dissertation, direct ROS measurement gives concrete evidence about the involvement of oxidant events (Chapters II and III). Although more studies are required to elucidate detailed mechanisms for the role of oxidative stress in signaling events, imaging detection of the second messenger  $H_2O_2$  via PG-1 and HyPer in this study following zinc and 1,2-NQ exposures fit into the gap between environmental exposure and activation of signaling events studied in Dr. Samet's laboratory research.

How and where oxidant insults result in environmental stimulus-induced adverse effects are complex questions. Exogenous and endogenous ROS are intertwined in activating multiple cascades. These studies were able to identify mitochondria as the origin of  $H_2O_2$  following  $Zn^{2+}$  and 1,2-NQ exposure. An elevated level of ROS may lead to the inhibition of PTPase and activate relevant signaling events such as AP-1 and NF- $\kappa$ B translocation into the nucleus or transcription of cytokine genes. Also, the disruption of redox homeostasis may stimulate ROS production from other major cellular sources such as NADPH oxidase and xanthine oxidase which can result in an effective amplification of the

reaction. Although technically challenging, it is therefore critical to locate the source of the initiating event stimulated by xenobiotic exposure.

The recognition of the role of thiology in antioxidant defense and redox regulation crates a new concept in metabolic regulations via redox reactions. The elucidation of detailed mechanisms for redox regulated signaling events requires more studies. General classifications according to different cellular cysteine functions can be made including metal-binding, catalytic, regulatory cysteine, and structural disulfide switches. Computational tools have been dedicated to categorize and predict cysteine function (Meyer and Dick 2010). Efficient predictions of catalytic redox cysteine, metal-binding cysteine, and disulfide bonds are examples of encouraging progress (Dickinson and Chang 2011). Nonetheless, more efforts are required for regulatory cysteine calculation and detection of redox switches in computational-based approaches (Chudakov et al. 2010). Extensive experimental datasets and the development of theoretical tools can fill in the gap of system biology application in regards to thiology topics. It would be beneficial to develop global computational predictions that are based on the integration of specific local pathways on oxidant signaling studies. The imaging approaches developed in this current study provide high temporal spatial resolution with flexible study design and demonstrates potential for adaptation to a higher throughput method that can generate large quantities of data for computational studies of redox regulation in toxicology.

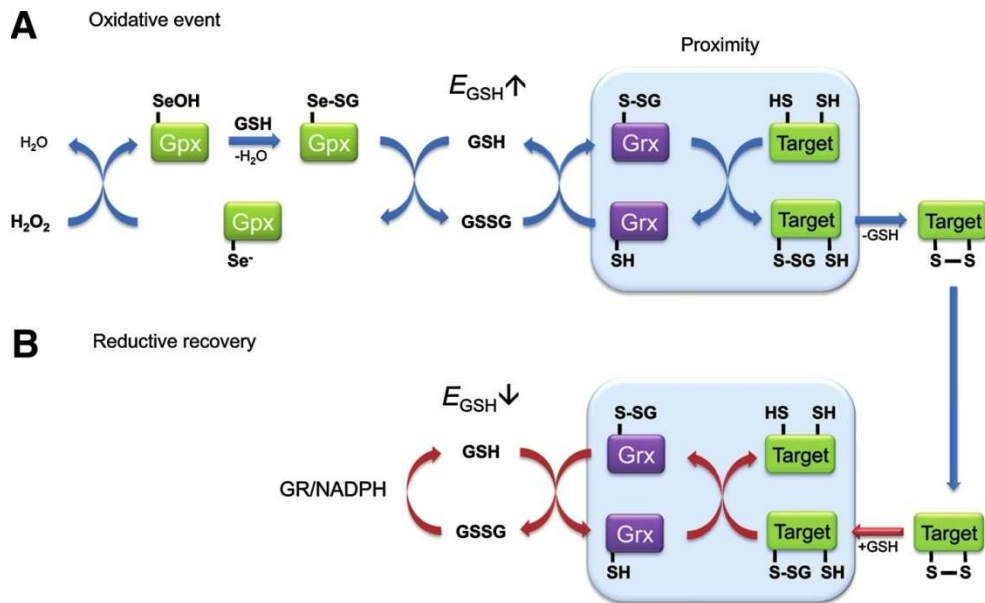


Figure 5- A. Glutaredoxin as a general mediator of reversible protein thiol oxidation (Merzlyak et al. 2007; Subach et al. 2008).

## **5-B. Toxicological applications of the imaging approach to oxidant detection**

As discussed in the previous chapters, oxidative stress is a critical hub linking toxic exposures and adverse outcomes. Therefore it is strategically advantageous to invest in methodology for the assessment of oxidant stress in toxicology and environmental health. However, a major limitation for oxidant studies in toxicology has been the availability of an integrated approach for the real-time detection of ROS production and oxidative damage in living cells. The onset of oxidant events can be very rapid and the duration is typically transient. Moreover production of ROS can be highly localized in specific compartments. Compared with conventional biochemical assays, live-cell imaging methods offer superior temporal and spatial resolution targeted to specific cellular processes.

Modern imaging methods can be used to monitor oxidative stress by visualizing immunohistochemical markers such as free radical modified molecules, antioxidants, and translocation of transcription factors. These methods can also be beneficial for monitoring the participation of ROS mediated signaling events. However, samples for immunohistochemistry analysis require fixation with formalin which limits method applications and temporal resolution. Therefore, chemical and genetic indicators for live-cell imaging are preferable in oxidative studies. The small molecule probe applied in Chapter II for ROS detection is both reaction-based and highly specific for H<sub>2</sub>O<sub>2</sub>. However, membrane permeability is both the strength and weakness for PG-1. PG-1 can easily cross the cytoplasm membrane driven by a concentration gradient;

however, unlike other biosensors, PG-1 cannot be trapped intracellularly, which restricts the interpretation of results obtained with this sensor. Recent efforts have been made ensuring that the next generation of indicators is enhanced by the addition of cytosolic trapping groups and organelle targeting capabilities (Meyer and Dick 2010). As is the case with many fluorophores, PG-1 also suffers from issues such as photo bleaching and an irreversible reactivity, which restricts sensitivity and prohibits dynamic detection. On the other hand, chemical sensors have the advantage of ready application. Generally, no specific technique or reagent is required for applying small molecular sensors as long as it is membrane permeable. Therefore, it is recommended for identifying the presence of a specific ROS in many situations.

Imaging detection with different strategies other than small molecular sensors was introduced in the subsequent projects (Chapters III and IV). Genetically engineered sensors demonstrate good photostability and brightness, especially for green and yellow fluorescence proteins. However, several parameters should be taken into account such as transcription and translational efficiency, construct stability, and protein maturation rate (Meyer and Dick 2010). High efficiency expression may result in cytotoxicity when cells are forced to express these highly stable constructs. pH stability is another strength of fluorescence proteins, particularly for blue, red, and far-red variants (Meyer and Dick 2010). GFP variants used in the current study are largely pH insensitive under physiological conditions. However, due to its sensitivity to hydrogen ion concentrations, monitoring pH is recommended when using YFP in live-cell

experiments (Meyer and Dick 2010). A GFP based indicator developed for pH detection, pHluorin, was tested in a pilot study. However, limited protein expression was reported in BEAS-2B cells, which prevented its interpretation under the conditions used in this experiment.

The GFP based probes utilized in this study for monitoring oxidative stress were delivered through 2 different methods, reagent transfection and lenti-viral transduction. Reagent transfection is convenient for screening purposes. Mixtures of plasmid DNA and transfection reagent can be directly applied to different cell types. A minimum of 24-48 hrs incubation is required for transfection and a 20-40 % transfection efficiency is expected. Another application for transfection that should be noted is manipulating the given amount of plasmid DNA. This is a practical strategy for expressing different constructs simultaneously in order to optimize similar levels of performance, such as indicator brightness. On the other hand, lenti-viral transduction to deliver target DNA requires a longer incubation time to establish a stably transduced cell line. Theoretically, a high expression rate is expected by using a lenti virus. 50-60 % of cells were successfully transduced with oxidant-imaging sensors in our study. In theory, once the construct DNA is incorporated into the target genome, no further procedure is needed to maintain expression. However, reduced percentages of transduced cells were observed for cells expressing HyPer and roGFP following 10-15 cell passages. Storage and periodical revival of early stage viral transduced cells is recommended to ensure consistent responses across experiments over time.

roGFP and HyPer utilize a similar principle to report changes in redox and H<sub>2</sub>O<sub>2</sub>, respectively. Namely, the reactivity of these sensors is based on a structural alteration by the formation or distortion of a cysteine disulfide bridge to influence chromophore emission intensity (Bolton et al. 2000). The surface exposed cysteine pairs at position 147 and 204 are the critical modification for roGFP to sense redox changes in its surroundings. As mentioned earlier, the enzymatic catalyses with Gpx and Grx are crucial for the disulfide bridge formation which is the fundamental step for the modulation of roGFP fluorescence intensity (Figure 5-A). However, by incubating roGFP protein in a cell-free system, the addition of H<sub>2</sub>O<sub>2</sub>, DTT, and 1,2-NQ can alter roGFP emission intensity in the absence of enzymatic proteins. One possibility underlying this observation is that overwhelming concentrations of oxidizing and reducing reagents overcome the high pK<sub>a</sub> needed for cysteine dissociation, and promote the formation or dissociation of the disulfide crosslink. A strong electrophile like 1,2-NQ may create a direct covalent modification with roGFP protein to change fluorescence intensity as well. Further validations are recommended when applying roGFP as a sensor for the detection of redox status. Modification of enzyme activity of Grx and Gpx with inhibitors or genetically overexpressed/knock-down systems to alter sensor responses in an exposure system is preferable in order to validate the roGFP system. Protein analysis by mass spectrometry for roGFP and exposure chemical co-incubated samples can be helpful in determining whether direct attack is involved in the reaction. Another complication in our detection system is that roGFP is designed for responding to the changing ratio between oxidized and

reduced glutathione; whereas HyPer is oxidized by the presence of H<sub>2</sub>O<sub>2</sub> and reduced through the glutathione pool (Valko et al. 2005). The communication with different redox pairs (2H<sub>2</sub>O/H<sub>2</sub>O<sub>2</sub> and 2GSH/GSSG) brings up a complication of HyPer detection and should be taken into account when monitoring exposures that may not only induce H<sub>2</sub>O<sub>2</sub> production but also modulate the reduced to oxidized glutathione balance.

The indicators discussed in previous paragraphs are applicable with different detection methods such as microscopy, plate readers, and flow cytometry. In the current study, we exploit instruments such as the confocal microscope and fluorescence plate reader for specific purposes. Microscopy served as the more sensitive method, where addition of 10  $\mu$ M H<sub>2</sub>O<sub>2</sub> is detectable when using roGFP and HyPer as indicators in the cytosol. A good signal-to-noise ratio and stable signal output are the major benefits of utilizing confocal microscopes to monitor living cells throughout the exposure period. With the combination of Perfect Focus system to maintain scanning focal plane and stable temperature and humidity control, overnight measurements have been performed in our laboratory. However, the major limitation of using a microscope as a means of detection is that the practical sample quantity is limited. Only one specific condition can be tested at a time. Therefore, we turned our attention to integrate a plate reader into our detection system for high throughput screening. The noise level is increased in plate reader detection; therefore, multiple repeats are suggested when implementing this type of detection. It is both beneficial and efficient to test different experimental parameters using 96 well plates.

Verification is suggested by using independent methods such as a confocal microscope or flow cytometry. Another limitation regarding imaging detection that should be mentioned is the difficulty to derive quantitative values. In the current study, we measured indicator responses by comparing fluorescence intensity before and after exposure. Only relative changes can be calculated and plotted. Theoretically, it is possible to generate a standard curve based on the calibration of absolute redox value for a ratiometric based sensor such as roGFP (Quig 1998). Overall, it is desirable to have quantitative microscopy detection, but efforts are required to overcome certain practical limitations such as cell-to-cell variations that occur even within a uniform cell line.

### **5-C. PM induced oxidant toxicity and its evaluation**

PM is one of the air pollutants that most frequently exceeds federal regulation standards. It is responsible for elevated levels of mortality and morbidity in developed as well as developing countries (Guo et al.). The inflammatory effects of PM are associated with the strong oxidant potential from various sources, such as DEP. DEP accounts for 80% of the total mass of PM<sub>10</sub> in samples collected from urban areas (BeruBe et al. 2007). The organic and inorganic fractions of DEP components are believed to be the major cause for ROS production. Therefore, we employed a potent organic electrophile (1,2-NQ) and a redox inert heavy metal (zinc) that are related to DEP-induced oxidative stress as our model toxicants.

Quinone toxicity involves two major mechanisms: 1,4 addition and redox cycling. Reports of quinones' adverse effects are focused on carcinogenesis and mutagenesis mediated through quinone adduct formation (WHO 2002). Quinones are also known for undergoing redox cycling, which generates ROS by single electron reduction of oxygen. While ROS production induced by DEP is believed to induce inflammatory responses (Rahman and MacNee 2000), few studies delve into the mechanisms for 1,2-NQ-induced inflammation. In Chapter III, elevated levels of *IL-8* and *COX-2* gene expression were observed after 1,2-NQ exposure. This verifies the hypothesis of inflammation as one of the end points for adverse health effects resulting from quinone exposure.

The observation we made in Chapter III by utilizing HyPer and roGFP reported that 1,2-NQ exposure stimulated H<sub>2</sub>O<sub>2</sub> production and redox changes in an independent manner. Catalase over-expression did not protect against 1,2-NQ-induced roGFP signals indicative of a loss of reducing potential. Based on Figure 5-A, there are several potential targets for 1,2-NQ to trigger roGFP changes including attack on Gpx, GSH, or Grx. By-product formation that oxidizes Gpx other than the generation of H<sub>2</sub>O<sub>2</sub> is a possibility as well.

Furthermore, activation of the *HO-1* gene through 1,2-NQ exposure is independent from inflammatory gene responses. Strong electrophiles like 1,2-NQ may activate Nrf2 signaling pathways by promoting the dissociation of the Nrf2 repressor, Kelch-like ECH-associated protein (Keap1) (Niture et al.). It is possible that phase II enzymes and antioxidants are activated during 1,2-NQ detoxification

and excretion processes by the modulation of Nrf2. Instead of potentiating gene expression, the addition of H<sub>2</sub>O<sub>2</sub> actually blunted 1,2-NQ-induced *HO-1* gene expression (Chapter III), raising the possibility that biomolecular covalent modifications by 1,2-NQ are involved in *HO-1* gene expression induced by an electrophilic attack.

Modifications of DNA bases and enhanced lipid peroxidation are well-known mechanisms for metal induced toxicity (Ruckerl et al. 2011). The redox-inert transition metal zinc induces cellular damage through covalent modification of critical sulfhydryl groups of cellular biomolecules. The observation made in Chapter II that zinc-stimulated H<sub>2</sub>O<sub>2</sub> production through mitochondrial dysfunction indicates that potential zinc-targeting sites are associated with maintaining mitochondrial membrane potential. Also, it could be an underlying mechanism for zinc-induced signaling dysregulation leading to increased expression of inflammatory mediators, as well as apoptotic and necrotic cell death (Kim et al. 2006; Tal et al. 2006; Tang et al. 2001; Franklin and Costello 2009).

The model toxicants studied in this research provides interesting contrasts and similarities. They represent two major mechanisms for PM/DEP induced toxicity. The separation of electrophile attack and ROS production produce insights that are pertinent to the study for multi-pollutant models. PM exposure could induce important gene-environment interactions through oxidative stress, as revealed in Chapter III. Although we studied single exposures, application of the

system to multi-pollutants is desirable as representing a closer approximation to the ambient environment.

#### **5-D. From imaging oxidative stress in vitro to protecting the public health from environmental exposures**

Worldwide air pollution exposure is a major public health concern that involves the death of more than 800,000 people annually, according to the World Health Report 2002 . Major strategies to limit the air contaminants which impose health burdens are engineering controls designed to decrease pollutant concentrations. However, it is unlikely that these interventions can completely remove polluting agents from the atmosphere. This awareness raises the urgency with which efforts aimed at obtaining a better understanding of air pollutant-mediated adverse health effects should be pursued. The efforts to decipher toxicological mechanisms induced by contaminant exposure can assist in the development of strategies to remove the most highly toxic components of air pollutants and design strategies to protect sensitive groups through targeted interventions.

Air pollution is a complex mixture and its composition varies according to multiple parameters such as locations, seasons, and sources. The deposition, solubility, and intake of contaminants in the lungs is critical for initiating toxic responses, since different physical properties can determine the susceptible cell types ranging from ciliated epithelium and macrophages in bronchial branching to alveolar epithelial cells in the alveoli region, or even endothelial cells in blood

vessels. Although, diverse responses have been observed once pollutants reach the cellular level, oxidative stress is involved to varying degrees in almost all of the exposures. Elevated levels of ROS in the lungs is observed after exposure to PM, ozone, nitrogen oxides, sulphur dioxide, and tobacco smoke (Biswas and Rahman 2009). The exposure duration and dose determine biological responses. Based on epidemiological studies, acute exposure to increased concentrations of particulate air pollution is associated with increased mortality, hospitalization, and incidence of respiratory symptoms (Pope et al. 1995). Oxidative stress stimulated by potent oxidants reacts directly with cellular organelles, interferes with physiological functions, and mediates acute cell death (Irani 2000; Rahman and MacNee 2000). The observation that antioxidant supplements have moderated the effects of air pollution on lung function from several case control studies also points to the relevance of oxidant insults (Tashakkor et al.). On the other hand, mortality risk and chronic respiratory disease are associated with long-term exposure to air pollutants (Pope et al. 1995). Mechanisms of oxidative stress-induced chronic responses are associated with inflammation. Fibrosis, bronchitis, and even carcinogenesis are related to oxidant mediated inflammation .

The commonality of oxidant insults in air pollutant exposure raises the importance of reaching a fundamental understanding of oxidative stress as a pivotal toxic mechanism. Application of the latest imaging tools to investigate the transient nature and spatial specificity of ROS production is perhaps the major contribution of this dissertation. The improved detection methods developed here allow rapid and accurate identification of oxidant insults in a cellular system.

These are fundamental steps for depicting the mechanisms of air pollutant induced adverse health effects. The tools applied in this study can also utilize different experimental models including animal testing or even biomarker development. Furthermore, the model system developed from the oxidant paradigm (Figure 1-C) can be employed in mechanistic studies of multiple components of air pollution.

There is a growing awareness of the role that redox dysregulations plays in the adverse health effects induced by air pollution exposure. This dissertation applies recently developed reporters of redox state and ROS to interface real-time measurement of oxidative stress with mechanistic studies of the toxicity of contaminants. Two structurally disparate environmental contaminants ( $Zn^{2+}$  and 1,2-NQ) were employed in this dissertation as model toxicants. Distinct mechanisms were observed for the inorganic and organic air pollutants, linking adverse outcomes to the induction of oxidative stress in cells. The utilization of an integrated imaging approach to study oxidative stress has considerable potential to continue providing insights into the adverse health effects of air pollution inhalation.

## REFERENCES

[EPA US. 2007. National air quality: status and trends through 2007. Available: http://www.epa.gov/airtrends/2008/index.html.](http://www.epa.gov/airtrends/2008/index.html)

[Anonymous]. 1995. 8th International IUPAC (International Union of Pure and Applied Chemistry) Symposium on Mycotoxins and Phycotoxins. Mexico City, Mexico, 6-13 November 1992. *Food Addit Contam* 12(3): 291-525.

Andreyev AY, Kushnareva YE, Starkov AA. 2005. Mitochondrial metabolism of reactive oxygen species. *Biochemistry (Mosc)* 70(2): 200-214.

Aust AE, Eveleigh JF. 1999. Mechanisms of DNA oxidation. *Proc Soc Exp Biol Med* 222(3): 246-252.

Austin CD, Wen X, Gazzard L, Nelson C, Scheller RH, Scales SJ. 2005. Oxidizing potential of endosomes and lysosomes limits intracellular cleavage of disulfide-based antibody-drug conjugates. *Proc Natl Acad Sci U S A* 102(50): 17987-17992.

Awasthi YC, Sharma R, Cheng JZ, Yang Y, Sharma A, Singhal SS, et al. 2003. Role of 4-hydroxynonenal in stress-mediated apoptosis signaling. *Mol Aspects Med* 24(4-5): 219-230.

Bai Y, Suzuki AK, Sagai M. 2001. The cytotoxic effects of diesel exhaust particles on human pulmonary artery endothelial cells in vitro: role of active oxygen species. *Free Radic Biol Med* 30(5): 555-562.

Becker S, Mundandhara S, Devlin RB, Madden M. 2005. Regulation of cytokine production in human alveolar macrophages and airway epithelial cells in response to ambient air pollution particles: further mechanistic studies. *Toxicol Appl Pharmacol* 207(2 Suppl): 269-275.

Belousov V, Fradkov AF, Lukyanov KA, Staroverov DB, Shakhbazov KS, Terskikh AV, et al. 2006. Genetically encoded fluorescent indicator for intracellular hydrogen peroxide. *Nature Methods* 3(4): 6.

Benedetti PA, Evangelista V, Guidarini D, Vestri S. 1992. Confocal-line microscopy. *J Microsc* 165(Pt 1): 119-129.

Berg RH. 2004. Evaluation of spectral imaging for plant cell analysis. *J Microsc* 214(Pt 2): 174-181.

Berube K, Balharry D, Sexton K, Koshy L, Jones T. 2007. Combustion-derived nanoparticles: mechanisms of pulmonary toxicity. *Clin Exp Pharmacol Physiol* 34(10): 1044-1050.

Biswas SK, Rahman I. 2009. Environmental toxicity, redox signaling and lung inflammation: the role of glutathione. *Mol Aspects Med* 30(1-2): 60-76.

Bjornberg O, Ostergaard H, Winther JR. 2006. Measuring intracellular redox conditions using GFP-based sensors. *Antioxid Redox Signal* 8(3-4): 354-361.

Blanc PD, Boushey HA, Wong H, Wintermeyer SF, Bernstein MS. 1993. Cytokines in metal fume fever. *Am Rev Respir Dis* 147(1): 134-138.

Bogeski I, Bozem M, Sternfeld L, Hofer HW, Schulz I. 2006. Inhibition of protein tyrosine phosphatase 1B by reactive oxygen species leads to maintenance of Ca<sup>2+</sup> influx following store depletion in HEK 293 cells. *Cell Calcium* 40(1): 1-10.

Bolton JL, Trush MA, Penning TM, Dryhurst G, Monks TJ. 2000. Role of quinones in toxicology. *Chem Res Toxicol* 13(3): 135-160.

Bossy-Wetzel E, Talantova MV, Lee WD, Scholzke MN, Harrop A, Mathews E, et al. 2004a. Crosstalk between Nitric Oxide and Zinc Pathways to Neuronal Cell Death Involving Mitochondrial Dysfunction and p38-Activated K Channels. *Neuron* 41: 15.

Bossy-Wetzel E, Talantova MV, Lee WD, Scholzke MN, Harrop A, Mathews E, et al. 2004b. Crosstalk between Nitric Oxide and Zinc Pathways to Neuronal Cell Death Involving Mitochondrial Dysfunction and p38-Activated K Channels. *Neuron* 41: 15.

Brook RD, Franklin B, Cascio W, Hong Y, Howard G, Lipsett M, et al. 2004. Air pollution and cardiovascular disease: a statement for healthcare professionals from the Expert Panel on Population and Prevention Science of the American Heart Association. *Circulation* 109(21): 2655-2671.

Brown AM, Kristal BS, Effron MS, Shestopalov AI, Ullucci PA, Sheu KF, et al. 2000. Zn<sup>2+</sup> inhibits alpha-ketoglutarate-stimulated mitochondrial respiration and the isolated alpha-ketoglutarate dehydrogenase complex. *J Biol Chem* 275(18): 13441-13447.

Brown AM, Kristal BS, Effron MS, Shestopalov AI, Ullucci PA, Sheu K-FR, et al. 2000. Zn<sup>2+</sup> Inhibits alpha -Ketoglutarate-stimulated Mitochondrial Respiration and the Isolated alpha -Ketoglutarate Dehydrogenase Complex. *Journal of Biological Chemistry* 275(18): 7.

Cannon MB, James Remington S. 2009. Redox-sensitive green fluorescent protein: probes for dynamic intracellular redox responses. A review. *Methods Mol Biol* 476: 50-64.

Cannon MB, Remington SJ. 2006. Re-engineering redox-sensitive green fluorescent protein for improved response rate. *Protein Sci* 15(1): 45-57.

Cannon MB, Remington SJ. 2008. Redox-sensitive green fluorescent protein: probes for dynamic intracellular redox responses. A review. *Methods Mol Biol* 476: 51-65.

Cao D, Bromberg PA, Samet JM. 2007a. COX-2 expression induced by diesel particles involves chromatin modification and degradation of HDAC1. *Am J Respir Cell Mol Biol* 37(2): 232-239.

Cao D, Bromberg PA, Samet JM. 2009. Diesel Particle-induced Transcription Expression of P21 Involves Activation of EGFR, SRC and STAT3. *Am J Respir Cell Mol Biol*.

Cao D, Tal TL, Graves LM, Gilmour I, Linak W, Reed W, et al. 2007b. Diesel exhaust particulate-induced activation of Stat3 requires activities of EGFR and Src in airway epithelial cells. *Am J Physiol Lung Cell Mol Physiol* 292(2): L422-429.

Chang MB, Huang CK, Wu HT, Lin JJ, Chang SH. 2000. Characteristics of heavy metals on particles with different sizes from municipal solid waste incineration. *J Hazard Mater* 79(3): 229-239.

Cheng WY, Currier J, Bromberg PA, Silbajoris R, Simmons SO, Samet JM. 2011. Linking Oxidative Events to Inflammatory and Adaptive Gene Expression Induced by Exposure to an Organic PM Component. *Environ Health Perspect*.

Cheng WY, Tong H, Miller EW, Chang CJ, Remington J, Zucker RM, et al. 2010. An integrated imaging approach to the study of oxidative stress generation by mitochondrial dysfunction in living cells. *Environ Health Perspect* 118(7): 902-908.

Cho AK, Stefano ED, You Y, Rodriguez CE, Schmitz DA, Kumagai Y, et al. 2004. Determination of four quinones in diesel exhaust particles, SRM 1649a, and atmospheric PM<sub>2.5</sub>. *Aerosol Science and Technology* 38(S1): 14.

Choi H, Kim S, Mukhopadhyay P, Cho S, Woo J, Storz G, et al. 2001. Structural basis of the redox switch in the OxyR transcription factor. *Cell* 105(1): 103-113.

Chudakov DM, Matz MV, Lukyanov S, Lukyanov KA. 2010. Fluorescent proteins and their applications in imaging living cells and tissues. *Physiol Rev* 90(3): 1103-1163.

Chung C, Srikun D, Lim CS, Chang CJ, Cho BR. 2011. A two-photon fluorescent probe for ratiometric imaging of hydrogen peroxide in live tissue. *Chem Commun (Camb)* 47(34): 9618-9620.

Claiborn CS, Larson T, Sheppard L. 2002. Testing the metals hypothesis in Spokane, Washington. *Environ Health Perspect* 110 Suppl 4: 547-552.

Cobbett CS, May MJ, Howden R, Rolls B. 1998. The glutathione-deficient, cadmium-sensitive mutant, *cad2-1*, of *Arabidopsis thaliana* is deficient in gamma-glutamylcysteine synthetase. *Plant J* 16(1): 73-78.

Crow JP. 1997. Dichlorodihydrofluorescein and dihydrorhodamine 123 are sensitive indicators of peroxynitrite in vitro: implications for intracellular measurement of reactive nitrogen and oxygen species. *Nitric Oxide* 1(2): 145-157.

Dickinson BC, Chang CJ. 2011. Chemistry and biology of reactive oxygen species in signaling or stress responses. *Nat Chem Biol* 7(8): 504-511.

Dickinson BC, Tang Y, Chang Z, Chang CJ. 2011. A nuclear-localized fluorescent hydrogen peroxide probe for monitoring sirtuin-mediated oxidative stress responses in vivo. *Chem Biol* 18(8): 943-948.

Dickinson ME, Bearman G, Tille S, Lansford R, Fraser SE. 2001. Multi-spectral imaging and linear unmixing add a whole new dimension to laser scanning fluorescence microscopy. *Biotechniques* 31(6): 1272, 1274-1276, 1278.

Donaldson K, Tran L, Jimenez LA, Duffin R, Newby DE, Mills N, et al. 2005. Combustion-derived nanoparticles: a review of their toxicology following inhalation exposure. *Part Fibre Toxicol* 2: 10.

Dooley CT, Dore TM, Hanson GT, Jackson WC, Remington SJ, Tsien RY. 2004. Imaging dynamic redox changes in mammalian cells with green fluorescent protein indicators. *J Biol Chem* 279(21): 22284-22293.

Ecker RC, de Martin R, Steiner GE, Schmid JA. 2004. Application of spectral imaging microscopy in cytomics and fluorescence resonance energy transfer (FRET) analysis. *Cytometry A* 59(2): 172-181.

Endo A, Sumi D, Kumagai Y. 2007. 1,2-Naphthoquinone disrupts the function of cAMP response element-binding protein through covalent modification. *Biochem Biophys Res Commun* 361(1): 243-248.

Ercal N, Gurer-Orhan H, Aykin-Burns N. 2001. Toxic metals and oxidative stress part I: mechanisms involved in metal-induced oxidative damage. *Curr Top Med Chem* 1(6): 529-539.

Esterbauer H. 1996. Estimation of peroxidative damage. A critical review. *Pathol Biol (Paris)* 44(1): 25-28.

Faraci FM, Didion SP. 2004. Vascular protection: superoxide dismutase isoforms in the vessel wall. *Arterioscler Thromb Vasc Biol* 24(8): 1367-1373.

Finkelstein JN, Johnston CJ. 2004. Enhanced sensitivity of the postnatal lung to environmental insults and oxidant stress. *Pediatrics* 113(4 Suppl): 1092-1096.

Flohe L. 2010. Changing paradigms in thiology from antioxidant defense toward redox regulation. *Methods Enzymol* 473: 1-39.

Forman HJ, Maiorino M, Ursini F. 2010. Signaling functions of reactive oxygen species. *Biochemistry* 49(5): 835-842.

Fourquet S, Guerois R, Biard D, Toledano MB. 2010. Activation of NRF2 by nitrosative agents and H<sub>2</sub>O<sub>2</sub> involves KEAP1 disulfide formation. *J Biol Chem* 285(11): 8463-8471.

Franklin RB, Costello LC. 2009. The important role of the apoptotic effects of zinc in the development of cancers. *J Cell Biochem* 106(5): 750-757.

Groeger G, Quiney C, Cotter TG. 2009. Hydrogen peroxide as a cell-survival signaling molecule. *Antioxid Redox Signal* 11(11): 2655-2671.

Guo Y, Tong S, Zhang Y, Barnett AG, Jia Y, Pan X. The relationship between particulate air pollution and emergency hospital visits for hypertension in Beijing, China. *Sci Total Environ* 408(20): 4446-4450.

Guthrie HD, Welch GR. 2008. Determination of high mitochondrial membrane potential in spermatozoa loaded with the mitochondrial probe 5,5',6,6'-tetrachloro-1,1',3,3'-tetraethylbenzimidazolyl-carbocyanine iodide (JC-1) by using fluorescence-activated flow cytometry. *Methods Mol Biol* 477: 89-97.

Haghdoust S, Czene S, Naslund I, Skog S, Harms-Ringdahl M. 2005. Extracellular 8-oxo-dG as a sensitive parameter for oxidative stress in vivo and in vitro. *Free Radic Res* 39(2): 153-162.

Hanson GT, Aggeler R, Oglesbee D, Cannon M, Capaldi RA, Tsien RY, et al. 2004. Investigating mitochondrial redox potential with redox-sensitive green fluorescent protein indicators. *J Biol Chem* 279(13): 13044-13053.

Hanson GT, Aggeler R, Oglesbee D, Cannon M, Capaldi RA, Tsien RY, et al. 2004. Investigating mitochondrial redox potential with redox-sensitive green fluorescent protein indicators. *The Journal of Biological Chemistry* 279(13): 10.

Hinkle PC, Butow RA, Racker E, Chance B. 1967. Partial resolution of the enzymes catalyzing oxidative phosphorylation. XV. Reverse electron transfer in the flavin-cytochrome beta region of the respiratory chain of beef heart submitochondrial particles. *J Biol Chem* 242(22): 5169-5173.

Hirst J, King MS, Pryde KR. 2008. The production of reactive oxygen species by complex I. *Biochem Soc Trans* 36(Pt 5): 976-980.

Inoue K, Takano H, Hiyoshi K, Ichinose T, Sadakane K, Yanagisawa R, et al. 2007b. Naphthoquinone enhances antigen-related airway inflammation in mice. *Eur Respir J* 29(2): 259-267.

Inoue K, Takano H, Ichinose T, Tomura S, Yanagisawa R, Sakurai M, et al. 2007a. Effects of naphthoquinone on airway responsiveness in the presence or absence of antigen in mice. *Arch Toxicol* 81(8): 575-581.

Irani K. 2000. Oxidant signaling in vascular cell growth, death, and survival : a review of the roles of reactive oxygen species in smooth muscle and endothelial cell mitogenic and apoptotic signaling. *Circ Res* 87(3): 179-183.

Iwamoto N, Sumi D, Ishii T, Uchida K, Cho AK, Froines JR, et al. 2007. Chemical knockdown of protein-tyrosine phosphatase 1B by 1,2-naphthoquinone through covalent modification causes persistent transactivation of epidermal growth factor receptor. *J Biol Chem* 282(46): 33396-33404.

Jakober CA, Riddle SG, Robert MA, Destailats H, Charles MJ, Green PG, et al. 2007. Quinone emissions from gasoline and diesel motor vehicles. *Environ Sci Technol* 41(13): 4548-4554.

Jaspers I, Samet JM, Erzurum S, Reed W. 2000. Vanadium-induced kappaB-dependent transcription depends upon peroxide-induced activation of the p38 mitogen-activated protein kinase. *Am J Respir Cell Mol Biol* 23(1): 95-102.

Jaspers I, Sheridan PA, Zhang W, Brighton LE, Chason KD, Hua X, et al. 2009. Exacerbation of allergic inflammation in mice exposed to diesel exhaust particles prior to viral infection. *Part Fibre Toxicol* 6: 22.

Jones DP. 2006. Redefining oxidative stress. *Antioxid Redox Signal* 8(9-10): 1865-1879.

Jones DP. 2008. Radical-free biology of oxidative stress. *Am J Physiol Cell Physiol* 295(4): C849-868.

Kelly FJ, Mudway IS. 2003. Protein oxidation at the air-lung interface. *Amino Acids* 25(3-4): 375-396.

Kelly KA, Havrilla CM, Brady TC, Abramo KH, Levin ED. 1998. Oxidative stress in toxicology: established mammalian and emerging piscine model systems. *Environ Health Perspect* 106(7): 375-384.

Kikuno S, Taguchi K, Iwamoto N, Yamano S, Cho AK, Froines JR, et al. 2006. 1,2-Naphthoquinone activates vanilloid receptor 1 through increased protein tyrosine phosphorylation, leading to contraction of guinea pig trachea. *Toxicol Appl Pharmacol* 210(1-2): 47-54.

Kim YM, Reed W, Wu W, Bromberg PA, Graves LM, Samet JM. 2006. Zn<sup>2+</sup>-induced IL-8 expression involves AP-1, JNK, and ERK activities in human airway epithelial cells. *Am J Physiol Lung Cell Mol Physiol* 290(5): L1028-1035.

Kinter M. 1995. Analytical technologies for lipid oxidation products analysis. *J Chromatogr B Biomed Appl* 671(1-2): 223-236.

Kodavanti UP, Schladweiler MC, Ledbetter AD, Hauser R, Christiani DC, Samet JM, et al. 2002. Pulmonary and systemic effects of zinc-containing emission particles in three rat strains: multiple exposure scenarios. *Toxicol Sci* 70(1): 73-85.

Kowaltowski AJ, de Souza-Pinto NC, Castilho RF, Vercesi AE. 2009. Mitochondria and reactive oxygen species. *Free Radic Biol Med* 47(4): 333-343.

Kumagai Y, Arimoto T, Shinyashiki M, Shimojo N, Nakai Y, Yoshikawa T, et al. 1997. Generation of reactive oxygen species during interaction of diesel exhaust particle components with NADPH-cytochrome P450 reductase and involvement of the bioactivation in the DNA damage. *Free Radic Biol Med* 22(3): 479-487.

Kuroda H, Takeno M, Murakami S, Miyazawa N, Kaneko T, Ishigatsubo Y. 2010. Inhibition of heme oxygenase-1 with an epidermal growth factor receptor inhibitor and cisplatin decreases proliferation of lung cancer A549 cells. *Lung Cancer* 67(1): 31-36.

Kussmaul L, Hirst J. 2006. The mechanism of superoxide production by NADH:ubiquinone oxidoreductase (complex I) from bovine heart mitochondria. *Proc Natl Acad Sci U S A*

103(20): 7607-7612.

Kuwahara I, Lillehoj EP, Lu W, Singh IS, Isohama Y, Miyata T, et al. 2006. Neutrophil elastase induces IL-8 gene transcription and protein release through p38/NF- $\kappa$ B activation via EGFR transactivation in a lung epithelial cell line. *Am J Physiol Lung Cell Mol Physiol* 291(3): L407-416.

Lam M, Oleinick NL, Nieminen AL. 2001. Photodynamic therapy-induced apoptosis in epidermoid carcinoma cells. Reactive oxygen species and mitochondrial inner membrane permeabilization. *J Biol Chem* 276(50): 47379-47386.

Lambert AJ, Brand MD. 2004. Inhibitors of the quinone-binding site allow rapid superoxide production from mitochondrial NADH:ubiquinone oxidoreductase (complex I). *J Biol Chem* 279(38): 39414-39420.

Lame MW, Jones AD, Wilson DW, Segall HJ. 2003. Protein targets of 1,4-benzoquinone and 1,4-naphthoquinone in human bronchial epithelial cells. *Proteomics* 3(4): 479-495.

Larson JM. 2006. The Nikon C1si combines high spectral resolution, high sensitivity, and high acquisition speed. *Cytometry A* 69(8): 825-834.

Laumbach RJ. 2010. Outdoor air pollutants and patient health. *Am Fam Physician* 81(2): 175-180.

Le SB, Hailer MK, Buhrow S, Wang Q, Flatten K, Padiaditakis P, et al. 2007. Inhibition of mitochondrial respiration as a source of adaphostin-induced reactive oxygen species and cytotoxicity. *J Biol Chem* 282(12): 8860-8872.

Lerner JM, Zucker RM. 2004. Calibration and validation of confocal spectral imaging systems. *Cytometry A* 62(1): 8-34.

Li N, Sioutas C, Cho A, Schmitz D, Misra C, Sempf J, et al. 2003. Ultrafine particulate pollutants induce oxidative stress and mitochondrial damage. *Environ Health Perspect* 111(4): 455-460.

Li P-F, Dietz R, Harsdorf R. 1999. p53 regulates mitochondrial membrane potential through reactive oxygen species and induces cytochrome c-independent apoptosis blocked by Bcl-2. *EMBO Journal* 18: 9.

Lim HB, Ichinose T, Miyabara Y, Takano H, Kumagai Y, Shimojyo N, et al. 1998. Involvement of superoxide and nitric oxide on airway inflammation and hyperresponsiveness induced by diesel exhaust particles in mice. *Free Radic Biol Med* 25(6): 635-644.

Link TA, von Jagow G. 1995. Zinc ions inhibit the QP center of bovine heart mitochondrial bc1 complex by blocking a protonatable group. *J Biol Chem* 270(42): 25001-25006.

Lippert AR, New EJ, Chang CJ. 2011b. Reaction-based fluorescent probes for selective imaging of hydrogen sulfide in living cells. *J Am Chem Soc* 133(26): 10078-10080.

Lippert AR, Van de Bittner GC, Chang CJ. 2011a. Boronate oxidation as a bioorthogonal reaction approach for studying the chemistry of hydrogen peroxide in living systems. *Acc Chem Res* 44(9): 793-804.

Livak KJ, Schmittgen TD. 2001. Analysis of relative gene expression data using real-time quantitative PCR and the  $2^{-\Delta\Delta C(T)}$  Method. *Methods* 25(4): 402-408.

Lohman JR, Remington SJ. 2008. Development of a family of redox-sensitive green fluorescent protein indicators for use in relatively oxidizing subcellular environments. *Biochemistry* 47(33): 8678-8688.

Marchesi E, Rota C, Fann YC, Chignell CF, Mason RP. 1999. Photoreduction of the fluorescent dye 2'-7'-dichlorofluorescein: a spin trapping and direct electron spin resonance study with implications for oxidative stress measurements. *Free Radic Biol Med* 26(1-2): 148-161.

Marino SM, Gladyshev VN. 2011. Redox biology: computational approaches to the investigation of functional cysteine residues. *Antioxid Redox Signal* 15(1): 135-146.

Mason DE, Liebler DC. 2000. Characterization of benzoquinone-peptide adducts by electrospray mass spectrometry. *Chem Res Toxicol* 13(10): 976-982.

Merzlyak EM, Goedhart J, Shcherbo D, Bulina ME, Shcheglov AS, Fradkov AF, et al. 2007. Bright monomeric red fluorescent protein with an extended fluorescence lifetime. *Nat Methods* 4(7): 555-557.

Meyer AJ, Brach T, Marty L, Kreye S, Rouhier N, Jacquot JP, et al. 2007. Redox-sensitive GFP in *Arabidopsis thaliana* is a quantitative biosensor for the redox potential of the cellular glutathione redox buffer. *Plant J* 52(5): 973-986.

Meyer AJ, Dick TP. 2010. Fluorescent protein-based redox probes. *Antioxid Redox Signal* 13(5): 621-650.

Miller E, Tulyathan O, Isacoff E, Chang C. 2007. Molecular imaging of hydrogen peroxide produced for cell signaling. *Nature Chemical Biology* 3: 5.

Miller EW, Dickinson BC, Chang CJ. 2010. Aquaporin-3 mediates hydrogen peroxide uptake to regulate downstream intracellular signaling. *Proc Natl Acad Sci U S A* 107(36): 15681-15686.

Miura T, Shinkai Y, Jiang HY, Iwamoto N, Sumi D, Taguchi K, et al. 2011. Initial Response and Cellular Protection through the Keap1/Nrf2 System during the Exposure of Primary Mouse Hepatocytes to 1,2-Naphthoquinone. *Chem Res Toxicol*.

Monks TJ, Hanzlik RP, Cohen GM, Ross D, Graham DG. 1992. Quinone chemistry and toxicity. *Toxicol Appl Pharmacol* 112(1): 2-16.

Murphy MP. 2009. How mitochondria produce reactive oxygen species. *Biochem J* 417(1): 1-13.

Nakamura H, Nakamura K, Yodoi J. 1997. Redox regulation of cellular activation. *Annu Rev Immunol* 15: 351-369.

Nel A. 2005. Atmosphere. Air pollution-related illness: effects of particles. *Science* 308(5723): 804-806.

Nel AE, Diaz-Sanchez D, Ng D, Hiura T, Saxon A. 1998. Enhancement of allergic inflammation by the interaction between diesel exhaust particles and the immune system. *J Allergy Clin Immunol* 102(4 Pt 1): 539-554.

Nemery B. 1990. Metal toxicity and the respiratory tract. *Eur Respir J* 3(2): 202-219.

Niture SK, Kaspar JW, Shen J, Jaiswal AK. Nrf2 signaling and cell survival. *Toxicol Appl Pharmacol* 244(1): 37-42.

Ohashi T, Mizutani A, Murakami A, Kojo S, Ishii T, Taketani S. 2002. Rapid oxidation of dichlorodihydrofluorescein with heme and hemoproteins: formation of the fluorescein is independent of the generation of reactive oxygen species. *FEBS Lett* 511(1-3): 21-27.

Ormo M, Cubitt AB, Kallio K, Gross LA, Tsien RY, Remington SJ. 1996. Crystal structure of the *Aequorea victoria* green fluorescent protein. *Science* 273(5280): 1392-1395.

Ostergaard H, Henriksen A, Hansen FG, Winther JR. 2001. Shedding light on disulfide bond formation: engineering a redox switch in green fluorescent protein. *EMBO J* 20(21): 5853-5862.

Ouhabi R, Boue-Grabot M, Mazat JP. 1998. Mitochondrial ATP synthesis in permeabilized cells: assessment of the ATP/O values in situ. *Anal Biochem* 263(2): 169-175.

Palmieri B, Sblendorio V. 2007. Oxidative stress tests: overview on reliability and use. Part I. *Eur Rev Med Pharmacol Sci* 11(5): 309-342.

Pastore A, Piemonte F, Locatelli M, Lo Russo A, Gaeta LM, Tozzi G, et al. 2001. Determination of blood total, reduced, and oxidized glutathione in pediatric subjects. *Clin Chem* 47(8): 1467-1469.

Pautke C, Vogt S, Tischer T, Wexel G, Deppe H, Milz S, et al. 2005. Polychrome labeling of bone with seven different fluorochromes: enhancing fluorochrome discrimination by spectral image analysis. *Bone* 37(4): 441-445.

Penning TM, Burczynski ME, Hung CF, McCoull KD, Palackal NT, Tsuruda LS. 1999. Dihydrodiol dehydrogenases and polycyclic aromatic hydrocarbon activation: generation of reactive and redox active o-quinones. *Chem Res Toxicol* 12(1): 1-18.

Pinchuk I, Schnitzer E, Lichtenberg D. 1998. Kinetic analysis of copper-induced peroxidation of LDL. *Biochim Biophys Acta* 1389(2): 155-172.

Pope A, Dockery D, Schwartz J. 1995. Review of Epidemiological Evidence of Health

Effects of Particulate Air Pollution. *Inhal Toxicol* 7(1): 1-18.

Pope A. 2010. Review: Epidemiological Basis for Particulate Air Pollution Health Standards. *Aerosol Science and Technology* 32(1): 4-14.

Pourazar J, Mudway IS, Samet JM, Helleday R, Blomberg A, Wilson SJ, et al. 2005. Diesel exhaust activates redox-sensitive transcription factors and kinases in human airways. *Am J Physiol Lung Cell Mol Physiol* 289(5): L724-730.

Quig D. 1998. Cysteine metabolism and metal toxicity. *Altern Med Rev* 3(4): 262-270.

Radi R, Peluffo G, Alvarez MN, Naviliat M, Cayota A. 2001. Unraveling peroxynitrite formation in biological systems. *Free Radic Biol Med* 30(5): 463-488.

Rahman I, MacNee W. 2000. Oxidative stress and regulation of glutathione in lung inflammation. *Eur Respir J* 16(3): 534-554.

Reddel RR, Ke Y, Gerwin BI, McMenamin MG, Lechner JF, Su RT, et al. 1988. Transformation of human bronchial epithelial cells by infection with SV40 or adenovirus-12 SV40 hybrid virus, or transfection via strontium phosphate coprecipitation with a plasmid containing SV40 early region genes. *Cancer Res* 48(7): 1904-1909.

Reers M, Smith TW, Chen LB. 1991. J-aggregate formation of a carbocyanine as a quantitative fluorescent indicator of membrane potential. *Biochemistry* 30: 7.

Rhee SG. 2007. Measuring H<sub>2</sub>O<sub>2</sub> produced in response to cell surface receptor activation. *Nat Chem Biol* 3(5): 244-246.

Riganti C, Gazzano E, Polimeni M, Costamagna C, Bosia A, Ghigo D. 2004. Diphenyliodonium inhibits the cell redox metabolism and induces oxidative stress. *J Biol Chem* 279(46): 47726-47731.

Riley MR, Boesewetter DE, Kim AM, Sirvent FP. 2003. Effects of metals Cu, Fe, Ni, V, and Zn on rat lung epithelial cells. *Toxicology* 190(3): 171-184.

Rodriguez CE, Shinyashiki M, Froines J, Yu RC, Fukuto JM, Cho AK. 2004. An examination of quinone toxicity using the yeast *Saccharomyces cerevisiae* model system.

Toxicology 201(1-3): 185-196.

Roebuck KA. 1999. Regulation of interleukin-8 gene expression. *J Interferon Cytokine Res* 19(5): 429-438.

Rosen GM, Pou S, Ramos CL, Cohen MS, Britigan BE. 1995. Free radicals and phagocytic cells. *FASEB J* 9(2): 200-209.

Rota C, Fann YC, Mason RP. 1999. Phenoxy free radical formation during the oxidation of the fluorescent dye 2',7'-dichlorofluorescein by horseradish peroxidase. Possible consequences for oxidative stress measurements. *J Biol Chem* 274(40): 28161-28168.

Ruckerl R, Schneider A, Breitner S, Cyrus J, Peters A. 2011. Health effects of particulate air pollution: A review of epidemiological evidence. *Inhal Toxicol* 23(10): 555-592.

Sagai M, Saito H, Ichinose T, Kodama M, Mori Y. 1993. Biological effects of diesel exhaust particles. I. In vitro production of superoxide and in vivo toxicity in mouse. *Free Radic Biol Med* 14(1): 37-47.

Samet JM, Dewar BJ, Wu W, Graves LM. 2003. Mechanisms of Zn(2+)-induced signal initiation through the epidermal growth factor receptor. *Toxicol Appl Pharmacol* 191(1): 86-93.

Samet JM, Dominici F, Curriero FC, Coursac I, Zeger SL. 2000. Fine particulate air pollution and mortality in 20 U.S. cities, 1987-1994. *N Engl J Med* 343(24): 1742-1749.

Samet JM, Graves LM, Quay J, Dailey LA, Devlin RB, Ghio AJ, et al. 1998. Activation of MAPKs in human bronchial epithelial cells exposed to metals. *Am J Physiol* 275(3 Pt 1): L551-558.

Samet JM, Tal TL. 2010. Toxicological disruption of signaling homeostasis: tyrosine phosphatases as targets. *Annu Rev Pharmacol Toxicol* 50: 215-235.

Santa-Maria I, Smith MA, Perry G, Hernandez F, Avila J, Moreno FJ. 2005. Effect of quinones on microtubule polymerization: a link between oxidative stress and cytoskeletal alterations in Alzheimer's disease. *Biochim Biophys Acta* 1740(3): 472-480.

Schwarzlander M, Fricker MD, Sweetlove LJ. 2009. Monitoring the in vivo redox state of plant mitochondria: effect of respiratory inhibitors, abiotic stress and assessment of recovery from oxidative challenge. *Biochim Biophys Acta* 1787(5): 468-475.

Senft AP, Dalton TP, Nebert DW, Genter MB, Puga A, Hutchinson RJ, et al. 2002. Mitochondrial reactive oxygen production is dependent on the aromatic hydrocarbon receptor. *Free Radic Biol Med* 33(9): 1268-1278.

Shimomura O, Johnson FH, Saiga Y. 1962. Extraction, purification and properties of aequorin, a bioluminescent protein from the luminous hydromedusan, *Aequorea*. *J Cell Comp Physiol* 59: 223-239.

Shutes A, Onesto C, Picard V, Leblond B, Schweighoffer F, Der CJ. 2007. Specificity and mechanism of action of EHT 1864, a novel small molecule inhibitor of Rac family small GTPases. *J Biol Chem* 282(49): 35666-35678.

Simmons SO, Fan C-Y, Yeoman K, Wakefield J, Ramabhadran R. 2011. NRF2 Oxidative Stress Induced by Heavy Metals is Cell Type Dependent. *Current Chemical Genomics* 5: 12.

Smiley ST, Reers M, Mottola-Hartshorn C, Lin M, Chen A, Smith TW, et al. 1991. Intracellular heterogeneity in mitochondrial membrane potentials revealed by a J-aggregate-forming lipophilic cation JC-1. *Proc Natl Acad Sci U S A* 88(9): 3671-3675.

Stadtman ER. 2004. Role of oxidant species in aging. *Curr Med Chem* 11(9): 1105-1112.

Starkov AA, Fiskum G, Chinopoulos C, Lorenzo BJ, Browne SE, Patel MS, et al. 2004. Mitochondrial alpha-ketoglutarate dehydrogenase complex generates reactive oxygen species. *J Neurosci* 24(36): 7779-7788.

Starkov AA. 2008. The role of mitochondria in reactive oxygen species metabolism and signaling. *Ann N Y Acad Sci* 1147: 37-52.

Steinberg JJ, Gleeson JL, Gil D. 1990. The pathobiology of ozone-induced damage. *Arch Environ Health* 45(2): 80-87.

Subach OM, Gundorov IS, Yoshimura M, Subach FV, Zhang J, Gruenwald D, et al. 2008.

Conversion of red fluorescent protein into a bright blue probe. *Chem Biol* 15(10): 1116-1124.

Sumi D, Akimori M, Inoue K, Takano H, Kumagai Y. 2010. 1,2-Naphthoquinone suppresses lipopolysaccharide-dependent activation of IKKbeta/NF-kappaB/NO signaling: an alternative mechanism for the disturbance of inducible NO synthase-catalyzed NO formation. *J Toxicol Sci* 35(6): 891-898.

Sun Y, Taguchi K, Sumi D, Yamano S, Kumagai Y. 2006. Inhibition of endothelial nitric oxide synthase activity and suppression of endothelium-dependent vasorelaxation by 1,2-naphthoquinone, a component of diesel exhaust particles. *Arch Toxicol* 80(5): 280-285.

Tak PP, Firestein GS. 2001. NF-kappaB: a key role in inflammatory diseases. *J Clin Invest* 107(1): 7-11.

Tal TL, Bromberg PA, Kim Y, Samet JM. 2008. Epidermal growth factor receptor activation by diesel particles is mediated by tyrosine phosphatase inhibition. *Toxicol Appl Pharmacol* 233(3): 382-388.

Tal TL, Graves LM, Silbajoris R, Bromberg PA, Wu W, Samet JM. 2006. Inhibition of protein tyrosine phosphatase activity mediates epidermal growth factor receptor signaling in human airway epithelial cells exposed to Zn<sup>2+</sup>. *Toxicol Appl Pharmacol* 214(1): 16-23.

Tal TL, Simmons SO, Silbajoris R, Dailey L, Cho SH, Ramabhadran R, et al. 2010. Differential transcriptional regulation of IL-8 expression by human airway epithelial cells exposed to diesel exhaust particles. *Toxicol Appl Pharmacol* 243(1): 46-54.

Tang ZL, Wasserloos K, St Croix CM, Pitt BR. 2001. Role of zinc in pulmonary endothelial cell response to oxidative stress. *Am J Physiol Lung Cell Mol Physiol* 281(1): L243-249.

Tashakkor AY, Chow KS, Carlsten C. Modification by antioxidant supplementation of changes in human lung function associated with air pollutant exposure: a systematic review. *BMC Public Health* 11: 532.

Trachootham D, Lu W, Ogasawara MA, Nilsa RD, Huang P. 2008. Redox regulation of cell survival. *Antioxid Redox Signal* 10(8): 1343-1374.

Tsatsanis C, Androulidaki A, Venihaki M, Margioris AN. 2006. Signalling networks

regulating cyclooxygenase-2. *Int J Biochem Cell Biol* 38(10): 1654-1661.

Valavanidis A, Fiotakis K, Vlahogianni T, Papadimitriou V, Pantikaki V. 2006. Determination of Selective Quinones and Quinoid Radicals in Airborne Particulate Matter and Vehicular Exhaust Particles. *Environmental Chemistry* 3(2): 6.

Valko M, Morris H, Cronin MT. 2005. Metals, toxicity and oxidative stress. *Curr Med Chem* 12(10): 1161-1208.

Valko M, Rhodes CJ, Moncol J, Izakovic M, Mazur M. 2006. Free radicals, metals and antioxidants in oxidative stress-induced cancer. *Chem Biol Interact* 160(1): 1-40.

Vanhaesebroeck B, Leever SJ, Ahmadi K, Timms J, Katso R, Driscoll PC, et al. 2001. Synthesis and function of 3-phosphorylated inositol lipids. *Annu Rev Biochem* 70: 535-602.

Vernoux T, Wilson RC, Seeley KA, Reichheld JP, Muroy S, Brown S, et al. 2000. The ROOT MERISTEMLESS1/CADMIUM SENSITIVE2 gene defines a glutathione-dependent pathway involved in initiation and maintenance of cell division during postembryonic root development. *Plant Cell* 12(1): 97-110.

Vesce S, Jekabsons MB, Johnson-Cadwell LI, Nicholls DG. 2005. Acute glutathione depletion restricts mitochondrial ATP export in cerebellar granule neurons. *J Biol Chem* 280(46): 38720-38728.

Wamelink MM, Struys EA, Jakobs C. 2008. The biochemistry, metabolism and inherited defects of the pentose phosphate pathway: a review. *J Inher Metab Dis* 31(6): 703-717.

WHO. 2002. World Health Report. Reducing risks, promoting healthy life. Geneva: World Health Organization.

Wolf E, Schubler A. 2005. Phycobiliprotein fluorescence of *Nostoc punctiforme* changes during the life cycle and chromatic adaptation: characterization by spectral confocal laser scanning microscopy and spectral unmixing. *Plant, Cell and Environment* 28: 480-491.

Wu W, Graves LM, Jaspers I, Devlin RB, Reed W, Samet JM. 1999. Activation of the EGF receptor signaling pathway in human airway epithelial cells exposed to metals. *Am J Physiol* 277(5 Pt 1): L924-931.

Wu W, Samet JM, Silbajoris R, Dailey LA, Sheppard D, Bromberg PA, et al. 2004. Heparin-binding epidermal growth factor cleavage mediates zinc-induced epidermal growth factor receptor phosphorylation. *Am J Respir Cell Mol Biol* 30(4): 540-547.

Xia T, Korge P, Weiss JN, Li N, Venkatesen MI, Sioutas C, et al. 2004. Quinones and aromatic chemical compounds in particulate matter induce mitochondrial dysfunction: implications for ultrafine particle toxicity. *Environ Health Perspect* 112(14): 1347-1358.

Zelikoff JT, Chen LC, Cohen MD, Fang K, Gordon T, Li Y, et al. 2003. Effects of inhaled ambient particulate matter on pulmonary antimicrobial immune defense. *Inhal Toxicol* 15(2): 131-150.

Zhang L, Yu L, Yu CA. 1998. Generation of superoxide anion by succinate-cytochrome c reductase from bovine heart mitochondria. *J Biol Chem* 273(51): 33972-33976.

Zimmermann T, Rietdorf J, Pepperkok R. 2003. Spectral imaging and its applications in live cell microscopy. *FEBS Lett* 546(1): 87-92.

Zucker RM, Lerner JM. 2005. Wavelength and alignment tests for confocal spectral imaging systems. *Microsc Res Tech* 68(5): 307-319.

Zucker RM, Rigby P, Clements I, Salmon W, Chua M. 2007. Reliability of confocal microscopy spectral imaging systems: use of multispectral beads. *Cytometry A* 71(3): 174-189.

Zucker RM. 2006a. Quality assessment of confocal microscopy slide-based systems: instability. *Cytometry A* 69(7): 677-690.

Zucker RM. 2006b. Quality assessment of confocal microscopy slide based systems: performance. *Cytometry A* 69(7): 659-676.